Stockholm University

# A quantum for a quantum

Quantum simulators in exotic lattices

Pil Maria Saugmann

Doctoral Thesis in Theoretical Physics at Stockholm University, Sweden 2022

# A quantum for a quantum
## Quantum simulators in exotic lattices

**Pil Maria Saugmann**

Academic dissertation for the Degree of Doctor of Philosophy in Theoretical Physics at Stockholm University to be publicly defended on Friday 9 September 2022 at 13.00 in Albano, details about the location is available at the department website.

### Abstract
This thesis centers on how to use exotic lattices in different ways to design potential quantum simulators. These exotic lattices are either real physical objects in the form of ultra cold atoms in bipartite optical lattice systems or lattice models revealed in state space. For optical lattices, the potential wells forms a lattice, such that the atoms of the system will be highly localized at the potential minima, and where the bipartite nature of the lattice ensures that the lattice sites will alternate between two different types. When studying the atoms in the optical lattices they can be described by a Bose-Hubbard model, where it turns out that bipartite lattice systems provides a route to realizing frustration through competing nearest and next nearest neighbor couplings in both the superfluid phase and the Mott insulating phase.

For state space lattices are no longer objects in real space, but instead they live in state space. Though such state space lattice models can be represented as single particle systems, they still hold a potential for realizing quantum simulators. For this type of exotic lattices, the focus is on how to study quantum optical models in terms of their Fock space lattices (FSLs). Such models only have a few degrees-of-freedom which together with symmetries of these system, make it simple to identify the emerging FSLs with know lattice models from the condensed matter. Thus shedding new light on the quantum optical systems at hand. The three-mode Jaynes-Cummings model in the large detuned limit, is used as an example to display the strength of this method. It is the growth of a systems state space, that determines whether the system is a potential quantum simulator or not. For a system to be a quantum simulator, the growth of the phase space has to be such, that it becomes computational hard to find the systems energy. This means, that if we can design a state space lattice, which grows exponential, then we have a potential candidate for a quantum simulator. The Bethe lattice is one such example that grows exponentially.

**Keywords:** *quantum physics, condensed matter physics, quantum optics, optical lattices. Fock state lattices, exotic lattices, frustration.*

Stockholm 2022
http://urn.kb.se/resolve?urn=urn:nbn:se:su:diva-206468

ISBN 978-91-7911-940-9
ISBN 978-91-7911-941-6


**Department of Physics**

Stockholm University, 106 91 Stockholm

A QUANTUM FOR A QUANTUM

Pil Maria Saugmann


Stockholm
University

# A quantum for a quantum

Quantum simulators in exotic lattices

Pil Maria Saugmann

©Pil Maria Saugmann, Stockholm University 2022

ISBN print 978-91-7911-940-9
ISBN PDF 978-91-7911-941-6

Printed in Sweden by Universitetsservice US-AB, Stockholm 2022

*Er lyset for de lærde blot*
*til ret at slet at stave*
*Nej himlen under flere godt*
*og lys er himlens gave.*

# List of Papers

The following papers, referred to in the text by their Roman numerals, are included in this thesis.

PAPER I: **Magnetic phases of orbital bipartite optical lattices**
Pil Saugmann, Jonas Larson, *New Journal of Physics*, **Volume 22**, page (2020).
DOI: Magnetic phases of orbital bipartite optical lattices

PAPER II: **Route towards classical frustration and band flattening via optical lattice distortion**
Pil Saugmann, José Vargas, Yann Kiefer, Max Hachman, Raphael Eichberger, Andreas Hemmerich and ,Jonas Larson, *Submitted: Phys. Rev. Lett*,
DOI: ArXiv: Route towards classical frustration and band flattening via optical lattice distortion

PAPER III: **A Fock state lattice approach to quantum optics**
Pil Saugmann, Jonas Larson, *Submitted: Phys. Rev. A.*,
DOI: ArXiv: A Fock state lattice approach to quantum optics

# Contents

# List of Figures

# List of Tables

# The story of this PhD

This became a twisted path, and I took turns and loops I never imagined that I would take. I can say that this PhD was both everything and nothing at all of what I imagined it would be. For me, this PhD was a lot more than the research, and I take the chance to share a glimpse of this. This whole experience was first and foremost shaped by all people I crossed paths with and who I would like to thank.

My supervisor **Jonas**, is one of the people who has had the biggest impact. It is hard to capture all of our interactions in a few sentences, but what stays with me is the last thing he said in my interview. That **KOMKO** is a very nice place to work. It resonated with me, and while there has been ups and downs, I am to this day, still happy that I got the chance to work here, and that is very much due to him. KOMKO is indeed an amazing place to work, and it so due to all the people who have passed through these corridors. As academia is international and filled with short term contracts, a lot of people passed through. People like **Fabian**, **Gerard**, **Massi**, **Quentin**, **Naemi**, and **Marion** who I had countless of strange conversations with, **Iman** and **Sreekanth** who I tricked into eating Danish candy, **Julia** who I could talk for hours with, **Themis** who I shared the most EU friendly office with and who enabled an unhealthy obsession with British politics, and **Axel**, who I can simply not envision how this PhD would have been without.

Academia is precarious, and it can be a tough working environment with a lot uncertainty, and management that does not always know what to do. I was lucky though, both with my **university**, my **faculty** and my **department**. My department has been supportive by providing structure and administrative help, by never hindering my representational endeavors, and by at both my licentiate and predefence, where **Edwin**, **Markus**, **Sten**, and **Johan**, gave much needed feedback. My co-supervisor **Eddy** and my mentor **Supriya**, did both in different ways provid the work environment everyone who does a PhD dreams about. It felt safe and like there was someone to catch me if needed.

The people in **Desert Island**, **Lunch and Guns**, **Fika and Guns**, and **K-gattan** first made me feel connected to Stockholm. And **Colin**,

**Ferran**, **Magda**, **Vlad**, **Maria**, **Sreyashi**, **Hannes**, **Joana**, **Vani**, and **Michelle** are who at various points made Stockholm a home for me.

Home is where the heart is, and I scattered mine all over the world. Besides Sweden, I store a piece in Belgrade, London, Wigan, France, and Denmark - in **Århus**, at **CF Richs vej 36**, but particular in **København**. I want to thank **Dave** for making me dare this and showing me that it would not make me any less rooted. Something of the finest my mother taught me was to let others in, and from knowing **Lise, Willy, Anne-Marie, Tove** and **Per** I learned that there are many ways of doing so. As a child, **Strandboulevarden** and **Holte** were where my world began and ended, and where **Søren**, **Birgitte** and **Peter** helped shape me to be me, **Christian**, **Marie**, **Kirstine**, **Tamaz**, and **Malaz** are my base in Copenhagen and beyond.

I feel like I spent most of my PhD in trains. Most trips have vanished into oblivion but one stands crystal clear. **Friday the 13th** of March 2020, I thought about if I should go north or south. Half an hour northwards bound, Denmark closed its borders, and while they were never closed to me, it made a profound impact.

During the pandemic I started a sourdough that died, I started running which I quit, and with **Irina** I started a podcast that didn't die and I didn't quit. **Nyfiken** grew into something more that **Mona**, **Maria**, **Aron**, **Emilia** and many others help shape in different ways.

As for many who did their PhD during the pandemic, the pandemic shaped the experience. If I learned one thing from it, it is that the most interesting things they happen due to interactions, I learned I won the supervisor lottery. While I more or less could carry on with my research, I missed interactions and the strange lunch conversations just before the pandemic where I was asked **Who would you bring on a Desert Island**. And I found my self in countless of Zoom meetings discussing the consequences of the pandemic had on PhD education.

A year earlier, I asked my student union to nominate for chair of the doctoral students committee in **Sveriges Förenade Studentkårer** (SFS). This is the single decision I made during my PhD that shaped it the most. It started with a trip to Östersund, and though it was in May it was snowing. I went to SFS-FUM and was totally at a loss. But beside feeling lost I felt in awe. In awe of all the students who were all so knowledgeable. The people I crossed path with in the **Swedish studentrörelse** impressed me by the work they do. At times they gave me more imposter syndrome than my research, but I was left with a feeling, that we are all in this together, and together we shape the future of higher education and research into something more **sustainable**.

**SUS** is **my** student union and without **Sara**, **Markus**, **Henrike**, **Anton**, **Elis**, and **Sofia** I would not have gotten hooked on this hobby I forgot I love. I look forward to see *What happens next* for all of you.

While SUS lured me in, **SSCO** provided me housing, it is SFS that stole my heart. For me SFS is not only *spetsig påverkansorganisation*, it is much more, it is the people who were, are or will be active. For me it is the **boardmembers** who introduced me to *på spåret*, patiently let me develop my Swedish skills. It is the **office** who makes things run. It is **KOMIT** and **SQC**. It is and **Gustav**, **Karl**, **Elisabet**, **Joel**, **Jacob**, **Philip**, **Leo** and **Oskar** who I worked closer with. And most importantly, it is the nicest place in Swedish student politics, my own committee SFS-DK, with its members **Ananda**, **Qiaoli**, **Emma**, **Emil**, **Christopher**, **Gustav**, **Katharina**, **Lakshmi**, **Marvin**, and in particular those who were with me all the way **Alex**, **Daniel** and **Sebastian**.

I am lousy at sports, but I like the metaphorically felling of playing on the same tem. SFS gave me that, and I got to be on a team with four of the most talented people I know, with **Linnéa**, who like me has an unhealthy interest in the Swedish doctoral education and British crime shows, with **Sara**, with whom I make an overambitious team and I would love to do so again, with **Linn**, who is hard to match and the only one in SFS with Danish skills, and with **Simon**, who I had so many meetings with that it was insane, and though he made me doubt my Swedish skills the most, always had my back and is one of the nicest people I have worked with.

I would have liked to be added to **Högskolaläckan** early so I would have what to small talk about in various boards and working groups. In these many meetings, at **Stockholm University**, **UKÄ** and **SUHF**, I got a tailored made culture and language classes and I was taught one or two things about leadership and where **Anders**, **Astrid**, **Sigbrit** and **Kerstin** were inspirations.

My language class were custom made, and while board rooms are not a scalable solution, I wish that more internationals get a chance to represent. Academia is international and precarious, and it never felt more so than with the Aliens Act. It changed the conditions for many of my international friends and colleagues overnight and some left academia or Sweden because of it. If there is a silver lining, it is that it brought the entire sector together, and for me it meant I got to work closely with **Mohammad**, **Paulina**, **Sandra**, **Kjell**, **Robert** and others in the **student unions** and **doctoral student councils** and organizations like **SULF**, **Fackförbundet ST**, **SNPA**, and **NJF**.

When I first wanted to learn Swedish, **Hans** laughed loudly. According to him if I spoke Danish I would be understood. Most times this didn't work! Between the lines, he stressed something important, that it takes a fourth order Taylor expansion to tell the difference between Denmark and Sweden. Representation was for me not a new hobby nor one I confined to Sweden. As a fan of the European Union, I went abroad as well. One of the finest European organizations I know of is **Eurodoc**. Here, first **Mathias**, then **Danila**, **Mariana**, **Sebastian**, **Olek**, **Aga**, **Sara** and lately **Patrizia**, **Joana**, **Nicola** and **Hannah** gave me friends and allies in Europe as well.

When it comes to representation you can choose to leave it to others or you can choose to do it your self. I chose the later. Evil tongues would say I have used to much time on all of this, and I loved it. For me it started back in Copenhagen and at **Fysisk Fagråd's** meetings in |RUM| with **Anine**, **Amalie**, **Allan**, **Esben**, **Ida**, **Jacob**, **Thomas R** and honorably members **Robert** and **Ian**. I loved to study at Niels Bohr Institutet, but it is a place where you are expected to feel a belonging to, and that is not always easy, **Niels**, **Karis**, **Christian**, **Jeppe**, **Anne**, **Elisabeth**, **Hjalte**, and **Yngve**, made me feel that I belonged.

To cite an **SUHF** report, it is the PhD education that shapes the future academia, this is only partially true. The future of academia is also shaped by all of those people in the sector who cares about it. And my PhD was shaped by all of those listed above and many others.

Were and how I fit in, is not something I find easy and I often doubt my self. But there are places I know I always fit in. It is the orange couch in Stockholm, were **Irina**, **David** and I outlasted the pandemic. With an internet connection and streaming subscriptions, the pandemic has not change my answer, and I would bring them with me on a Desert Island. It is with **Nanna** on the beach with the taste of salt in the air, it is with **Mona** who makes the world a better place, with **Jeanette** who sees me as I wished I saw myself, **Mikkel** who believes in me when I don't do so myself, it is with **Fie** who I do not wish to remember a world without, and with **Steen**, med hvem to plus to er fem og jeg er glad.

I care about research, education, academia, physics, and people. Most of all this is due to my mother. So last but not least, to my mother **Pernille**! This work was made possible because of the confidence in the world and myself you instilled in me. You gave me a hunger for knowledge, whether it came from books or interactions with others. And you were the first to teach me the difference between, **one**, **two** and **many** - something for this work proved to be quite useful.

# Part I

# Background

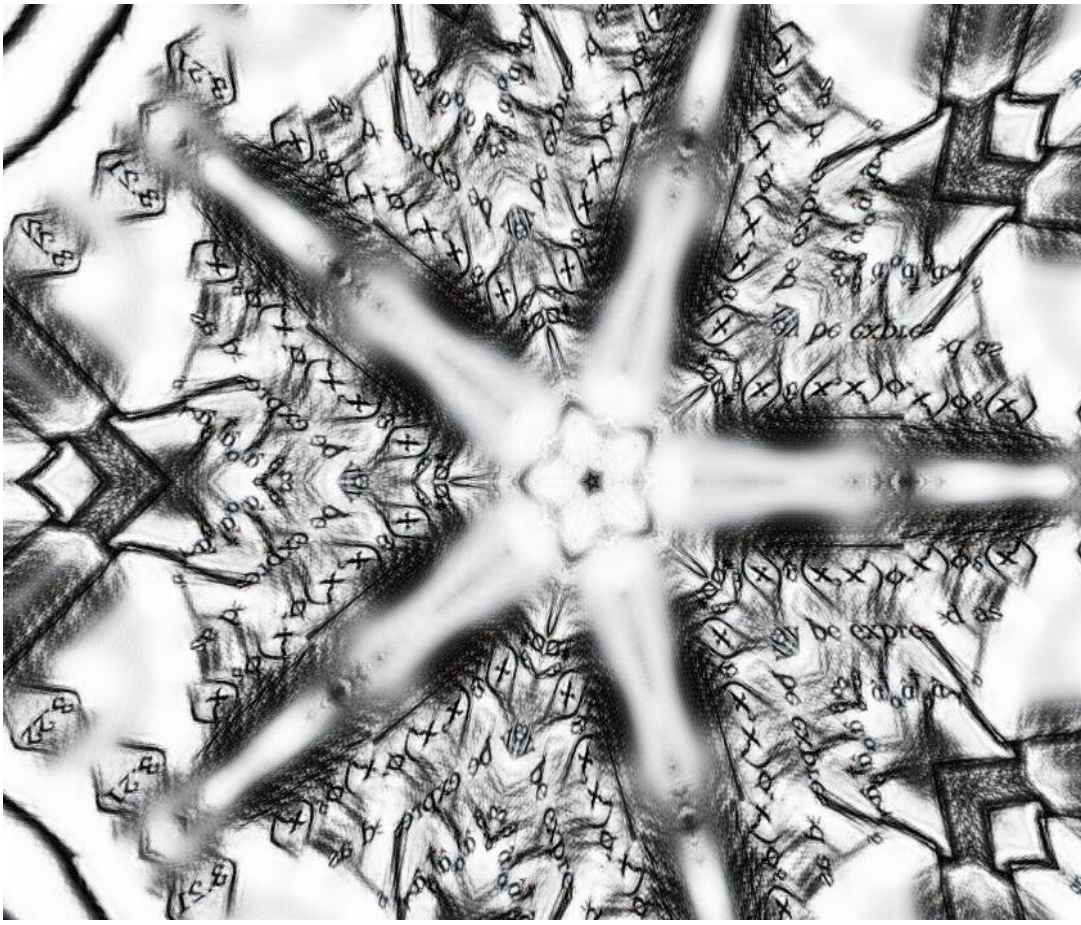

# 1. A quantum for a quantum

In the knowledge society, knowledge is what shapes society, and this raise the question of what knowledge is. A kind of knowledge that academia specialises in is research-based knowledge. The research done today hopefully lead to new knowledge and thus shape our futures. Research thus play an integral part in the knowledge society. With this, comes the responsibility that researchers share their findings broadly. This is true for all kinds of research and, of course, my own. The title of this thesis is *A quantum for a quantum* , and I hope no matter if you are a physicist or not, that this chapter explains what to expect if you continue to read on.

I do my research within the field of *Quantum physics*. Quantum physics is a field where its reputation is likely to reach you before you become fully acquainted, and it is rumoured to be so inaccessible that we cannot fully understand it. One reason for this reputation, is that the quantum world is very different from the classical one where we live our daily lives.

Some quantum systems are so complicated that we cannot study them using a classical computer. Instead, we must resort to a trick as old as physics and simulate their behaviour, However, we must do so using another quantum system.

When we simulate one quantum system with another quantum system, we get *A quantum for a quantum* or a quantum simulator. A quantum simulator is a quantum system that can teach us something about some quantum property of other quantum systems without us looking directly at these other systems. That we study systems by proxy is neither strange nor new. This is what one does when using a computer to simulate how a rocket may travel to the moon or how a disease spreads. If you are not a physicist, what might be new is that one can do this with a quantum system as the simulator. It is crucial that both systems are truly quantum, because if not then a classical computer could have done the job. A universal quantum simulator is a quantum simulator on which one could simulate (almost) all other quantum systems. Such a quantum simulator is called a *Quantum computer*.

The topic of quantum computers is hard to avoid these days. It is an excellent example of why research conducted in the field of physics holds the potential to shape society in a multitude of ways. In 2018 the European Union launched its research and innovation initiative, the Quantum Flagship, and earlier this year, NATO announced that a *Defense Innovation Accelerator for the North Atlantic* center would be placed at Niels Bohr Institutet, an institute with its history deeply entangled with quantum physics. These are two examples of why knowledge of quantum simulators is necessary if you want to understand future technologies, the geopolitical situation, or how the world functions.

## 1.1 Classical versus quantum

When we throw a ball up into the air, we can at all times know where the ball is and where it is heading. This is because the ball is a classical particle. Had it instead been quantum this would not be the case. Here, Heisenberg's uncertainty relation limits our combined knowledge about the velocity and position of the quantum particle. Where the classical world is deterministic, and we know where the ball is and is heading at all times, things are not as simple in the quantum world. Here, while the Schrödinger equation fully determines the wave function, the outcome of a measurement of it is nondeterministic. Instead, we must get used to describe the position and momentum of the quantum particle by probability distributions.

Quantum physics should still not be as frightening as it should scare anyone away. After all, we can visualise it using computer simulations on a classical computer. However, trouble do begin if we have more than one particle at hand. Here, the difference between the classical and quantum limits becomes even more profound. The classical particles are distinguishable, meaning can describe the whole system as a sum over every single particle. In the quantum limit, the particles are indistinguishable. Even though we know how to describe the movement of one particle or the interaction between two particles, piecing these pieces together cannot describe the entire system. The quantum particles become entangled; thus, one will have to solve for all particles simultaneously, rather than one at a time. And when we say that we are interested in truly quantum systems, this entanglement is what characterise these systems.

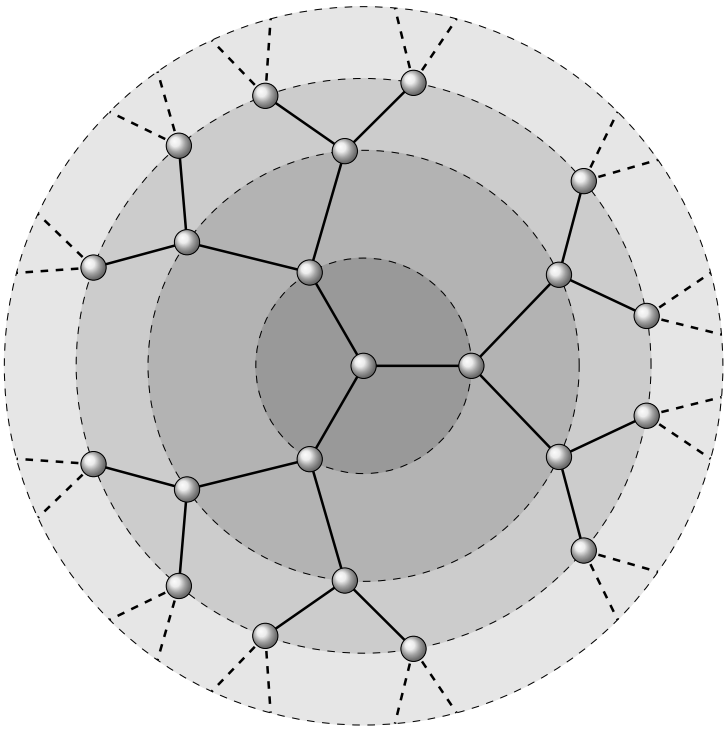

**Figure 1.1:** To illustrate what exponential growth means, the Bethe lattice is shown above. The number of lattice sites at each ring is respectively $1, 3, 6, 12...$ or expressed differently from the second ring, and onwards the number of sites on the $n$'th ring is $3 \cdot (2)^n$.

## 1.2 From entanglement to quantum simulators?

To understand what entanglement means, we suppose have a system with many particles and we are interested in describing how the system behaves. Often this means that we wish to find its groundstate. Here, the number of equations one needs to solve to find the state of the system grows exponentially with the number of particles in the system.

And herein lies a problem: if we are interested in many-body quantum systems of spin-half particles, trying to find the states of the system is a tedious job. With some skill, as long as we have only a few particles, we can ask a computer to solve this problem for us. The problem lies in that if the number of particles continues to increase, then the number of equations we need to solve to find the states of the system grows exponentially (see fig. 1.1 for an illustration of what exponential growth means). Thus, the number of bits that a classical computer would need

to solve the problem also grows exponentially, and it becomes a computationally hard problem meaning that the classical computer cannot solve it when the number of particles increases.

If a classical computer cannot solve the equations for us, we can either give up or try to circumvent the problem. The intrinsic obstacle is that the quantum particles are entangled, and their state-space grows exponentially. Since our computer is a classical system, it cannot keep up with the complexity of the quantum system. However, as Richard Feynman proposed, this intrinsic complexity of the many-body quantum systems can also pave the route to circumvent this challenge [1–3]. He suggested that instead of using a classical computer to analyze many-body quantum systems, one should use a quantum computer. A (universal) quantum computer is a programmable quantum system that allows us to solve any quantum systems (and some classical ones). Suppose we are less ambitious, and rather than aiming at solving all quantum problems, only aim at solving specific ones. In that case, we are left with a quantum simulator.

## 1.3 Towards quantum simulators

If a quantum simulator is a simulator which is governed by quantum physics instead of classical physics, then the simulator must be a quantum many-body system. Here, even though we know how each particle would move around and how two particles can interact, we have so many particles that a classical computer cannot describe the system completely. So rather than using a classical computer, or even worse, doing it with pen on paper, to investigate the system, we do it by looking at another quantum system, a real physical system in a laboratory.

We turn to the Hamiltonian, which specifies the total energy of a physical system, to get a feeling of how two different quantum systems can describe one another. The Hamiltonian is a mathematical object, *i.e.*, an equation, and it will have many different terms for many-body systems. If we include everything that affects the system, we should, in theory, include the whole world. We instead make a cutoff; when we express the Hamiltonian, we only include the relevant terms. This approach is what best can be called the art of approximation. While we have to address the approximations we make, and we have to argue for their validity, we are, however, left with a manageable Hamiltonian.

Typically, one ends up with a rather general Hamiltonian that describes the system at hand under several different conditions. However, we may then study the system under different limits. Given our Hamilto-

nian, we use it to derive the equations-of-motion which, when solved, tell how the system will evolve. Two seemingly different physical systems, described by some Hamiltonians, may generate equations of motion sharing the same mathematical structure. Hence, as other starting systems may lead us to the same effective Hamiltonian, we see an example of how one quantum system can describe another.

Two crucial questions should still be addressed. First, how do we, given that we cannot check it on a classical computer, know if the result of our quantum simulator is reliable? One way around this, is to consider systems with a limit where we know and where we understand their behaviour. Second, how one finds a suitable system for a quantum simulator? There are, more than one way to do so. In this thesis, we look at physical models that can be described as lattice models. We try to understand these models and what it is that makes them either suitable or unsuitable as quantum simulators. From this, we then try to change the models systematically, such that they can pave the way to a quantum simulator, and we do so using pen and paper.

## 1.4 From frustration to quantum simulator

To see how a quantum lattice system may be used to realise quantum simulators, we look at the phases of these. Quantum matter can, like classical matter, possess different phases, and it is the ground state of the system that determines the phase of the system. In the context of quantum simulators, what we search for is a system with a phase that cannot be understood without studying it with a quantum simulator.

Hence, a starting point will be to look at the ground state energy of the systems we are interested in. To distinguish different phases from one another one can introduce an *order parameter* which is a quantity that takes different values depending on the behaviour of the phase. The order parameter can be either zero or non-zero, with a zero value signalling lack of order. A phase without order is called a frustrated phase, here the system's ground state is highly degenerated due to competing forces that cannot simultaneously be fulfilled and in the quantum limit such a phase indicates that the particles are highly entangled [4; 5].

### 1.4.1 Frustration in lattices

Lattice systems provides a route for realising frustration systematically. A straightforward example of a frustrated system is the antiferromagnetic 2D triangular lattice of Ising spins. An Ising spin can only point

in two directions, *i.e.* up or down. When such spins are placed in a triangular lattice with antiferromagnetic couplings, it is impossible to satisfy all couplings simultaneously [6]. It would require that for all pairs of coupled spin, one spin should point up while the other point down, which will not be possible in the triangular lattice. Instead, we find that if we consider the three pairs of spins in a single triangle, then for two of the pairs, the spins will be anti-parallel, but for the last pair, the spins will be parallel. Thus, there are, in total, six different ground-states for a single triangle, leading to a highly degenerated ground state for the entire lattice [4; 6].

Frustration in systems like the triangular lattice is called geometric frustration because it is the geometry of the system that causes the frustration [7] as opposed that of coupling-induced frustration [8]. The Villain model, which consists of Ising spins on a square lattice, where tree of the couplings for every single square are ferromagnetic, while the last on is antiferromagnetic model [9] is an example of such a model where it is impossible satisfy all couplings, and also here one will end up with a frustrated ground state.

While the Ising spins were a good starting place to grasp frustration, we are interested in more complicated spins. When the temperature decreases, the spin will fluctuate and be correlated. Still, the system as a whole will lack order. In this sense, such systems mimic ordinary liquids, a dense and highly correlated form of matter that lacks static order, and such spin matter has therefor been coined spin liquids [4].

### 1.4.2 Quantum spin liquids

When the spin is small, it becomes quantum, and so do the fluctuations. Thus, in this limit, we have what is called a quantum spin liquid (QSL). Here the fluctuations will continue to exist down to $T = 0$, again due to Heisenberg's uncertainty relation. Thus the QSL can exist even at zero temperature [4; 10–12]. For a QSL even spins situated at lattice sites far apart will be entangled. The ground state of this kind of system is called a Resonant Valence Band (RVB) [10]. An RVB state is a superposition state of all the different possibilities that two spins can be paired, and thus the ground state is extremely degenerated, making a such a phase an ideal candidate for a quantum simulator.

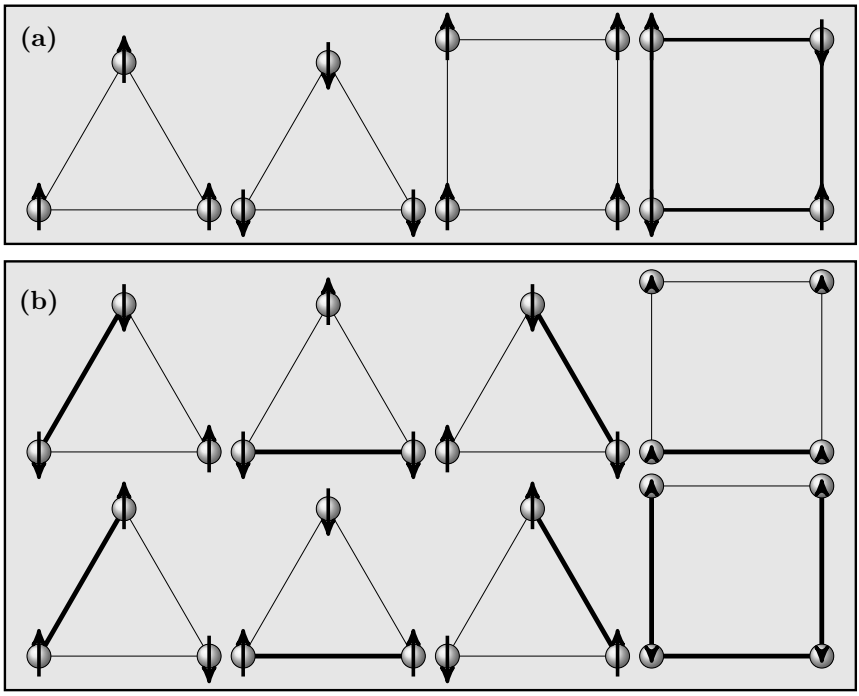


**Figure 1.2:** The ordering of Ising spins in a triangular versus square lattice. Thick lines mark antiferromagnetic coupling, while thin lines mark ferromagnetic couplings. In Fig.(a) ordering is possible, whereas in Fig. (b) it is not.

## 1.5 The structure of this thesis

The title of this thesis *A quantum for a quantum - Quantum simulators in exotic lattices* indicates that this thesis focuses on quantum simulators in exotic lattices. As a disclosure, I can now say that you will, in this thesis, not find a quantum simulator that has been realised. Instead, you will find two very different routes to how one can potentially design systems that could be quantum simulators. At the heart of both these routes are their lattice-like nature, which allows us to study the behaviour of the specific systems we have at hand and to use our findings to outline how to design new systems.

In Part 2 of this thesis, we look at *Ultra cold atoms in optical lattices* and in Part 3 move on *Fock state lattices*. Part 1, which includes this chapter and the two there follows, is designed to cover the common ground for both. In Chapter 2 *Exotic lattice structures* we discuss what is meant by lattices and exotic lattices, and in Chapter 3 we (re)capture the theoretical framework for dealing with many-body quantum systems.

In Part 2 (Chapter 4 - Chapter 6), we study ultracold optical lattice systems. We start in Chapter 4 by introducing optical lattice. In Chapter 5 we study such lattice systems in the superfluid limit and in Chapter 6 we study them in the Mott phase. In both chapters we see how the nature of bipartite lattices provides a route to realising a frustration.

We then change the setting, and in Part 3 (Chapter 7- Chapter 9), we look at Fock state lattices. As we will discuss later, Fock state lattices are conceptually very different from optical lattice. In Chapter 7, the introduce the theoretical framework for Fock state lattices, and in Chapter 8 we use this framework to study the multi-mode Jaynes Cummings model in the large detuned limit. In Chapter 9, we flip the question around. Here, we explore how we can use the knowledge from the previous two chapters to design Fock state lattices of interest.

Part 4 consists of a single chapter (Chapter 10). Here, ideas of how to proceed are presented.

# 2. Exotic lattice structures

Quantum simulators can take different shapes and forms. However, the ones you will encounter in this thesis have in common that they have a lattice-like structure.

Most likely, you have some intuitive understanding of what a lattice is. A neat example is a grid like the one on the squared paper. Here, the crossing of the lines will correspond to what we shall call lattice sites, and the line between two lattice sites will be the connections that allow us to move (electrons, atoms, or something else) around in the lattice. Strictly speaking, the squared paper is not what a mathematician would call a lattice.

A lattice is, mathematically speaking, an infinite set of points in the $d$ dimensional space $\mathbb{R}^d$, which fulfils that coordinate-wise addition or subtraction of any two points in the set will produce another element in the set. Thus, the mathematical lattice has no boundaries. The physical lattices we encounter are not infinite. In physics, however, one is often most interested in lattices in one, two, or three dimensions, but the definitions we encounter here can be extended to higher dimensions.

The squared paper is not infinite, and thus the structure we see on it is, strictly speaking, a lattice. For physicists, this is, however, not enough to call something a lattice. In physics, the probably most well-known physical example of a lattice is that of crystals formed by regular configurations of atoms found in some materials. Hence, a crystal is an actual physical object in a solid state that exhibits the order described before. While no crystal is infinite, it, of course, has a boundary. However, most atoms or molecules in it will be so far away from the boundary that their behaviour will not be influenced by it, and in that sense, the solid-state crystal is perfect. The behaviour of crystal lattices is the topic of solid-state physics, and they have proven to be a powerful method for studying condensed matter systems [13]. Thus such systems are finite, just as a piece of squared paper is. Most of the lattice sites are situated so far away from the system's boundary that we can disregard the effects of the boundary on these lattice sites. In this sense, the behaviour of the atoms that occupy these lattice sites can be studied by

describing them as being in the lattice. In this chapter, we review some of the basics of solid-state physics, but for readers who are interested in a more thorough introduction, we refer to standard textbooks [14; 15].

## 2.1 The crystal lattice

The crystals one encounters in nature are at most three-dimensional structures. In physics, the mathematical lattice is called a *Bravais lattice*, after the French physicist Auguste Bravais [14]. For a three-dimensional lattice, the condition given above can be expressed as

$$\mathbf{R} = n_1\mathbf{a}_1 + n_2\mathbf{a}_2 + n_3\mathbf{a}_3, \tag{2.1}$$

where $n_i$ are any integers and $a_i$ are the *primitive vectors* which span the lattice. The choice of these primitive vectors is not unique.

Mathematically speaking, a **lattice** in three dimensions is a Bravais lattice. However, the name lattice by physicists is often used more loosely, where the lattice describes an actual physical object, such as the crystal structure. This structure can have a basis of one or several atoms, and this group repeats indefinitely in three dimensions according to the arrangement of one of the Bravais lattices.

We shall, from here on, use the physicist convention, and by a lattice, we shall mean a periodic structure with a boundary. However, if it is large enough to be considered translational invariant, thus it can be described by its Bravais lattice. There are 5, 14, and 64 Bravais lattices in respectively 2, 3, and 4 dimensions [14; 15]. All crystalline materials recognised today, not including quasicrystals, fit in one of these arrangements.

### 2.1.1 The Unit cell versus the lattice plaquette

The area spanned by the primitive vectors is called the *unit cell*. The unit cell is the smallest building block of the lattice and reflects the symmetry and structure of the entire crystal. Just as there are many different primary vectors, there are many different unit cells. However, an often practical choice is the *Wigner-Seitz cell*. The Wigner-Seitz cell is found by first picking a lattice point. After this point is chosen, one draws lines to all nearby lattice points. Halfway through each line, another line is drawn perpendicularly. The smallest area enclosed by the perpendicular lines is the Wigner–Seitz primitive cell. In fig. 2.1 two different 2 dimensional lattices are shown. Both lattices are what we will call square lattices. However, whereas all atoms in the lattice

shown in fig. 2.1(a) are the same, the atoms in the lattice in fig. 2.1(b) alternate between two different kinds - we shall call this kind of lattice for a *bipartite lattice*.

Though the two lattices in fig. 2.1 are very similar, there are significant differences. In particular, the unit cell for the two lattices will be different. The unit cell in the bipartite lattice will be twice as big as the unit cell in the regular lattice (see the white cell in both fig. 2.1(a) and (b)).

The unit cell depends on the lattice grid and the atoms placed in it. However, we introduce another cell that only depends on the grid, which we call the *lattice plaquette*. The lattice plaquette is the cell captured by the smallest loop one can make in the lattice. As opposed to the unit cell, the lattice plaquette only depends on the lattice grid. Returning to fig. 2.1 we see how the lattice plaquette for the regular and bipartite square lattice coincide. Furthermore, we see how the lattice plaquette is also a unit cell in the standard square lattice.

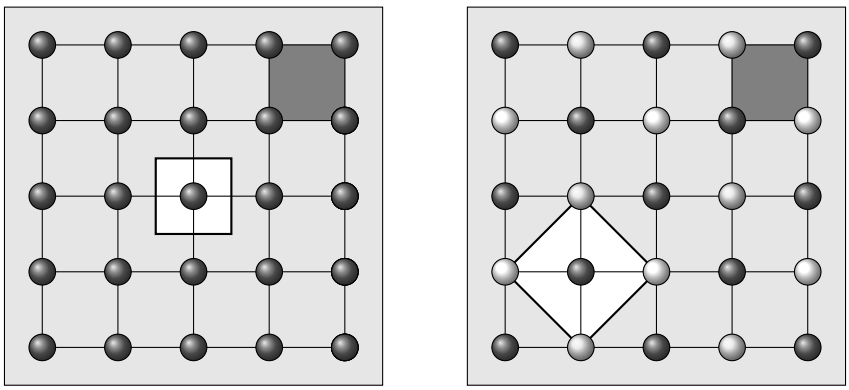

**Figure 2.1:** The unit cell (white) and the smallest lattice plaquette (dark grey) are shown for the regular versus the bipartite two-dimensional square lattice.

### 2.1.2 The reciprocal lattice and the Brillouin zones

That lattices are periodic structures means, from a physicist's point of view, that the resulting equations of motion follow the same periodicity, *i.e.*, the Hamiltonian is also periodic. Hence, one may perform a *Fourier transformation* to simplify such equations-of-motions. By doing so, one changes the domain from real space to *reciprocal space* (or k-space). The Bravais lattice in reciprocal space is called the *reciprocal lattice* and is

defined by a set of wave-vectors

$$\mathbf{G} = m_1\mathbf{b}_1 + m_2\mathbf{b}_2 + m_3\mathbf{b}_3, \tag{2.2}$$

which obey

$$\mathbf{a}_i \cdot \mathbf{b}_j = 2\pi\,\delta_{ij}, \tag{2.3}$$

Hence, when the periodicity of the real space lattice is $\mathbf{d}$, the periodicity of the reciprocal lattice must be $\mathbf{Q} = (\frac{2\pi}{a_1}, \frac{2\pi}{a_2}, \frac{2\pi}{a_3})$. In reciprocal space, the first *Brillouin zone* is a uniquely defined primitive cell. In the same way, as a Bravais lattice can be built up by the Wigner–Seitz cells in real space, the reciprocal lattice can be divided into cells by the first Brillouin zone. If the unit cell in real space is doubled, the corresponding unit cell in $k$-space is halved in size.

## 2.2 The Bloch theorem

The first Brillouin zone is important when it comes to *Bloch's theorem*. If we consider the *Schrödinger equation* for a periodic potential

$$\hat{H}\Psi(\mathbf{x}) = \left(-\frac{\hbar^2}{2m}\nabla^2 + V(\mathbf{x})\right)\Psi(\mathbf{x}) = E\Psi(\mathbf{x}), \tag{2.4}$$

where, $m$ is the mass of the atom, and $V(\mathbf{r}) = V(\mathbf{r}+\mathbf{d})$ is a periodic potential with a period $\mathbf{d}$. The *Bloch theorem* [14–16] states that the solutions to this equation will be given by the *Bloch functions* which have the form

$$\Psi_{\nu,\mathbf{q}}(\mathbf{x}) = e^{i\mathbf{q}\cdot\mathbf{x}}u_{\nu,\mathbf{q}}(\mathbf{x}). \tag{2.5}$$

Here, $u_{\nu,\mathbf{q}}(\mathbf{x})$ has the same periodicity as the lattice. The index $\mathbf{q}$ is the *crystal quasi-momentum* and is confined to the first *Brillouin zone*, while the index $\nu$ is the *band index* and appears because for each given $\mathbf{q}$ there will be many solutions, also called bands. Both $\mathbf{q}$ and $\nu$ are good quantum numbers. The energy associated with such a pair $E^{\nu}(\mathbf{q})$ is also confined to the first Brillouin zone $\mathbf{Q}$.

When evaluating the energy bands, one is often interested in finding the minima and maxima of each band. Often, the energy band's minima and maxima are located at the $\Gamma$-point (the centre of the Brillouin zone), the $M$-point (the centre of the edge), or at the $K$-point (the corner of the edges).

## 2.3 A note about symmetries

The geometrical regularity of crystals digs deeper than the question of translational invariance. It is also a question about the geometric transformations (such as rotations around an axis) one can perform that leave the appearance of the crystal unchanged or phrased differently depending on what inherent symmetries the crystal posses. The different kinds of symmetries the lattice may possess are listed below [14; 15]

- **Reflection**: mirrors the lattice across a reflection plane.
- **Rotation**: rotates the lattice with an angle $\alpha$ around some axis. In two and three-dimensional lattices, the rotations are limited to two-, three-, four-, and six-fold to preserve translational invariance. However, quasicrystals can have other rotational symmetries, such as five- or eight-fold [17; 18];
- **Inversion**: changes the sign of all coordinates of each lattice point with respect to an inversion point.
- **Improper rotation**: rotate the lattice around an axis followed by an inversion.

While all lattices have translational symmetry in all dimensions, not all lattices have all other symmetries. If a lattice has a given symmetry, performing the related symmetry operations on the lattice leaves the lattice unchanged. A complete classification of a crystal requires that all such symmetries are identified. To determine a lattice's symmetry, one can look at its Bravais lattice and its unit cell. The Bravais lattice exhibits all the symmetries the lattice may have, and then one can check if the unit cell exhibits these symmetries or not. It is not a requirement for a lattice to possess any symmetries beyond translational invariance, it may, in many situations, simplify equations of motion.

## 2.4 Quantum simulations in exotic lattices

Lattice systems where we can control the geometry and couplings between lattice sites can provide a route to realising a quantum simulator. It allows us both a method to design systems that may host a frustrated phase and a way to create systems with a state space that grows exponentially.

In this thesis, you will encounter examples of both types of lattice systems. In Part 2, we study *Ultracold atoms in optical lattice systems*

which are quantum many-body systems which may host a frustrated phase. In Part 3, we study *Fock state lattices* where one of the purposes is to see if they can be used to design systems with an exponentially growing state space lattice.

We call these types of lattice systems exotic. They are exotic as they do not occur naturally in nature and as they may be used to realise quantum simulators or *A quantum for a quantum.*

Optical lattices are lattices made out of light, with the ability to tune parameters in the experimental set-ups such that a large variety of lattices can be realised. As we shall discuss later, ultra-cold atoms trapped in such lattices offer a clean, controllable way of realising Bose–Hubbard models [19; 20]. Such a system possesses the periodicity required by a lattice, and it can be made large enough such that the physical characteristic of a periodic system is manifested, just as the real crystal can. Hence, we may treat it as if it was translational invariant to extract the relevant properties, just as we may treat the crystal lattice.

Exotic lattice-like structures also arise if we consider state space instead of real space. State-space lattices are lattice-like structures where the states of a physical system are the lattice points or vertices, and the coupling between different states are the edges or connections between these vertices. The state space lattice is not uniquely defined by the Hamiltonian. It depends on the basis chosen, and the systems we encounter in Part 3 are all that we call Fock-state lattices, indicating these lattice structures live in the Fock-space. As the strength of the coupling between two states will depend on the number of particles in the state, state space lattice-like structures are **not** translational invariant. However, the emerging structures are lattice-like, meaning they look like lattices. Viewing them as lattices will provide new insights and enhance our understanding of the corresponding physical system.

# 3. One, two, or many

This thesis centres around different many-body, interacting and non-interacting quantum lattice systems. The tradition in condensed matter physics is only to call interacting systems many-body systems. This convention is due to the non-interacting many-body Hamiltonian being quadratic. Thus, it is enough to solve it for a single particle. However, we shall in the following refer to **both** the interacting and non-interacting cases when speaking about many-body systems.

To understand how many-body quantum systems behave, one needs to understand how the behaviour of quantum systems differs from one of the classical systems. This chapter starts with a brief recap of basic quantum mechanics for single particles. We then turn to the Schrödinger equation for many-particle systems, and it becomes clear why a *first quantization* approach is unsuitable for many-particle systems. Thus, *Second quantization* is introduced, and we rewrite the many-particle Hamiltonian with this formalism. Finally, the chapter concludes with a discussion of how to solve many-body quantum systems. Here the connection between many-body quantum lattice systems and the possible realisation of quantum simulators becomes apparent.

## 3.1 Quantum mechanics 101

In the quantum realm, we describe the systems we are interested in by their wave-function $\Psi$. We are typically interested in the stationary properties of the ground state and how the system's states change over time. In quantum mechanics, Schrödinger's equations play a similar role to Newton's second law for classical systems, and it is natural to take it as our starting point. In its most general form, one can write Schrödinger's equation as

$$i\hbar\frac{d}{dt}\Psi(\mathbf{x},t) = \hat{H}\Psi(\mathbf{x},t), \tag{3.1}$$

where $\hat{H}$ is the Hamiltonian operator and $\Psi(\mathbf{x},t)$ is the wave-function. Like its classical counterpart, the Hamiltonian expresses the total energy

of the system and will, in most cases, contain both a kinetic and a potential part. For a single particle, the Hamiltonian can be written as

$$\hat{H} = \left( -\frac{\hbar}{2m}\nabla_i^2 + V(\mathbf{x}_i, t) \right). \tag{3.2}$$

Here, both the kinetic and the potential terms describe the energy of a single particle. However, for a many-body system, the potential term may also include interaction terms between two or more particles. Thus it will, in many situations, be more convenient to write the expression for the Hamiltonian as

$$\hat{H} = \hat{H}_0 + \hat{H}_I, \tag{3.3}$$

where $H_0$ now is the single-particle contributions to the Hamiltonian and $\hat{H}_I$ are the many-body contributions. For an $N$-particle system, we may write the single-particle contributions as

$$\hat{H}_0 = \sum_i^N \hat{h}(\mathbf{x}_i, t), \qquad \hat{h}(\mathbf{x}_i, t) = \left( -\frac{\hbar}{2m}\nabla^2 + V(\mathbf{x}, t) \right) \tag{3.4}$$

and where

$$\hat{H}_I = \hat{V}(\mathbf{x}_1, \mathbf{x}_2, \cdots, \mathbf{x}_n, t) \tag{3.5}$$

The expression 3.5 captures all interaction terms between particles in the system. However, it is unnecessary to include interaction terms to see how single-particle and many-body systems differ. Without the interaction term, the Schrödinger equation in 3.1 becomes separable and reduces to the eigenvalue equation

$$\hat{H}\,|\Psi\rangle = E\,|\Psi\rangle\,, \tag{3.6}$$

where the solution comes in the form of the stationary eigenstates $|\psi_k\rangle$ with corresponding eigenvalues $E_k$. At first glance, it seems straightforward to expand this to the case of many identical particles. However, there is an important difference between identical classical and quantum particles. While for identical classical particles, at least in theory, it is possible to label them in such a way that one can tell them apart, it is not the case for quantum particles. Here, identical means that all the intrinsic physical properties of the particles are the same, and the particles are not only identical but also indistinguishable. Hence the wave function for the full N-particle quantum system must obey

$$\begin{aligned} \Psi(\mathbf{x}_1, \ldots, \mathbf{x}_j, \ldots, \mathbf{x}_k, \ldots, \mathbf{x}_N) &= \lambda\Psi(\mathbf{x}_1, \ldots, \mathbf{x}_k, \ldots, \mathbf{x}_j, \ldots, \mathbf{x}_N), \\ &= \lambda^2\Psi(\mathbf{x}_1, \ldots, \mathbf{x}_l, \ldots, \mathbf{x}_k, \ldots, \mathbf{x}_N), \end{aligned} \tag{3.7}$$

such that $\lambda^2 = 1$. This condition allows for two kinds of quantum particles bosons and fermions. For bosons, the wave function is symmetric and thus remains unchanged under a permutation of two particles, $\Psi \xrightarrow{P} \Psi$. Contrary, fermions have antisymmetric wave functions meaning that a permutation of two particles changes the sign of the wave function $\Psi \xrightarrow{P} -\Psi$. While we can construct the proper symmetric or antisymmetric $N$ particle wave function from the single-particle wave functions, it quickly becomes tedious as $N$ grows large. To account for all possible permutations of two particles - and ensure that the overall wave function is symmetric or antisymmetric, one will have to include $N!$ terms in the expression. Even without any potential term, the large number of terms contributing to the wave function makes it infeasible to address many-body systems in such a manner. With the inclusion of potential, it would only become more complicated. While this should be enough to make us search for another approach, it is important to stress that there is another reason that this approach is unsuitable. It is not only that the calculations become tedious when the number $N$ grows large, but it is also that they depend explicitly on the actual $N$. The wave function and any operator working on such a wave function will depend on the number of particles. If we were to change the number of particles from 100 to 101, we would have to redo all derivations. Hence what we search for is a formulation of quantum mechanics where

1. symmetrisation and anti-symmetrisation are intrinsically built into the formalism

2. the description of the system does not depend explicitly on the number of particles $N$.

As it turns out, this is what second quantization, also called occupation number representation, does the trick.

## 3.2 Second quantization

In second quantization, the indistinguishability of the particles is used as an advantage. Instead of asking what the state of each particle is, one asks how many particles there are in a given state $\nu$ [21]. For a $N$ particle system, the basis states for the full system are thus given in terms of occupation numbers of each available single-particle state

$$|\Psi_N\rangle = |n_{\nu_1}, n_{\nu_2}, n_{\nu_3}, \ldots\rangle\,, \quad \sum_j n_{\nu_j} = N. \tag{3.8}$$

Defining the occupation number operator $\hat{n}_{\nu_j}$ which has the the basis states $|n_{\nu_j}\rangle$ as its eigenstates and the occupation number $n_{\nu_j}$ as it is eigenvalues, we note that the $n_{\nu_j}$ must obey

$$n_{\nu_j} = \begin{cases} 0,1 & \text{for fermions,} \\ 0,1,2,\ldots & \text{for bosons,} \end{cases} \tag{3.9}$$

Looking at the expression for the many-body state in eq. 3.8 a natural question is how does one transform these states as the many-body states are expressed in terms of occupation numbers of the single-particle states. For an intuitive way of viewing this, we can think of the operators in terms of which single-particle states they create or annihilate. We, therefore, introduce the annihilation $\hat{a}$ and creation $\hat{a}^\dagger$ operators that act on many-body states in the following way.

$$\begin{aligned} \hat{a}_j^\dagger |n_1, n_2, \ldots, n_j, \ldots\rangle &= A^+(n_j) |n_1, n_2, \ldots, n_{j+1}, \ldots\rangle, \\ \hat{a}_j |n_1, n_2, \ldots, n_j, \ldots\rangle &= A^-(n_j) |n_1, n_2, \ldots, n_{j-1}, \ldots\rangle, \end{aligned} \tag{3.10}$$

where $A^\pm(n_j)$ are normalisation constants to be determined. To do so, it is, however, necessary to treat bosons and fermions separately.

### 3.2.1 The difference between fermions and bosons

The normalisation constants $A^\pm(n_j)$ depend on whether we are dealing with bosons or fermions, as their respective commutation relations between the annihilation and creation operators are different. For bosons, this means that the creation and annihilation operators must satisfy the following commutation relations

$$\left[\hat{b}_{\nu_j}, \hat{b}_{\nu_k}\right] = 0, \quad \left[\hat{b}^\dagger_{\nu_j}, \hat{b}^\dagger_{\nu_k}\right] = 0, \quad \left[\hat{b}_{\nu_j}, \hat{b}^\dagger_{\nu_k}\right] = \delta_{\nu_j,\nu_k}, \tag{3.11}$$

which leads to the normalisation constants being

$$B^+(n_{\nu_j}) = \sqrt{n_{\nu_j} + 1}, \qquad B^-(n_{\nu_j}) = \sqrt{n_{\nu_j}}. \tag{3.12}$$

For fermions, we have that the annihilation and creation operators must obey the anti-commutation relations

$$\left\{\hat{c}_{\nu_j}, \hat{c}_{\nu_k}\right\} = 0, \quad \left\{\hat{c}^\dagger_{\nu_j}, \hat{c}^\dagger_{\nu_k}\right\} = 0, \quad \left\{\hat{c}_{\nu_j}, \hat{c}^\dagger_{\nu_k}\right\} = \delta_{\nu_j,\nu_k}. \tag{3.13}$$

This ensures that $(\hat{c}^\dagger_{\nu_j})^2 = 0$ and similarly $(\hat{c}_{\nu_j})^2 = 0$, such that two fermions cannot occupy the same state.

## 3.3 Fock space and Fock states

Let $|\Psi_N^\Lambda\rangle$ be an eigenstate of the $N$ particle system, where $\Lambda$ denotes the degrees-of-freedom, such as boson or fermion modes, available for the individual particles in the system to occupy. Note that this for a fermion system means that the number of degrees-of-freedoms must fulfil $\Lambda \geq N$. We shall use the notation $\mathcal{H}^\Lambda$ to denote the Hilbert space for a single-particle state that can occupy any of these $\Lambda$ modes. Hence, one should note that $\Lambda$ is the dimension of this single-particle Hilbert space. We are interested in many-body systems, and **not** only in the single-particle Hilbert space but also in the Hilbert space where the many-body states $|\Psi_N^\Lambda\rangle$ live. Recalling that the many-body eigenstate is nothing but a properly symmetrised or anti-symmetrised product state of single-particle states, it must thus live in a Hilbert space of the form

$$\mathcal{F}_N^\Lambda = \mathcal{S}_\nu H_\Lambda^{\otimes N}, \tag{3.14}$$

where $H_\Lambda^{\otimes N}$ is the direct product of $N$ single-particle Hilbert spaces $\mathcal{H}_\Lambda$ and $\mathcal{S}_\nu$, is the operator that symmetrises or antisymmeterises the many-body state. When the number of particles is unknown or when it may fluctuate, the systems' Hamiltonian includes terms that either create or annihilate single particles. Hence, this will connect two Hilbert spaces of the form given in eq. (3.14) through

$$\begin{aligned} \hat{a}_\nu^\dagger &: \mathcal{H}_N^\Lambda \to \mathcal{H}_{N+1}^\Lambda, \\ \hat{a}_\nu &: \mathcal{H}_N^\Lambda \to \mathcal{H}_{N-1}^\Lambda, \end{aligned} \tag{3.15}$$

full Hilbert space will thus be another direct product of subspaces of the form given above, such that it takes the form

$$\mathcal{F}^\Lambda = \bigotimes_i^\infty \mathcal{F}_i^\Lambda. \tag{3.16}$$

Here the index $i$ labels the number of particles in the system. When the number of modes available for the single-particle to occupy is infinite, the expression above is usually written as

$$\mathcal{F} = \bigotimes_i^\infty \mathcal{F}_i. \tag{3.17}$$

Those familiar with the topic of many-particle physics will recognise this as the *Fock-space*. However, throughout this thesis, we shall use this name to include Hilbert spaces on the form given in eq. (3.16). While

the traditional Fock space $\mathcal{F}$ is infinite-dimensional, it should be noted that $\mathcal{F}^{\Lambda}$ has a dimension smaller or equal than $|\Lambda|$. When all available modes are boson, when the number of particles is allowed to fluctuate, the dimension is $\Lambda$. At the same time, when the number of particles is held fixed, the dimension will be $(\Lambda - 1)$, as fixing the number of particles removes symmetry and thus reduces the number of dimensions by 1.

### 3.3.1 Mixture of particle types

Finally, we may expand the notation introduced above to include systems that consist of a mixture of particle types, such as boson-fermion mixtures of spin and boson states. In this case, the mixed Fock space is a product space of the two respective subspaces; the spin Fock space $\mathcal{F}_S$ and the boson Fock space $\mathcal{F}_B$

$$\mathcal{F}_{mix} = \mathcal{F}_S \otimes \mathcal{F}_B, \tag{3.18}$$

## 3.4 The many-body Hamiltonian

We now return to eq. 3.3 to provide a recipe for how one is to express the many-body Hamiltonian in the language of second quantization. First, we stress that a many-body Hamiltonian in the context of this thesis is simply a Hamiltonian for a many-body system. This Hamiltonian may or may not include interaction terms. In eq. 3.3 the many-body Hamiltonian had already been divided into a single-particle part $\hat{H}_0$ and a many-body part $\hat{H}_I$. Single-particle operators such as the $\hat{H}_0$ defined in eq. 3.1 can in first quantization be written as a sum of terms that only concern the coordinates of a single particle. However, moving to second quantization formalism makes us think in terms of the occupation number basis. Here, single-particle contributions to the Hamiltonian must come in the form of an operator that contains one annihilation and one creation operator. Thus, we also have a recipe for how to think about many-body contributions. Rather than considering how the individual particles are affected, we should consider how many particles are involved in the interaction. Thus the interaction part of the Hamiltonian will be split into two bodies, three bodies, and so on contributions. For the work presented in this thesis, two-body contributions are the only relevant many-body contributions, and we shall ignore higher-order contributions from here on. But it is important to stress that such contributions can be included using the same approach. The translation of one and two body operators from first quantization to second quantization can be

expressed as

$$\begin{aligned}\hat{H}_0 &= \sum_{i=1}^{N} \hat{h}(\mathbf{x}_i) \Rightarrow \sum_{\alpha,\beta} \langle \alpha | \hat{h} | \beta \rangle \hat{a}_\alpha^\dagger \hat{a}_\beta, \\ J_\beta^\alpha &= \langle \alpha | \hat{h} | \beta \rangle \int d\mathbf{x} \phi_\alpha^*(\mathbf{x}) \hat{h}(\mathbf{x}) \phi_\beta(\mathbf{x}),\end{aligned} \tag{3.19}$$

and

$$\hat{H}_I = \sum_{i,j=1, i\neq j}^{N} \hat{v}(\mathbf{x}_i, \mathbf{x}_j) \Rightarrow \sum_{\alpha,\beta,\gamma,\delta} \langle \alpha\beta | \hat{v} | \gamma\delta \rangle \hat{a}_\alpha^\dagger \hat{a}_\beta^\dagger \hat{a}_\gamma \hat{a}_\delta, \tag{3.20}$$

with

$$J_{\gamma\delta}^{\alpha\beta} = \langle \alpha, \beta | \hat{v} | \gamma, \delta \rangle = \int d\mathbf{x} d\mathbf{x}' \phi_\alpha^*(\mathbf{x}) \phi_\beta^*(\mathbf{x}) \hat{v}(\mathbf{x}, \mathbf{x}') \phi_\gamma(\mathbf{x}') \phi_\delta(\mathbf{x}'), \tag{3.21}$$

and thus, the many-body Hamiltonian may be expressed as

$$\hat{H} = \sum_{\alpha,\beta} J_\beta^\alpha \hat{a}_\alpha^\dagger \hat{a}_\beta + \frac{1}{2} \sum_{\alpha,\beta,\gamma,\delta} U_{\gamma\delta}^{\alpha\beta} \hat{a}_\alpha^\dagger \hat{a}_\beta^\dagger \hat{a}_\gamma \hat{a}_\delta. \tag{3.22}$$

### 3.4.1 The quadratic many-body Hamiltonians

We turn to the question of how to solve many-body Hamiltonians, which means how one can find their eigenvalues. For one-body Hamiltonians, this is straightforward. Consider a diagonal Hamiltonian

$$\hat{H} = \sum_\alpha J^\alpha \hat{a}_\alpha^\dagger \hat{a}_\alpha \tag{3.23}$$

here the eigenvalues will be $J^\alpha$. Any other one body Hamiltonians can be expressed as

$$\hat{H} = \sum_{\alpha,\beta} \left( J_\beta^\alpha \hat{a}_\alpha^\dagger \hat{a}_\beta + K_\alpha^\beta \hat{a}_\alpha^\dagger \hat{a}_\beta^\dagger + h.c. \right). \tag{3.24}$$

Thus, such Hamiltonians can be diagonalised by a Bogoliubov transformation [21], and one can also find the eigenvalues for these Hamiltonians. However, when we include many-body terms, we can no longer write the Hamiltonian on matrix form in terms of the single-particle states.

### 3.4.2 Non-quadratic many-body Hamiltonians

When it comes to the interaction terms for many-body Hamiltonians, it often contributes on the form

$$\hat{H}_I = \frac{1}{2} \sum_{\alpha,\beta,\gamma,\delta} U_{\gamma\delta}^{\alpha\beta} \hat{a}_\alpha^\dagger \hat{a}_\beta^\dagger \hat{a}_\gamma \hat{a}_\delta. \tag{3.25}$$

Such terms can, in general, not be put on a matrix form; hence, we cannot express the Hamiltonian on the quadratic form given eq. 3.24. Thus, we cannot find the energy spectrum analytically and will instead have to use numerical methods. Such methods are approximations, and while they are often a great place to start, we are not always able to fully understand the systems.

## 3.5 Towards quantum simulators

While quantum particles entangle even for non-interacting systems, it is the interactions that cause the correlations that make it necessary to study some systems with quantum simulators. Interactions in themselves are, however, not always not enough.

For the Hamiltonian in eq. 3.22, we see that it has a quadratic and a non-quadratic term. For the optical lattice systems, we are about to meet the quadratic part that comes from tunnelling processes and the non-quadratic part from onsite interactions. Though we have both quadratic and non-quadratic contributions to the Hamiltonian, it does not mean that we always have quantum systems where the correlations between the particles dominate their behaviour. For the optical lattice systems, the Hamiltonian in eq. 3.22 has two interesting limits, one where tunnelling dominate and one where onsite interaction does. The system is said to be in the *superfluid* limit in the first limit. Here, tunnelling processes dominate over onsite interactions, thereby suppressing quantum correlations, and we can thus describe the system's behaviour using a mean-field approach.

While it is in the other limit that the lattice system potentially hosts a frustrated phase, the superfluid limit is still interesting. Of course, in its own right, as interesting physics may happen in this limit, but also in the context of quantum simulators. Here, it can provide a limit where we understand the behaviour of the system without studying it using a quantum simulator.

# Part II

# Ultra cold atoms ins optical lattices

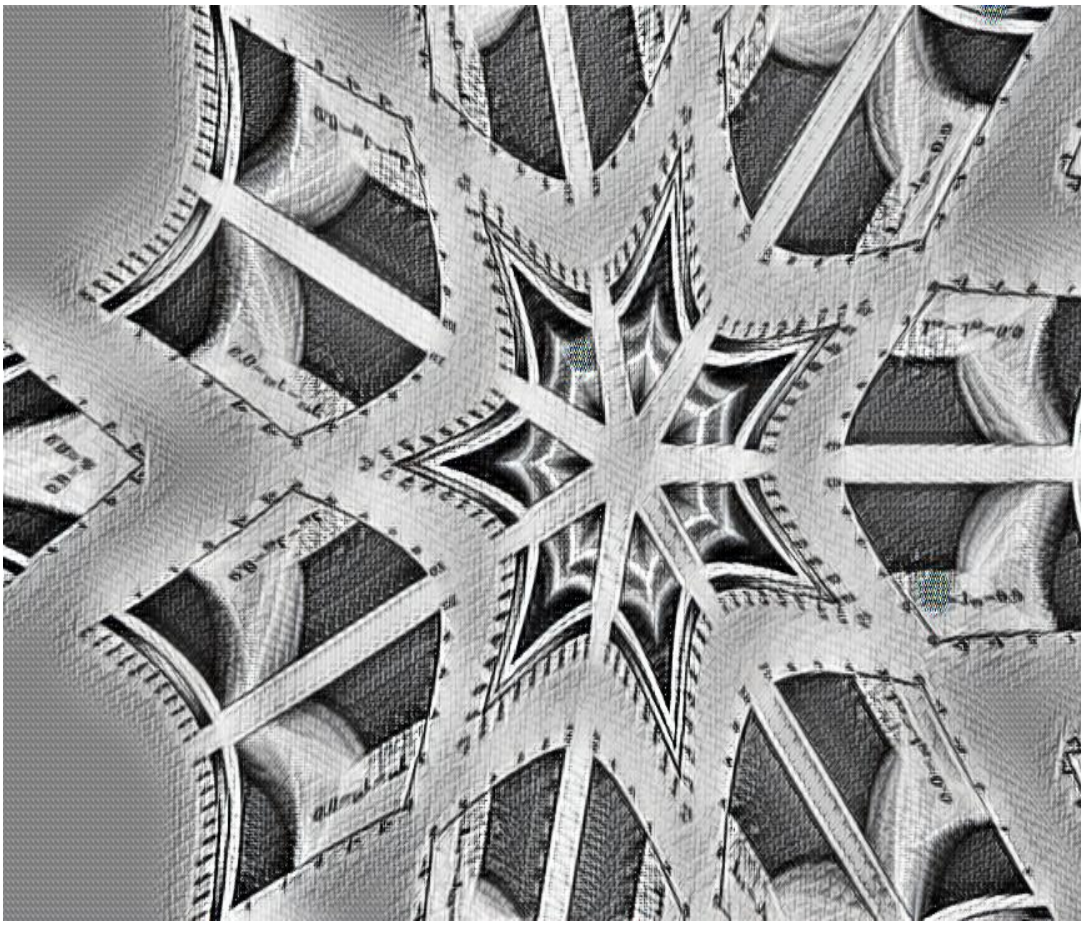

# 4. Ultracold atoms in optical lattices

Ultracold atoms in optical lattices are exotic lattice systems made by loading ultracold atoms into optical lattices. Such systems have two key ingredients, the optical lattice and the atoms. The optical lattice is a lattice made of light. It is a periodic potential created by counter-propagating laser beams (see fig. 4.1). The interference between these laser beams results in an optical standing wave, and when atoms are trapped in their potential wells, it forms a crystal-like structure. The combined system of atoms and the optical lattice thus form an artificial crystal - allowing us to treat the atoms in it as we would have treated electrons in a real crystal. There exists many good introductions to the topic of ultracold atoms in optical lattices and readers in more details are referred to [19; 22; 23].

Through the laser beams, one controls the geometrical structure of the lattice and the depth of the potentials. In this part of the thesis, we focus on how bipartite optical lattice systems provide a route for realising coupling-induced frustration in both the classical and quantum limit. In particular, we study the *s*-*s* and the *s*-*p* bipartite lattice. Before exploring these two systems, we need a theoretical understanding of ultra-cold atoms in optical lattices. To get the first crude idea about how atoms placed in an optical lattice behave, we first explore the behaviour of a two-level atom placed in an electrical field. Then an introduction to optical lattices follows before we look at a single particle in a periodic lattice. This chapter introduces several approximations related to the depth of the lattice potential. When these are valid, the atoms in the optical lattice can be described by the many-body Bose-Hubbard models discussed in the previous chapter. We then analyze the behaviour of such Bose-Hubbard models in *superfluid phase* and the *Mott insulating phase*.

Thus, the chapter focuses on developing the theoretical machinery for studying ultracold atoms in optical lattices and outlining how such systems may be used to realise interesting phases of quantum matter.

## 4.1 The two-level atom

To understand how atoms behave in an optical lattice, we first consider the *two-level atom*. At this level, the Hamiltonian can be written as

$$H_{\mathrm{A}} = E_g \left|g\right\rangle \left\langle g\right| + E_e \left|e\right\rangle \left\langle e\right|, \tag{4.1}$$

where $|g\rangle$ and $|e\rangle$ are the internal ground and excited states of the atom, and $E_g$ and $E_e$ the corresponding electronic energies. If such an atom is then placed in an electric field, it will typically be subject to a dipole coupling with the field. This coupling, in return, gives rise to an interaction term in the Hamiltonian, which can be expressed as

$$H_{\mathrm{I}} = -e\vec{r}\cdot\vec{E_0}\cos\left(\omega_L t\right), \tag{4.2}$$

where $e\vec{r}$ is the electric dipole moment, $\vec{E_0}$ is the electric field, and $\omega_L$ is the driving frequency of the laser. Due to parity rules $\langle g|\,\vec{r}\,|g\rangle = \langle e|\,\vec{r}\,|e\rangle = 0$. Labeling the *Rabi frequency* $\Omega = \frac{\vec{E_0}}{\hbar}\langle g|\,e\vec{r}\,|e\rangle$ the full Hamiltonian can be expressed on matrix form, in the $|g\rangle$ and $|e\rangle$ basis and up to an overall energy shift, as

$$H = H_{\mathrm{A}} + H_{\mathrm{I}} = \hbar \begin{bmatrix} -\omega_0/2 & \Omega\cos(\omega_L t) \\ \Omega^* \cos(\omega_L t) & \omega_0/2 \end{bmatrix}, \tag{4.3}$$

where $\omega_0 = E_e - E_g$.

### 4.1.1 On and off-resonance

The relative strength between $\omega_0$ and $\omega_L$ controls the system at large. There are two limits of interest, *on resonance* and *off-resonance*. When $\omega_0 \approx \omega_L$, the system is close to resonance. Here, the dipole coupling between the atom and the laser can be used to drive the atom into the excited state. The atoms in their excited states are exposed to spontaneous emission processes and losses; hence, decoherence cannot be ignored, so this is not the limit for implementing optical lattices. Nevertheless, this limit is still relevant in a broader context of cold atomic experiments. In particular, in a set-up where all the atoms initially are in the ground state, then a $\pi$-pulse is the cable of exciting the entire population to the excited state. In other words, the on-resonant lasers can be used to manipulate the internal atomic states.

In the other limit, when $|\omega_0 - \omega_L| \gg \omega_0, \omega_L$, the system is operating a far off-resonance regime. Defining the detuning of the laser with respect to the atomic transition as $\Delta = \omega_0 - \omega_l$ we can express the effective

Hamiltonian, in the *rotating wave-approximation* (RWA), with respect to the light field as

$$H = \frac{\hbar}{2}\begin{bmatrix} \Delta & 2\Omega \\ 2\Omega^* & -\Delta \end{bmatrix}. \tag{4.4}$$

This Hamiltonian is static, meaning it does not explicitly depend on the time $t$. Furthermore, if we tune the laser such that $\Delta \gg \Omega$ the Hamiltonian becomes approximately diagonal in the original basis of $|g\rangle$ and $|e\rangle$. This regime is called the large detuned limit, and we shall return to it in more detail later in this chapter. Including first-order corrections due to the atom-light interaction, one finds the energies of the ground and excited states to be

$$\varepsilon_g = -\frac{\hbar\omega_0}{2} + \frac{\hbar\left|\Omega\right|^2}{4\left(\omega_0 - \omega_L\right)}, \tag{4.5}$$

$$\varepsilon_e = +\frac{\hbar\omega_0}{2} - \frac{\hbar\left|\Omega\right|^2}{4\left(\omega_0 - \omega_L\right)}. \tag{4.6}$$

With the atom-light interaction, we have thus created a conservative potential with the shifts of the atomic energy levels, so-called *Stark shifts*. Since $|\Omega|^2 \propto \left|\vec{E_0}\right|^2$ and if $\vec{E_0}$ depends on $\vec{r}$ so does $\Omega$. If the intensity of the potential varies spatially, it will be energetically favourable for an atom experiencing to localise at the minima [24].

## 4.2 The optical lattice

The optical lattice is, in essence, an electric field with spatial periodicity. The atoms experience this field as a potential. Shaping such potentials as the potentials in crystal lattices allows one to form artificial lattices, with all the symmetries of the Bravais lattices we discussed in Chapter 2. One may even configure quasi-periodic lattice structures as well [25]. In fig. 4.1(a), a graphical representation of the principles behind an optical square lattice in two dimensions is shown. Here the top figure shows a gas of ultra-cold atoms being subject to four laser beams, while the lower one shows how the shape of the lattice potential may look. Fig. 4.1(b) shows how the lattice potential mimics that of a crystal lattice potential. Here, the top figure shows a cartoon representation of how the lattice potential from fig. 4.1(a) may trap atoms at the minima of the potential created by the lasers. In a regular crystal, the potential is instead created by ions, thereby trapping electrons at the potential minima. Thus,

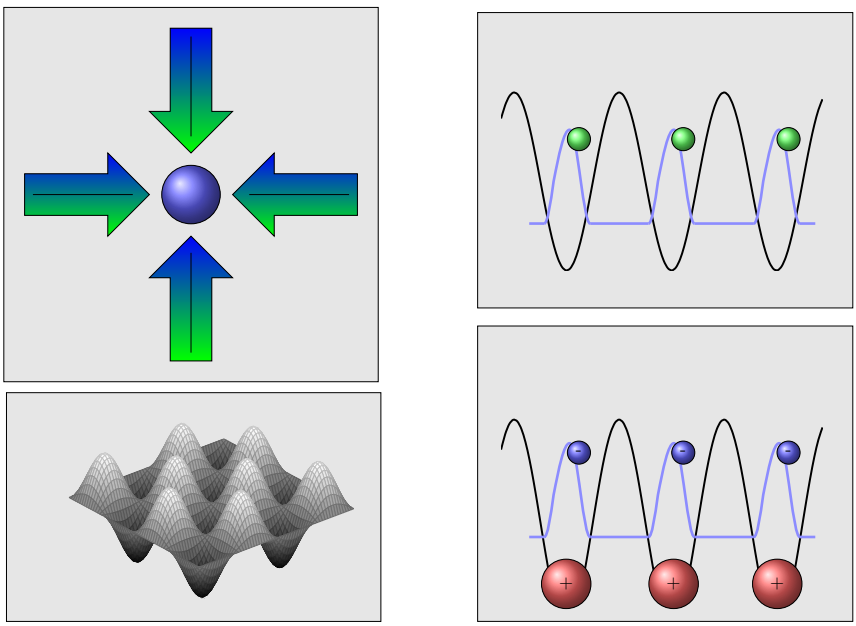


**Figure 4.1:** The principles behind the optical lattice are shown in (a). Here, the upper figure schematically shows how a gas of ultracold atoms is trapped by counter-propagating laser beams, whereas the lower figure shows how such a lattice potential can look. In (b) the upper figure, the black line shows a one-dimensional cut of the two-dimensional lattice potential shown in (a). Here, one sees how the atoms are trapped at the potential minima. In the lower figure (b), a schematic representation of a regular crystal is given as a comparison. Here, it is instead the ions at the lattice sites that create the potential, thereby trapping the electrons.

by comparing the upper and lower fig. 4.1(b), one sees how the artificial crystal systems of ultracold atoms mimic regular crystals. By changing the angle between the laser beams or by adding extra, one may change the lattice geometry. By varying the beams' intensity, the lattice's depth may be tuned. Thus, we are provided with a means to study the behaviour of periodic models similar to those found in condensed matter systems with control that would otherwise not be accessible.

## 4.3 A single particle in a periodic lattice

The first step towards describing a gas of ultracold atoms in an optical lattice is returning to the discussion of the single particle we started in Chapter 3. This time we will assume that it is subject to a periodic potential. The Schrödinger equation takes the form

$$\hat{H}\Psi(\mathbf{x}) = \left(-\frac{\hbar^2}{2m}\nabla^2 + V(\mathbf{x})\right)\Psi(\mathbf{x}) = E\Psi(\mathbf{x}). \tag{4.7}$$

Here, $m$ is the mass of the atom, and $V(\mathbf{x}) = V(\mathbf{x}+\mathbf{d})$ is a periodic potential with periodicity $\mathbf{d}$. From the *Bloch theorem* [14–16] we know that the solutions to this equation will be given by the *Bloch functions* which have the form

$$\Psi_{\nu,\mathbf{q}}(\mathbf{x}) = e^{i\mathbf{q}\cdot\mathbf{x}}u_{\nu,\mathbf{q}}(\mathbf{x}), \tag{4.8}$$

where $u_{\nu,\mathbf{q}}(\mathbf{x})$ has the same periodicity as the lattice. The index $\mathbf{q}$ is the crystal *quasi-momen*tum and is confined to the first Brillouin zone, while the index $\nu$ is the *band index* and appears because for each given $\mathbf{q}$ there will be many solutions, the so-called *bands*. They are both good quantum numbers. The energy associated with such a pair $E^{\nu}(\mathbf{q})$ is also periodic, this time with the periodicity of the Brillouin zone.

### 4.3.1 The square lattice

We now zoom in on an actual lattice, namely the square lattice shown in fig. 4.1a. Here, the lattice potential can be expressed as

$$V(x,y) = V_x \sin^2(k_x x) + V_y \sin^2(k_y y), \tag{4.9}$$

where for $\alpha \in \{x, y\}$, $V_\alpha$ denotes the potential amplitudes and $k_\alpha$ the wave-vectors in the same direction, and the square of the sin-functions

derives from the $|\Omega|^2$ terms in (4.5). Thus the Schrödinger equation in (4.7) can be written as

$$\left(-\frac{\hbar^2}{2m}\partial_x^2 + V_x \sin^2(k_x x) - \frac{\hbar^2}{2m}\partial_y^2 + V_y \sin^2(k_y y)\right)\Psi(x,y) = (E_x + E_y)\Psi(x,y). \tag{4.10}$$

Since the Hamiltonian is separable, we can find the solutions to it by solving for the $x$- and $y$- dependence independently. Here, the shape of the single-bands and the gap between them depends on $V_0$, which allows us to introduce a dimensionless potential amplitude $V_0 = \frac{V_x}{E_R}$ where $E_R$ is the recoil energy

$$E_R(\lambda) = \frac{h^2}{2m\lambda^2}, \tag{4.11}$$

here, $\lambda$ is the wavelength of the laser. The recoil energy provides a natural energy scale for optical lattices; physically, it corresponds to the kinetic energy gained or lost when the atom absorbs/emits a photon to the optical lattice. This connection highlights the crystal-like nature of optical lattices, as the neutral atoms exhibit the same behaviour as electrons in a crystal. In particular, they display the band structure where forbidden gaps separate allowed regions.

### 4.3.2 The harmonic approximation

In fig. 4.2 the band structure of the one-dimensional sinusoidal lattice is shown for different depths of the lattice potential. As $V_0$ increases, the bands become flattered, and the band gaps become larger, *i.e.*, in the limit of an infinitely deep lattice, the bands are completely flat. In this limit, the atoms at a single lattice experience a potential that mimics a harmonic potential. It is legitimate to apply the *harmonic approximation*. The harmonic approximation is nothing more than a Taylor expansion around a single potential minimum of the potential to second order. When this approximation is valid, we may replace the potential with $V_x \propto k_x^2 x^2$ in each spatial direction of the lattice potential. Hence, for the square lattice, the separable Schrödinger equation for the $x$-dependence reduces to

$$H_x\psi(x) = \left(-\frac{\hbar^2}{2m}\partial_x^2 + V_x k_x^2 x^2\right)\psi(x) = E_x\psi(x), \tag{4.12}$$

| $n$ | 0 | 1 | 2 | 3 |
|---|---|---|---|---|
| $H_n(\xi)$ | 1 | $2\xi$ | $4\xi^2-2$ | $8\xi^3-\xi$ |

**Table 4.1:** The table shows the first four Hermite polynomials.

Defining $\xi = \alpha x$ with $\alpha = \left(\frac{2V_x k_x^2 m}{\hbar^2}\right)^{1/4}$. The solutions to eq. (4.12) are on the form

$$\psi_n(z) = \left(\frac{\alpha^2}{\pi}\right)^{1/4} \frac{1}{\sqrt{2^n n!}} H_n(\xi) e^{-\frac{\xi^2}{2}}, \tag{4.13}$$

where $H_n(\xi)$ are the *Hermite polynomials*. The first four are given in table 4.1. If we use the notation $\mathbf{n} = (n_x, n_y)$ then

$$\psi_{\mathbf{n}} = \psi_{n_x}(x)\psi_{n_y}(y), \tag{4.14}$$

such that the groundstate ($\mathbf{n} = 0$) and the excited states ($\mathbf{n} = 1$) takes the form

$$\begin{aligned} \psi_0(x,y) &= \psi_0(x)\psi_0(y), \\ \psi_1(x,y) &= \psi_1(x)\psi_0(y), \\ \psi_1(x,y) &= \psi_0(x)\psi_1(y), \end{aligned} \tag{4.15}$$

and so on for higher $\mathbf{n}$.

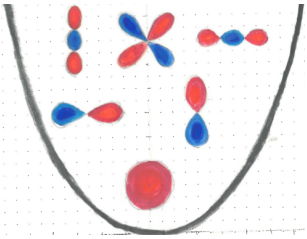

**Figure 4.2:** The shape of the Cartesian form of the *s*-,*p*-, and *d*-orbital states form of the wave-functions that arise from the Harmonic approximation in two dimensions.

### 4.3.3 Orbital states

In optical lattices, the atoms play the role of electrons in a crystal (see fig. 4.1). The atoms used are Alkali metals such as Rubidium which are easy to manipulate and control. Furthermore, as Alkali metals only have

one electron in their outer shell, they are theoretically easy to describe. Recalling that in quantum mechanics, an atomic orbital is a function describing the location and wave-like behaviour of an electron in an atom. Thus, a wave function describing the location of the atoms in the optical lattices is often referred to in the same way - as orbital states. The lowest locally energy eigenstate is labelled the $s$-orbital states, the first excited states as the $p$-orbital states, and so on. Strictly speaking, an $s$-orbital state is not the lowest energy eigenstate. The lowest energy eigenstate is a Bloch state with quasi momentum $q = 0$. However, from the perspective of the dynamics of the system, the $s$-orbital state is the lowest energy eigenstate that the atoms can occupy if the system has any dynamics such as tunnelling and onsite interaction.

We shall label the wave functions by this convention. As we in the following will encounter more situations where the atoms can occupy more than one orbital state, we will, in general, label the wave-function that creates or annihilates an atom in a given orbital state by this orbital state $\alpha$. Similarly, we will introduce an index $i$ to label the lattice site at which an atom is created or annihilated. Thus, we label the full wave-functions $\psi^\dagger_{\alpha_i}$ and $\psi_{\alpha_i}$ respectively.

## 4.4 Wannier functions

The potential given in (4.9) is periodic, but the harmonic one used in (4.12) is not, and therefore neither are the solutions to the Schrödinger equation that it gives rise to. These solutions are localised, highlighting an essential feature of the systems we are studying. When the potential is deep enough and the atoms are allowed to interact, they may localise in the potential wells. Thus, it will be beneficial to describe them in a basis that highlights this rather than in the eigenstate basis provided by the Bloch functions. Rather than replacing the potential with that of a harmonic oscillator, we seek an approach that is also valid when the harmonic approximation is not.

We may define another basis for our systems from the Bloch functions, namely the *Wannier functions* [14]. As the Bloch functions are spatially periodic, one may expand them in terms of a *Fourier series* of plane waves with wave-vectors in the reciprocal lattice. Thus the Bloch functions can be expressed as a sum over a product of a periodic function and plane waves, extending over the whole lattice. The periodic functions make the Bloch functions "modified" plane waves, but in the limit of a vanishing periodic potential, the Bloch functions become true plane waves.

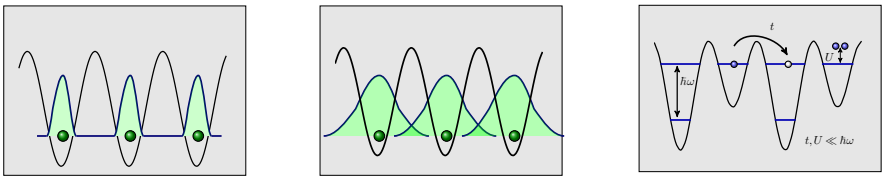


(a) (b) (c)

**Figure 4.3:** A cartoon description of how localised (a) versus delocalised wave functions are distributed in the lattice. In (c) a graphical description of tunneling ($t$), onsite interaction ($U$), and a decay process ($\hbar\omega$) f. The regime we are interested in is when $t, u \ll \hbar\omega$, that is, when tunnelling and onsite interaction dominate over the decay process.

Now, like for plane waves, a Fourier transform of the Bloch functions will generate a localised rather than extended function. This procedure is how the site localised Wannier functions are constructed, *i.e.*, a Fourier-type transformation of the Bloch functions, but where the integration is restricted to the first Brillouin zone.

Thus, we may write

$$\psi^{\nu}_{\mathbf{q}}(\mathbf{x}) = \sum_{\mathbf{R}} f_{\nu}(\mathbf{R}, \mathbf{x}) e^{i\mathbf{R}\cdot\mathbf{q}}, \tag{4.16}$$

where $\mathbf{R}$ is the *Fourier coefficients* $f_{\nu}(\mathbf{R}, \mathbf{x})$ are then found by

$$f_{\nu}(\mathbf{R}, \mathbf{x}) = \frac{1}{V} \int d\mathbf{q} e^{-i\mathbf{R}\cdot\mathbf{q}} \psi^{\nu}_{\mathbf{q}}(\mathbf{x}), \tag{4.17}$$

As a direct unitary transformation relating the two, the Bloch functions and the Wannier functions form two complete bases. Following the above, the Wannier functions are defined as [14; 15]

$$w_{\nu,j}(\mathbf{x}) = \sum_{q} e^{-iqR_j} \Psi_{\nu,q}(\mathbf{x}), \tag{4.18}$$

where $R_j$ labels the coordinates of the $j$, lattice site and the sums run over all quasi momenta.

### 4.4.1 The single particle Hamiltonian revisited

Recalling what we discussed in Chapter 3. We know a straightforward way to express the Hamiltonian in the language of second quantization. Let us consider a 1-dimensional system. Then the field operators, $\hat{\psi}^{\dagger}_{\nu}(x)$

and $\hat{\psi}_\nu(x)$, may be written in the basis of the Wannier functions $w^*_\nu(x - x_j)$ and $w_\nu(x - x_j)$, such that they become

$$\begin{aligned} \hat{\psi}_\nu(x) &= \sum_j w_\nu(x - x_j)\hat{a}_{\nu_j}, \\ \hat{\psi}^\dagger_\nu(x) &= \sum_j w^*_\nu(x - x_j)\hat{a}_{\nu_j}. \end{aligned} \tag{4.19}$$

where $*$ denotes complex conjugation. In this basis the $J^{\nu\nu'}_{i,j}$ becomes

$$J^{\nu\nu'}_{i,j} = \int dx w^{*\nu}(x - x_j)\left(-\frac{\hbar^2}{2m}\frac{\partial^2}{\partial x^2} + V(x)\right) w_{\nu'}(x - x_i), \tag{4.20}$$

such that the Hamiltonian can be written as

$$\hat{H} = \sum_{i,j}\sum_{\nu,\nu'} J^{\nu\nu'}_{i,j}\hat{a}^\dagger_{\nu_j}\hat{a}_{\nu'_i}. \tag{4.21}$$

## 4.5 Deep lattice approximations

As discussed in Chapter 1, approximations play an important role in physics, and the field of ultracold atoms in optical lattices is no exception. In fig. 4.3 one sees a cartoon description of localised versus delocalised wave functions. In the limit where the lattice potential is deep enough, the wave functions can be expressed as Wannier functions. As the lattice potential becomes deeper, the accuracy of the *Harmonic approximation* is improved.

### 4.5.1 The tight-binding approximation

In the limit where one may ignore all other contributions besides onsite interactions and nearest neighbour tunnelling, we have the *tight-binding approximation (TBA)*. Hence, the Hamiltonian in (4.21) reduces to

$$\hat{H} = \sum_{\langle i,j\rangle}\sum_{\nu,\nu'} J^{\nu\nu'}_{i,j}\hat{a}^\dagger_{\nu_j}\hat{a}_{\nu'_i} \tag{4.22}$$

where $\langle i, j\rangle$ means that we are only summing over nearest neighbours. One may relax this approximation step by step to include tunnelling beyond nearest neighbours.

### 4.5.2 The single-band approximation

When the system is cold enough, and the atom-atom interaction is not too strong, bosonic atoms occupy only the lowest energy band. However, if the lattice is deep enough, using various techniques, atoms may be excited to higher orbital states without escaping from the lattice on experimentally relevant time scales. Suppose the energy gap $\delta E$ between two consecutive energy bands is large enough. In that case, such excited states may be stable enough such that decays out of these bands can be suppressed on experimentally relevant time scales. The energy band is not entirely flat except for the limit of infinitely deep lattices. It has a width $\Delta E$. To only occupy the lowest band, then for a given temperature $T$ the thermal energy $k_B T \ll \delta E$, similarly if one includes interactions in the system, then the interaction strength $U$ should also obey, $U < \delta E$ for other bands not to be populated via interactions. Thus, the atoms at the lattice sites can be described in terms of a single (degenerate) energy band. This limit is called the *single-band approximation*. Strictly speaking, all lattice sites host the same orbital state in the single-band approximation. However, we shall use this name slightly broader. We shall also use it to describe the situation where the lattice site hosts two or more orbital states with the exact symmetry - such as when both $p_x$- and $p_y$- orbital states are hosted. Similarly, we also allow that not all lattice sites support the same orbitals, as in the bipartite $s$-$p$ lattice, where the shallow lattice sites host $s$-orbitals while the deep lattice sites host $p$-orbitals.

### 4.5.3 Making a lattice out of approximations

Returning to the lattice potential given in eq. (4.9), we see that this potential is expressed as a function of a continuous variable $\mathbf{x}$. The above discussion highlights that under the right conditions, when the approximations mentioned above become valid, this continuous system behaves as a discrete one, and we may treat it as a lattice model. When the lattice depth increases, we replace the basis of Bloch functions with the basis of Wannier functions as the basis of choice. The single-band approximation is valid when the band gap is tuned such that we may ignore all but one (degenerate) energy band. The tight-binding approximation is valid when the states of the atoms are localised. Then we may assume that only onsite interaction and (a few) nearest neighbour tunnelling will contribute. However, under the right conditions, the system turns into a lattice system, and we may describe it by lattice models such as the (Bose)-Hubbard model [20].

## 4.6 From one to many

A general expression for the Hamiltonian for a gas of $N$ atoms with mass $m$ is

$$\hat{H} = \sum_{i,j}^{N} \left( \frac{p_i^2}{2m} - V_{ext}(\mathbf{r}_i) \right) + V_{\text{int}}\left(\{\mathbf{r}_i, \mathbf{r}_j\}\right). \tag{4.23}$$

The first term gives the individual single-particle contributions, while the second describes the interactions between any two atoms in the gas [13; 21]. The single-particle term has two contributions, the kinetic term and one from an external potential. For an optical lattice experiment, the external lattice potential has two contributions; a lattice potential, which gives the shape of the periodic lattice, and a trapping potential, which prohibits the atoms from escaping the lattice. Compared with the length scales relevant for optical lattices, *i.e.*, the wavelength $\lambda$, the trapping potential can be considered constant, and its contribution to the Hamiltonian will therefore be a local constant energy shift [26; 27]. This approximation is the so-called *local density approximation*, where a constant energy shift acts as a local varying chemical potential that determines the atomic density locally. The gas of atoms in an optical lattice is generally very dilute, and we may continue including only two-body collisions. As the strength of the lattice potential is controllable, we assume a regime in which both the tight-binding and single-band approximation are valid.

### 4.6.1 The Hamiltonian parameters

As the atoms are neutral and occupying low energy states only onsite interactions are included, and hence we replace the interaction in (4.23) by that of a contact interaction $V_{\text{int}}(r_i, r_j) = g\delta(r_i - r_j)$. Here, $g = 2\pi\hbar^2 a/\mu$ with the scattering length $a$ and where $\mu$ is the reduced mass of the two scattered atoms, which in the case of identical particles is half the mass of a single atom. Hence, as the scattering length is experimentally tunable via *Feshbach resonances*, one has control over the interaction strengths [23; 28–31]. The interaction potential takes the form

$$V_{\text{int}}\left(\mathbf{r}_i, \mathbf{r}_j\right) = \frac{4\pi\hbar^2 a}{m} \delta\left(\mathbf{r}_i - \mathbf{r}_j\right), \tag{4.24}$$

and thus, the interaction term in the Hamiltonian (4.23) can be rewritten as

$$\begin{aligned}\hat{V}_{\text{int}} &= \frac{4\pi\hbar^2 a}{m}\int \mathrm{d}\mathbf{r}'\ \mathrm{d}\mathbf{r}\,\hat{\psi}^\dagger(\mathbf{r}')\hat{\psi}^\dagger(\mathbf{r})\delta(\mathbf{r}-\mathbf{r}')\hat{\psi}(\mathbf{r})\hat{\psi}(\mathbf{r}') \\ &= \frac{4\pi\hbar^2 a}{m}\int \mathrm{d}\mathbf{r}\,\hat{\psi}^\dagger(\mathbf{r})\hat{\psi}^\dagger(\mathbf{r})\hat{\psi}(\mathbf{r})\hat{\psi}(\mathbf{r}).\end{aligned} \tag{4.25}$$

With this, the full Hamiltonian in terms of the field operators from eq. (4.19) becomes

$$\begin{aligned}\hat{H} = \int \mathrm{d}\mathbf{r}\Bigg\{\hat{\psi}^\dagger(\mathbf{r})\left(-\frac{\hbar^2\nabla^2}{2m}+V_l(\mathbf{r})\right)\hat{\psi}(\mathbf{r}) \\ + \frac{\tilde{U}_0}{2}\hat{\psi}^\dagger(\mathbf{r})\hat{\psi}^\dagger(\mathbf{r})\hat{\psi}(\mathbf{r})\hat{\psi}(\mathbf{r})\Bigg\},\end{aligned} \tag{4.26}$$

where the tunnelling parameter is defined as

$$t^\sigma_{\alpha\beta} = \int \mathrm{d}(\mathbf{r})\ w^*_{\beta_{\mathbf{j}+\sigma}}(\mathbf{r})\left(-\frac{\hbar^2\nabla^2}{2m}+V_l(\mathbf{r})\right)w_{\alpha_{\mathbf{j}}}(\mathbf{r}), \tag{4.27}$$

and the onsite interaction parameter as

$$U^{\beta\beta'}_{\alpha\alpha'} = U_0\int \mathrm{d}\mathbf{r}\ w^*_{\beta_{\mathbf{j}}}(\mathbf{r})w^*_{\beta'_{\mathbf{j}}}(\mathbf{r})w^*_{\alpha_{\mathbf{j}}}(\mathbf{r})w_{\alpha'_{\mathbf{j}}}(\mathbf{r}). \tag{4.28}$$

Summing up, the Hamiltonian takes the form

$$\hat{H} = \sum_{\alpha,\beta}\sum_{\langle\mathbf{i},\mathbf{j}\rangle_\sigma} t^\sigma_{\alpha\beta}\hat{a}^\dagger_{\beta,\mathbf{j}}\hat{a}_{\alpha,\mathbf{i}} + \sum_{\substack{\alpha,\alpha'\\ \beta,\beta'}}\sum_{\mathbf{j}} U^{\beta\beta'}_{\alpha\alpha'}\hat{a}^\dagger_{\beta,\mathbf{j}}\hat{a}^\dagger_{\beta,\mathbf{j}}\hat{a}_{\alpha,\mathbf{j}}\hat{a}_{\alpha,\mathbf{j}}, \tag{4.29}$$

where $\mathbf{i}$ ($\mathbf{j}$) labels the lattice sites, $\alpha$ ($\beta$) labels the orbital states (i.e. band index but possible also spins), and $\sigma$ labels the spatial direction of a given tunneling process.

### Tunneling in the harmonic limit

If we take the Harmonic limit, we will find that up to constants, the orbital states will have the same shapes as they did for the square lattice. They will take the quantitative form of Hermitian polynomials and be even or odd in both variables.

While the true orbital states are the Wannier functions, we know that these will approach the Hermitian polynomials in the Harmonic limit. Thus, we may use the latter to find the allowed tunnelling processes. The potential is an even function, and the orbital states are either even or odd. We can thus analyze when the tunnelling process between two orbital states is allowed or forbidden.

### 4.6.2 The Hamiltonian

If we write the Hamiltonian as

$$\hat{H} = \hat{H}_0 + \hat{H}_{nn} + \hat{H}_{nn'} + \hat{H}_{fc}, \tag{4.30}$$

the first term can be identified as the free Hamiltonian, which describes nearest neighbour tunnelling, while the remaining terms are different kinds of interactions. In a lattice, where sites may host different orbital states, the tunnelling is expressed as an $\alpha$-orbital state tunnelling into a $\beta$-orbital along the $\sigma$-direction.

#### Density-density interactions

The second and the third terms in eq. (4.30) describe the two types of density-density interactions that allow for two-body interactions. Here,

$$\hat{H}_{nn} = \sum_{\alpha} \sum_{\mathbf{i}} \frac{U_{\alpha\alpha}}{2} \hat{n}_{\alpha,\mathbf{i}} \left( \hat{n}_{\alpha,\mathbf{i}} - 1 \right), \tag{4.31}$$

describes the density-density interaction between two atoms in the same orbital state, whereas

$$\hat{H}_{nn'} = \sum_{\alpha\beta} \sum_{\mathbf{i}} \frac{U_{\alpha\beta}}{2} \hat{n}_{\alpha,\mathbf{i}} \hat{n}_{\beta,\mathbf{i}}, \tag{4.32}$$

describes the density-density interaction between two atoms in different orbital states.

#### Orbital changing interactions

The orbital changing terms are terms where two atoms in state $\alpha$ and $\alpha'$ are transformed into two states $\beta$ and $\beta'$ where we require that the initial and final states are different, *i.e.*,

$$\hat{H}_{fc} = \sum_{\substack{\alpha,\alpha',\beta,\beta' \\ \alpha \neq \beta}} \sum_{\mathbf{i}} \frac{U_{\alpha\alpha'}^{\beta\beta'}}{4} \left( \hat{a}_{\beta,\mathbf{i}}^{\dagger} \hat{a}_{\beta',\mathbf{i}}^{\dagger} \hat{a}_{\alpha,\mathbf{i}} \hat{a}_{\alpha',\mathbf{i}} \right) + \text{h.c.}. \tag{4.33}$$

Contributions that include changing the states of the Hamiltonians are restricted by what states are supported in a given lattice site and what transitions are allowed. For lattice sites that support $s$-orbitals, there is no contribution from such a term as the lattice site only supports one state. However, for a two-dimensional lattice that supports $p$-orbitals, the terms from (4.33) must be included.

### 4.6.3 Bose Hubbard models

While the original Hubbard model describes spin-full fermions in a lattice [32], we are interested in bosons and various Bose-Hubbard models.

The first Bose-Hubbard model we shall consider is one where all the lattice sites support $s$-orbital states. Here the Hamiltonian in (4.29) reduces to

$$\hat{H}_{BH} = -t\sum_i \sum_{\vec{\sigma}} \hat{a}^\dagger_{\mathbf{i}+\vec{\sigma}}\hat{a}_{\mathbf{i}} + \frac{U}{2}\sum_i \hat{n}_{\mathbf{i}}(\hat{n}_{\mathbf{i}}-1) + h.c.. \tag{4.34}$$

This Hamiltonian is the original Bose–Hubbard model and, strictly speaking, the one named the Bose-Hubbard model [33]. However, we shall use this name a bit looser and include extended Bose-Hubbard models in this terminology.

#### The Bose-Hubbard model for the bipartite s-p lattice

An example of such a model is the Bose-Hubbard Hamiltonian for the $s$-$p$ bipartite lattice. The kind of bipartite lattice we are interested in is a square lattice where the depth of lattice sites alternate. Here, deep lattice sites are only connected to shallow ones and vice versa.

When the atoms in the deep lattice sites occupy $p$- orbital states and those in the shallow lattice sites occupy $s$-orbital states, then when we split the Hamiltonian in a kinetic and interaction part, $\hat{H} = \hat{H}_{\text{kin}} + \hat{H}_{\text{int}}$, we can express the kinetic part as

$$\begin{aligned} \hat{H}_{\text{kin}} \quad = \quad & -t_x \sum_{\langle \mathbf{ij}\rangle_x} \left(\hat{a}^\dagger_{s\mathbf{i}}\hat{a}_{x\mathbf{j}} + h.c.\right) + \Delta\sum_{\mathbf{i}} \hat{n}_{s\mathbf{i}} \\ & -t_y \sum_{\langle \mathbf{ij}\rangle_y} \left(\hat{a}^\dagger_{s\mathbf{i}}\hat{a}_{y\mathbf{j}} + h.c.\right) + \frac{\delta}{2}\sum_{\mathbf{j}} (\hat{n}_{x\mathbf{j}} - \hat{n}_{x\mathbf{j}}). \end{aligned} \tag{4.35}$$

The interaction term $\hat{H}_{\text{int}} = \hat{H}_{nn} + \hat{H}_{\text{fc}}$ can be further decomposed into 'density-density' interactions

$$\hat{H}_{nn} = \sum_\alpha \sum_{\mathbf{j}\in\mathcal{P}} \frac{U_{\alpha\alpha}}{2}\hat{n}_{\alpha\mathbf{j}}(\hat{n}_{\alpha\mathbf{j}}-1) + \sum_{\mathbf{i}\in\mathcal{S}} \frac{U_{ss}}{2}\hat{n}_{s\mathbf{i}}(\hat{n}_{s\mathbf{i}}-1) + \sum_{\alpha\beta,\alpha\neq\beta} \sum_{\mathbf{j}\in\mathcal{P}} U_{\alpha\beta}\hat{n}_{\alpha\mathbf{j}}\hat{n}_{\beta\mathbf{j}}, \tag{4.36}$$

and 'orbital-changing' interactions

$$\hat{H}_{\text{fc}} = \sum_{\alpha\beta,\alpha\neq\beta} \sum_{\mathbf{j}\in\mathcal{P}} \frac{U_{\alpha\beta}}{2}\left(\hat{a}^\dagger_{\alpha\mathbf{j}}\hat{a}^\dagger_{\alpha\mathbf{j}}\hat{a}_{\beta\mathbf{j}}\hat{a}_{\beta\mathbf{j}} + h.c.\right). \tag{4.37}$$

The system that this Hamiltonian describes is one where the lattice sites alternate in depth provided that $\Delta \neq 0$. In the shallow lattice sites, the atoms are in the $s$-orbital states, whereas in the deep lattice sites, the atoms are in a $p$-orbital state. One needs to keep track of four types of parameters: tunnellings $t$, interactions $U$, anisotropy between the $p$-orbitals $\delta$, and the offset between the onsite energies of the two types of lattice sites $\Delta$. We shall often assume that the lattice is isotropic, $\delta = 0$. In this case, there are only two different tunnelling parameters, one where the tunnelling happens parallel to the node of the $p_\alpha$ state, labelled $t_\alpha^\alpha$, and one where it happens perpendicular to the node similarly labelled $t_\alpha^\beta$. However as the eigenfunction for the groundstate is an even function and the one for the first excited state is an odd function, then only $t_\alpha^\alpha \neq 0$ while $t_\alpha^\beta = 0$. When $\Delta = 0$ the $s$- and $p$-orbital states are resonant, whereas when $\Delta \neq 0$ they are off-resonant. As long as $\Delta, t, U \ll \delta E$ the single-band approximation is still valid. However, if $\Delta \gg t, U$, the system is in the large detuned limit.

**The large detuned limit**

When the detuning $|\Delta|$ is much larger than the remaining parameters in the Hamiltonian, the system is far off-resonance.

For the $s$-$p$ bipartite lattice, the above implies that the energy of the $s$-orbital level is expressed in terms of the detuning $\Delta$. The $s$-atoms will then evolve with the smallest characteristic time-scale and adiabatically follow the evolution of the $p$-orbital states [34]. Hence, we can adiabatically eliminate the $s$-orbital states to derive an effective Hamiltonian for the $p$-orbitals alone. The derivation for this is found in [(I)]. When the detuning $|\Delta|$ is much larger than the remaining parameters in the Hamiltonian, the energy of the $s$-orbital level can be expressed in terms of the detuning $\Delta$ from the $p$-orbital energy level, and population transfer between the two different kinds of lattice sites are largely suppressed. To see how the system evolves, we may write the corresponding Heisenberg equations [34]

$$\begin{aligned}
\partial_t \hat{a}_{s_{\mathbf{i}}} &= -i\Delta \hat{a}_{s_{\mathbf{i}}} - iU_{ss}\hat{n}_{s_{\mathbf{i}}}\hat{a}_{s_{\mathbf{i}}} \\
&\quad it_x\left(\hat{a}_{x_{\mathbf{i}+\mathbf{1}_x}} + \hat{a}_{x_{\mathbf{i}-\mathbf{1}_x}}\right) + t_y\left(\hat{a}_{y_{\mathbf{i}+\mathbf{1}_y}} + \hat{a}_{y_{\mathbf{i}-\mathbf{1}_y}}\right), \\
\partial_t \hat{a}_{x\mathbf{j}} &= it_x\left(\hat{a}_{s_{\mathbf{j}+\mathbf{1}_x}} + \hat{a}_{s_{\mathbf{j}-\mathbf{1}_x}}\right) + \text{int. terms}, \\
\partial_t \hat{a}_{y_{\mathbf{j}}} &= it_y\left(\hat{a}_{s_{\mathbf{j}+\mathbf{1}_y}} + \hat{a}_{s_{\mathbf{j}-\mathbf{1}_y}}\right) + \text{int. terms}.
\end{aligned} \tag{4.38}$$

The notation $\mathbf{i} \pm \mathbf{1}_x$ is used for the neighbouring horizontal sites to the site $\mathbf{i}$, and similarly $\mathbf{i} \pm \mathbf{1}_y$ is used in the vertical direction. We find the steady state solution for the $s$-orbitals from $\partial_t \hat{a}_{s\mathbf{i}} = 0$. If we assume that the $\mathcal{S}$-sites are initially empty, then for all times $\langle \hat{n}_{s\mathbf{i}} \rangle \ll 1$ and we can neglect the shift deriving from onsite interaction on these sites, and thereby express the steady state solution for the $s$-orbitals as

$$\hat{a}^{(\mathrm{ss})}_{s_\mathbf{i}} = \frac{t_x}{\Delta}\left(\hat{a}_{x_{\mathbf{i}+\mathbf{1}_x}} + \hat{a}_{x_{\mathbf{i}-\mathbf{1}_x}}\right) + \frac{t_y}{\Delta}\left(\hat{a}_{y_{\mathbf{i}+\mathbf{1}_y}} + \hat{a}_{y_{\mathbf{i}-\mathbf{1}_y}}\right). \tag{4.39}$$

When substituting this expression for the $s$-orbital operators in the equations-of-motion for $\hat{a}_{x_\mathbf{j}}$ we obtain a series of terms. The interaction terms remain unaffected, but all other terms become two-step processes that only involve $p_x$- and $p_y$- orbital atoms, and hence only operators on half of the sites. We write

$$\partial_t \hat{a}_{x\mathbf{j}} = \hat{f}_2 + \hat{f}_1. \tag{4.40}$$

Here we divide the terms into two types. The first

$$\hat{f}_2 = iJ_{2x}\left(\hat{a}_{x_{\mathbf{j}+\mathbf{2}_x}} + \hat{a}_{x\mathbf{j}-\mathbf{2}_x} + 2\hat{a}_{x_\mathbf{j}}\right), \tag{4.41}$$

with the amplitude $J_{2x} = |t_x|^2/\Delta$, as the subscripts indicate, this couples twp $\mathcal{P}$-orbital sites along either the horizontal or vertical direction. It should be noted that this is a next nearest neighbouring (NNN) coupling. Similarly, there are terms which describe a coupling in the diagonal directions between two $\mathcal{P}$-lattice sites, these are nearest neighbouring (NN) couplings, and such terms take the form

$$\hat{f}_1 = iJ_1\left(\hat{a}_{y_{\mathbf{j}+\mathbf{1}_x+\mathbf{1}_y}} + \hat{a}_{y_{\mathbf{j}+\mathbf{1}_x-\mathbf{1}_y}} + \hat{a}_{y_{\mathbf{j}-\mathbf{1}_x+\mathbf{1}_y}} + \hat{a}_{y_{\mathbf{j}-\mathbf{1}_x-\mathbf{1}_y}}\right). \tag{4.42}$$

Here, the amplitude $J_1 = t_x t_y/\Delta$. Equivalently one could have found the equations for $\partial_t \hat{a}_{y_\mathbf{j}}$. From these equations, it is straightforward to derive an effective Hamiltonian for the $p$-orbital atoms via

$$\partial \hat{a}_{\alpha_\mathbf{j}} = -i\left[\hat{a}_{\alpha_\mathbf{j}}, \hat{H}_{\mathrm{eff}}\right]. \tag{4.43}$$

Though we have performed the derivation for an optical lattice system consisting of $s$- and $p$- orbitals, this method also works for other lattice systems where the evolution of particles at one type of lattice site follows the evolution of particles at the other sites. We shall also apply adiabatic elimination in Part 3 of this thesis when studying state-space lattices.

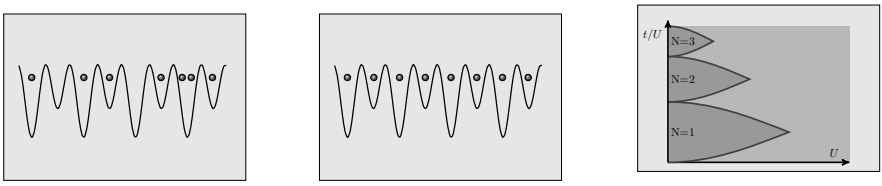


**(a)** **(b)** **(c)**

**Figure 4.4:** Cartoon description of the superfluid Fig. 4.4a versus the Mott insulating Fig. 4.4b phase. The final figure Fig. 4.4c shows a typical phase diagram.

## 4.7 Quantum phases of matter

The relative strength of the Hamiltonian parameters, $t$ and $U$, determines the overall phase of the system. When the tunnelling parameters $t$ are large compared to the interaction parameters $U$, the atoms are free to move around in the lattice, and the system is in what is called the *superfluid phase*. When the opposite is the case, and the tunnelling parameters are small compared to the interaction parameters, the system is effectively frozen with a fixed number of atoms per lattice site. This phase is called the *Mott* phase. In fig. 4.4 we show a graphical description of the superfluid phase 4.4(a), the Mott insulating phase 4.4(b), as well as a phase diagram over phase transitions between these phases. In the phase diagram (see fig. 4.4(c)), the $Mott_N$ phase is characterised by the number $N$ of particles per lattice site as a whole number, while in the superfluid phase, this number is allowed to fluctuate.

The superfluid and Mott phases are overall phases of the system. While these two phases give us an understanding of the system *i.e.* if the number of particles per lattice site froze or not, they do not give us a complete understanding of the system. Within these phases, there can even be sub-phases depending on the Hamiltonian one has at hand.

### 4.7.1 The superfluid phase

When $t$ is large compared to $U$, one can often treat the superfluid phase from a mean-field point of view [35; 36]. Such a mean-field approach is justified if the onsite particle number is at least around 10 [30]. When describing a weakly interacting many-body system from a mean-field point of view, one can apply the following three-step process. The first step is the *coherent state ansatz*, where a coherent state is assigned to every boson mode, and the mean-field Hamiltonian is thereby obtained [34].

This is done by replacing all of the operators $\hat{a}_{\alpha,\mathbf{j}}$ with complex numbers $\psi_{\alpha,\mathbf{j}}$, which is equivalent to assigning a coherent state at every site

$$|\Psi\rangle = \prod_{\mathbf{j}} |\psi\rangle_{\mathbf{j}}, \tag{4.44}$$

where $\hat{a}_{\alpha,\mathbf{j}}|\Psi\rangle = \psi_{\alpha,\mathbf{j}}|\Psi\rangle$. The second step is to express the equations of motions for the relevant *order parameters* $\psi_{\alpha,\mathbf{i}}$. In this thesis, we only encounter order parameters which can be expressed as complex numbers

$$\psi_{\alpha,\mathbf{i}} = e^{i\phi_{\alpha,\mathbf{i}}} \left|\psi_{\alpha,\mathbf{i}}\right|. \tag{4.45}$$

The full characterisation of the configuration of the order parameters, which gives the minimum energy, still depends on both the phase and the density of the order parameter. Finally, the Euler-Lagrange equations are propagated in imaginary time to find the configuration of order parameters that minimise the groundstate energy [27]. The last step is usually done numerically.

### 4.7.2 The Mott phase

In the other limit, when the interaction dominates, the system is highly correlated, and quantum effects are important [24; 37; 38]. In this limit, one can treat the tunnelling perturbatively and expand the full Hamiltonian in terms of $t$ order by order [39]. When doing so, the number of atoms in each lattice site stays frozen (see fig. 4.4b), and any tunnelling process must return the atom to the original lattice site. We shall throughout this thesis assume that we are in the $\text{Mott}_1$ phase, meaning that in unperturbed lattice, there will be one atom in each occupied lattice site.

We obtain an effective Hamiltonian by perturbation of the full in terms of the tunnelling parameter. The fixed number of atoms per lattice site is effectively handled by dividing the Hilbert space into two orthogonal subspaces using the projection operators $\hat{P}^2 = \hat{P}$, $\hat{Q}^2 = \hat{Q}$ with $\hat{P} + \hat{Q} = 1$. $\hat{P}$ projects onto the subspace $\mathcal{H}_P$ where all lattice sites are occupied with one atom, and $\hat{Q}$ projects onto the complementary subspace $\mathcal{H}_Q$ [23; 39]. Then the eigenvalue problem may be rewritten as

$$\left(\hat{Q}+\hat{P}\right)\hat{H}\left(\hat{Q}+\hat{P}\right)\psi = \left(\hat{Q}+\hat{P}\right)\left(\hat{H}_K+\hat{H}_U\right)\left(\hat{Q}+\hat{P}\right)\psi = E\psi, \tag{4.46}$$

where $\hat{H}_K$ is the kinetic part of the Hamiltonian, and $\hat{H}_U$ is the interaction part of the Hamiltonian. Since $\hat{P}\hat{H}_K\hat{P}$ and $\hat{Q}\hat{H}_U\hat{P}$ compute the

overlap between two disjoint subspaces of the Hilbert space they must both be zero, Furthermore, in the Mott$_1$ phase $\hat{P}\hat{H}_U\hat{P} = 0$. Using this allows us to write an effective Hamiltonian $\hat{H}_1$ in the Mott$_1$ phase with unit filling [23]

$$\hat{H}_1\psi = -\hat{P}\hat{H}_U\hat{Q}\frac{1}{\hat{Q}\hat{H}\hat{Q} - E}\hat{Q}\hat{H}_K\hat{P}\psi. \tag{4.47}$$

So far, our treatment is exact, and the Hamiltonian in (4.47) serves as the starting point for treating the tunneling perturbatively, *i.e.*, one expands $\frac{1}{\left(\hat{Q}\hat{H}\hat{Q}-E\right)}$. Making the approximation $\frac{1}{\hat{Q}\hat{H}\hat{Q}-E} \approx \frac{1}{\hat{H}-E}$ it follows that

$$\frac{1}{\hat{Q}\hat{H}\hat{Q} - E} \approx \frac{1}{\hat{H}_U}\frac{1}{\left(1 + \hat{H}_U^{-1}\left(\hat{H}_K - E\right)\right)} \quad . \tag{4.48}$$

As the tunnelling coefficient is much smaller than the interaction coefficient, one may expand around $\hat{H}_U^{-1}\left(\hat{H}_K - E\right)$.

$$\hat{K} \equiv \frac{1}{\hat{H}_U}\left[1 + \frac{1}{\hat{H}_U}\left(\hat{H}_K - E\right) + \frac{1}{\hat{H}_U}\left(\hat{H}_K - E\right)\frac{1}{\hat{H}_U}\left(\hat{H}_K - E\right)\right], \tag{4.49}$$

such that the effective Hamiltonian may be expressed as

$$\hat{H} \sim -t\hat{K}t. \tag{4.50}$$

When writing out the effective Hamiltonian, one has to sum over all paths that take an atom from a given lattice site and end the transition by returning the atom to the lattice site of origin (such that one remains in the Mott phase). Hence, all transitions will be of even order for a square lattice.

As we are in the Mott phase, then $t$ is small. Hence, we seek the transitions that require the smallest number of tunnellings but may change the lattice's dynamics.

If all lattice sites are occupied by $s$-orbitals, the *Mott*-phase is trivial as the interactions among $s$-orbitals cannot change the state of the system but only provide an energy shift. However, when the Hamiltonian in eq. (4.23) includes higher orbital states, the orbital-changing interaction changes the state of the system.

When an atom moves around in such processes, it will create a new orbital state when it tunnels into a lattice site and annihilates an orbital state when it tunnels out of a lattice site. Thus, if no interaction happens to change the orbital state, the contribution from such a process will have the form $\hat{a}^\dagger_{\alpha_i}\hat{a}_{\beta_i}$. If the lattice site happens to host an $s$-orbital state we have that $\alpha = \beta = s$, thus in the Mott-$n$ phase $\hat{a}^\dagger_{s_i}\hat{a}_{s_i} = n$ and one sees how any contribution from $s$-orbital states freezes out.

**The Mott phase for p-orbitals**

In a two-dimensional square lattice, where some of the lattice sites host $p$-orbital states and as these sites may occupy either a $p_x$ or an $p_y$-orbital state, one may introduce the *Schwinger spin bosons* mapping [39]

$$\begin{aligned} \hat{S}^Z_{\mathbf{i}} &= \tfrac{1}{2}\left(\hat{a}^\dagger_{x_{\mathbf{i}}}\hat{a}_{x_{\mathbf{i}}} - \hat{a}^\dagger_{y_{\mathbf{i}}}\hat{a}_{y_{\mathbf{i}}}\right), \\ \hat{S}^+_{\mathbf{i}} &= \hat{S}^X_{\mathbf{i}} + i\hat{S}^Y_{\mathbf{i}} = \hat{a}^\dagger_{x_{\mathbf{i}}}\hat{a}_{y_{\mathbf{i}}}, \\ \hat{S}^-_{\mathbf{i}} &= \hat{S}^X_{\mathbf{i}} - i\hat{S}^Y_{\mathbf{i}} = \hat{a}^\dagger_{y_{\mathbf{i}}}\hat{a}_{x_{\mathbf{i}}}. \end{aligned} \tag{4.51}$$

Using this mapping, we may map the effective Hamiltonian with one atom per site onto one of spin-1/2 particles. Throughout this thesis, we are interested in the $\text{Mott}_1$ phase, where the occupied lattice sites host exactly one atom in an unperturbed state. That we are in the $\text{Mott}_1$ phase thus ensures that $\hat{n}_{x_{\mathbf{i}}} + \hat{n}_{y_{\mathbf{i}}} = 1$ and we can thus express both $\hat{n}_{x_{\mathbf{i}}}$ and $\hat{n}_{y_{\mathbf{i}}}$ in terms of the $\hat{S}^Z_{\mathbf{i}}$

$$\hat{n}_{x_{\mathbf{i}}} = \tfrac{1}{2} + \hat{S}^Z_{\mathbf{i}} \quad , \quad \hat{n}_{y_{\mathbf{i}}} = \tfrac{1}{2} - \hat{S}^Z_{\mathbf{i}}, \tag{4.52}$$

In a regular square lattice in the tight-binding limit, this results in a spin model with nearest-neighbour couplings [23]. However, in a bipartite $s$-$p$ square lattice, while the effects of the $s$-orbitals freeze out, the $s$-site ensures that one needs to include up to fourth-order tunnelling processes to couple two $p$-sites. Thus, one is left with an effective Hamiltonian for a system of quantum particles with competing nearest and next-nearest neighbour couplings.

## 4.8 The scope of (bipartite) optical lattice systems

Through the realisation of spin-models in the Mott phase, we see how ultracold atoms in optical lattices hold the potential of realising a frustrated quantum phase. However, one thing is that something is theoretically possible, another one is whether it is doable.

Throughout this chapter, we have introduced approximation after approximation. Each approximation restricts the regime for which our effective model is valid. To realise a quantum spin-1/2 model, the lattice needs to support a double degenerated orbital state (like the $p_x$-$p_y$ pair). Thus, a crucial question is whether one for such an orbital state can realise a regime where all the necessary approximations are valid.

In the next two chapters, we study bipartite square lattice systems. First the superfluid limit in Chapter 5 and then the $\text{Mott}_1$ phase in Chapter 6. We see first how that if the tight-binding approximation is valid, one can, in the large detuned limit, realise a frustrated phase in the superfluid limit, and in the the Mott phase how quantum spin models with competing nearest and next-nearest neighbor coupling emerge.

For both the superfluid and the Mott phase, the key to realising these potentially frustrated phases is to freeze out one type of lattice site. Rather than contributing directly to the effective Hamiltonian, these lattice sites act as mediators of both nearest and next nearest neighbour couplings. Thus, with bipartite lattice systems one may realise nearest and next-nearest neighbouring couplings and do so systematical. Thus, bipartite lattice models are exciting because they provide a systematic route to realising coupling-induced frustration.

# 5. Frustration in bipartite lattices

We start our search for frustration in bipartite square lattices by considering the superfluid limit. Here, quantum correlations are suppressed, simplifying the situation so we may study this limit through a mean-field approach. The mean-field approach makes it relatively easy to see when and why frustration happens. However, when a mean-field approach is valid, it has a price. In the superfluid limit, any frustrated phase is, of course, not a quantum simulator. However, even within this limit, there are still open questions regarding coupling-induced frustration in a square lattice.

We first explore the general bipartite square lattice potential, wishing to understand the mechanisms that allow this potential to realise different bipartite lattice systems.

We then study *s*-*s* bipartite optical lattice. Under the assumption that the tight-binding approximation is valid in the large detuned limit, we see a perfect classical $J_1$-$J_2$ model emerges. However, while the tight binding approximation is not valid in this limit, the bipartite *s*-*s* model is still interesting. It is simple enough to be realised experimentally with the tunable relative depths between two lattice sites. This control over the lattice depths allows us to explore a regime other than the large detuned one. We find that when close to resonance, nearest and next-nearest neighbour tunnellings cause competing anti-ferromagnetic couplings for this system.

With experimental signs of a frustrated phase for the *s*-*s*-bipartite lattice, we wish to explore if other bipartite lattice systems may host frustrated phases. We turn to the bipartite *s*-*p* and see how this model, in the large detuned limit, also leads to a perfect classical $J_1$-$J_2$ model. Thus we discuss this model in more detail and how bipartite square lattice models provide a route for realising it.

## 5.1 The bipartite lattice

To understand bipartite square lattice systems better, we start by looking at the potential that causes them. The bipartite lattice potential

can be expressed as

$$V(x,y) = -V_0\Big[\cos^2(x) + \cos^2(y) + 2\cos(\theta)\cos(x)\cos(y)\Big]. \tag{5.1}$$

and thus it differs from the one for the regular square lattice given in (4.9) by a term of $2\cos(\theta)\cos(x)\cos(y)$. The parameter $\theta$ controls the energy offset between the deep and the shallow lattice sites. Choosing $\theta = \pi/2$ reproduces the lattice potential for the regular square lattice. However, even the slightest deviation from this value of $\theta$ produces a bipartite lattice. The lattice potential in eq. (5.1) reduces to that of (4.9) where $\theta = \frac{\pi}{2}$. Here, the potential is separable, *i.e.*, it can be written as $V(x,y) = V(x) + V(y)$. However, when $\theta \neq \frac{\pi}{2}$ the lattice potential in eq. 5.1 is non-separable.

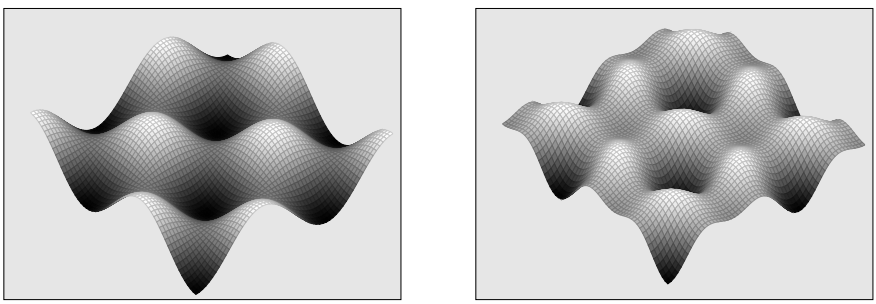

**(a)** The square lattice potential **(b)** The bipartite lattice potential.

**Figure 5.1:** The 2D lattice potentials for the regular versus the bipartite square lattice. For the regular square lattice $\theta = \frac{\pi}{2}$ while for the bipartite square lattice we consider here $\theta = \frac{2\pi}{5}$. One sees how in the bipartite square lattice, the depth of the lattice sites alternates between deep and shallow as opposed to the regular square lattice, where they all have the same depth.

We can also view the bipartite lattice from above and compare it to the regular square lattice (see Fig. 5.2). Here, one sees that all lattice sites are identical in the standard square lattice. However, for the bipartite square lattice, the lattice sites alternate between what we shall call shallow $\mathcal{S}$ (white) and deep $\mathcal{D}$ (grey) lattice sites.

### 5.1.1 Designing bipartite lattices

In eq. (5.1) the two parameters, $V_0$ and $\theta$, control the shape of the lattice potential. Among these two, $V_0$ is the one that controls the maximum depth of the lattice, while $\theta$ is the one that controls the energy offset between the two kinds of lattice sites.

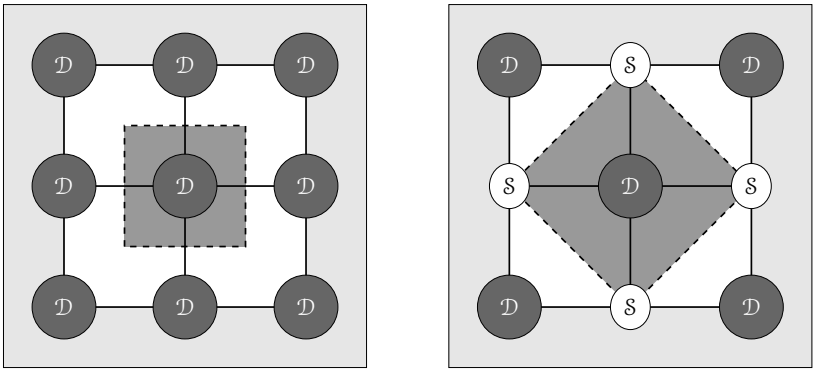


**Figure 5.2:** The regular versus the bipartite square lattice. The blue sites mark deep lattice sites, whereas the sites mark shallow lattice sites. The grey area shows the unit cell in each case.

Assuming that the single-band approximation is valid, one may realise several different bipartite square lattice models by tuning these two parameters. For some parameter choices, all lattice sites will support the same orbital states. In contrast, the two types of lattice sites support different orbital states for other options.

Suppose we start by considering the limit, where $\theta \approx \frac{\pi}{2}$, then the deep and the shallow lattice sites both support the same orbital state. Which one depends on the strength of the potential $V_0$. In general, one can say that the higher an orbital state one wishes to realise, the deeper the lattice potential has to be, and thus the larger $V_0$ has to be.

As long as $\theta \approx \frac{\pi}{2}$, the energies of the orbital states at the different lattice sites are close to resonance. Thus, when we define the detuning $\Delta = E_S - E_D$, it will be very small. Whether $\theta$ is larger or smaller than $\frac{\pi}{2}$, is not important as it only changes which lattice sites are deep and which are shallow.

However, increasing $\tilde{\theta} = |\theta| - \frac{\pi}{2}$ leads to the energies at deep and shallow lattice sites becoming increasingly off-resonance. At first, this leads to $\Delta \gg t, U$, and thus the system is in the far detuned limit. Suppose we continue to increase $\tilde{\theta}$. In that case, we can reach a situation where the two lattice sites each support different orbital states. At first, these orbital states will be off-resonant. If $\tilde{\theta}$ increases, the orbital states will once again become resonant. However, the deep and shallow lattice sites now support different orbital states; thus, the different orbitals will hybridise. Controlling $V_0$ and $\theta$ allows us to realise a variety of bipartite square lattice systems.

## 5.2 The Bose-Hubbard Hamiltonian

Assuming that both the single-band approximation and the tight-binding approximation are valid, we may express the system's dynamics in terms of its Bose-Hubbard Hamiltonian. For a bipartite lattice system, we express the Bose-Hubbard Hamiltonian below by introducing a notation that allows us to separate the onsite contributions in contributions from deep and shallow lattices, respectively. To do so we shall call the set of deep (shallow) lattice sites by $\mathcal{D}(\mathcal{S})$, and label a deep (shallow) lattice site by the index $\mathbf{i}$ ($\mathbf{j}$). Thus we can write the Hamiltonian as

$$\begin{aligned}\hat{H}_{ss} &= -\sum_{\langle \mathbf{i},\mathbf{j}\rangle}\sum_{\alpha\beta}\sum_{\sigma}\left(t^{\sigma}_{\alpha,\beta}\hat{a}^{\dagger}_{\alpha_i}\hat{a}_{\beta_\mathbf{j}} + h.c\right) \\ &\quad + E_{\mathcal{D}}\sum_{\mathbf{i}\in\mathcal{D}}\sum_{\alpha}\hat{n}_{\alpha_\mathbf{i}} + E_{\mathcal{S}}\sum_{\mathbf{j}\in\mathcal{S}}\sum_{\beta}\hat{n}_{\beta_\mathbf{j}} + \hat{H}^{\mathcal{D}}_{I} + \hat{H}^{\mathcal{S}}_{I},\end{aligned} \tag{5.2}$$

where the index $\sigma$ accounts for the different directions that the tunnelling can take place. We have included an index $\alpha$ ($\beta$) that allows us to sum over the possible orbital states. We can use the same notation in Chapter 6. However, when both lattice sites are $s$-orbital sites, the Hamiltonian can be written as

$$H^{s}_{I} = U_0\sum_{\mathbf{k}}\hat{n}_{s_\mathbf{k}}(\hat{n}_{s_\mathbf{k}} - 1). \tag{5.3}$$

Hence, if we introduce the notation $\Delta = E_{\mathcal{D}} - E_{\mathcal{S}}$, we can shift the energy such that $E_{\mathcal{S}} = 0$, such that we may write

$$E_{\mathcal{D}}\sum_{\mathbf{i}\in\mathcal{D}}\hat{n}_{\mathbf{i}} + E_{\mathcal{S}}\sum_{\mathbf{j}\in\mathcal{S}}\hat{n}_{\mathbf{j}} = \Delta\sum_{\mathbf{i}\in\mathcal{D}}\hat{n}_{\mathbf{i}}. \tag{5.4}$$

With this in mind, the Bose-Hubbard Hamiltonian takes the form

$$\begin{aligned}\hat{H}^{ss} &= -t\sum_{\langle \mathbf{i},\mathbf{j}\rangle}\left(\hat{a}^{\dagger}_{\mathbf{i}}\hat{a}_{\mathbf{j}} + h.c.\right) + \Delta\sum_{\mathbf{i}\in\mathcal{D}}\hat{n}_{\mathbf{i}} \\ &\quad + U_0\left(\sum_{\mathbf{i}\in\mathcal{D}}\hat{n}_{s_\mathbf{i}}(\hat{n}_{s_\mathbf{i}} - 1) + \sum_{\mathbf{j}\in\mathcal{S}}\hat{n}_{s_\mathbf{j}}(\hat{n}_{s_\mathbf{j}} - 1)\right),\end{aligned} \tag{5.5}$$

and we have now expressed the Hamiltonian in terms of the detuning $\Delta$. This expression is valid for any detuning $\Delta$. When detuning $\Delta >> t, U$, we can derive an effective Hamiltonian only in terms of either the shallow or deep lattice sites.

### 5.2.1 The large detuned limit

When detuning $\Delta \gg t, U$, we may use adiabatic elimination to derive an effective Hamiltonian for only the atoms in the $\mathcal{D}$-sites [34]. The procedure is similar to the one we described in Chapter 4, only now, the deep and shallow sites support $s$-orbital states. Performing adiabatic elimination leads to an effective Hamiltonian on the form

$$\begin{aligned} \hat{H}_{\text{eff}} &= \varepsilon \sum_{\mathbf{j}} \hat{n}_{\mathbf{j}} + \tau_1 \sum_{\langle \mathbf{ij} \rangle} \left( \hat{a}_{\mathbf{i}}^{\dagger} \hat{a}_{\mathbf{j}} + h.c. \right) \\ &\quad + \tau_2 \sum_{\{\mathbf{ij}\}} \left( \hat{a}_{\mathbf{i}}^{\dagger} \hat{a}_{\mathbf{j}} + h.c. \right) + U \sum_{\mathbf{j}} \hat{n}_{\mathbf{j}} (\hat{n}_{\mathbf{j}} - 1). \end{aligned} \tag{5.6}$$

The parameters are $\varepsilon = 4\tau$, $\tau_1 = 2\tau$, $\tau_2 = \tau$ and $\tau = t^2/\Delta$. Since the particle number is preserved, the first sum adds an overall energy shift and can be disregarded.

## 5.3 A naively frustrated s-s bipartite lattice

The large detuned limit is an obvious place to start studying bipartite lattice systems with competing nearest and next-nearest neighbours. In this limit, the system must exhibit a bipartite structure, as the two types of lattice sites are far off-resonant from one another.

As we are in the superfluid limit we may follow the procedure we outlined in Chapter 4 and replace the annihilation and creation operators with their coherent function

$$\psi_{s_{\mathbf{i}}} = e^{i\phi_{s_{\mathbf{i}}}} \left| \psi_{s_{\mathbf{i}}} \right|. \tag{5.7}$$

Thus, we can express a mean-field version of these Bose-Hubbard Hamiltonians by replacing the annihilation and creation operators with these functions. We then minimise this Hamiltonian with respect to the variables $\phi_{s_{\mathbf{i}}}$ and $|\psi_{s_{\mathbf{i}}}|$ to find the groundstate configuration. The coherent functions thus play the role of order parameters in the superfluid phase.

In the isotropic limit, the density is equally distributed and one only has to minimise the effective Hamiltonian with respect to the phases, to find the configuration of order parameters that minimises the energy. In order to find the configuration of order parameters that minimises the energy, we introduce an energy functional $E\left[\phi_{s,\mathbf{i}}\right]$. For the bipartite $s$-$s$ lattice, the energy functional is

$$E_{ss}^{\Delta}[\phi_{\mathbf{i}}] \quad = \quad 2\tau \sum_{\{\mathbf{i},\mathbf{j}\}} \cos(\phi_{\mathbf{i}} - \phi_{\mathbf{j}}) + 4\tau \sum_{\langle \mathbf{i},\mathbf{j} \rangle} \cos(\phi_{\mathbf{i}} - \phi_{\mathbf{j}}). \tag{5.8}$$

Introducing $J_1 = 4\tau$ we see how the above mean-field Hamiltonian becomes identical to the maximally frustrated $XY$ model [9]. Since $J_1 = 2J_2 > 0$, we sit at exactly the frustration point, where the condensate throughout the lattice should have difficulties ordering globally. A manifestation should show up in terms of seemingly random phases $\phi_{\mathbf{i}}$

### 5.3.1 Close to resonance and (almost) frustrated

Realising the $J1-J2$ model in the large detuned limit requires that the tight-binding approximation is valid. If tunnelling terms beyond nearest and next-nearest neighbours are non-vanishing strict fluctuations will be destroyed. To check how the tunnelling coefficients drops of, we evaluate the first few tunnelling coefficients numerically. If the tight-binding approximation were to hold, the next-nearest neighbour tunnelling strength must be significantly smaller than the nearest neighbour tunnelling. Unfortunately, in the large detuned limit, we do not have frustration.

That the tight-binding approximation breaks down does not mean that frustration cannot occur in this lattice. In the large detuned limit, one aims at realising competing nearest and next-nearest neighbour coupling only through nearest-neighbour tunnelling. Still, in another regime, frustration can be realised if nearest and next-nearest neighbour tunnellings compete.

We wish to explore if the bipartite $s$-$s$ lattice may have anti-ferromagnetic nearest and next-nearest neighbour couplings in another parameter regime. It turns out that for $V_0 = 10E_{\mathrm{R}}$, when close to resonance $\Delta \to 0$, there is a parameter regime where nearest and next nearest neighbour couplings are competing. Thus, we move away from the large detuned limit.

### 5.3.2 Experimental realisation of frustration

The regime of competing nearest and next-nearest neighbour tunnelling was experimentally explored in [II] in a setup consisting of an optical lattice formed by two orthogonal optical standing waves, thereby trapping a Bose-Einstein condensate of rubidium ($^{87}$Rb) atoms.

The experiment consisted of four stages, labelled (I)-(IV) in fig. 5.3. In the first stage, the atoms were loaded adiabatically into the lowest band in the lattice. This was done by increasing the lattice depth $V_0$

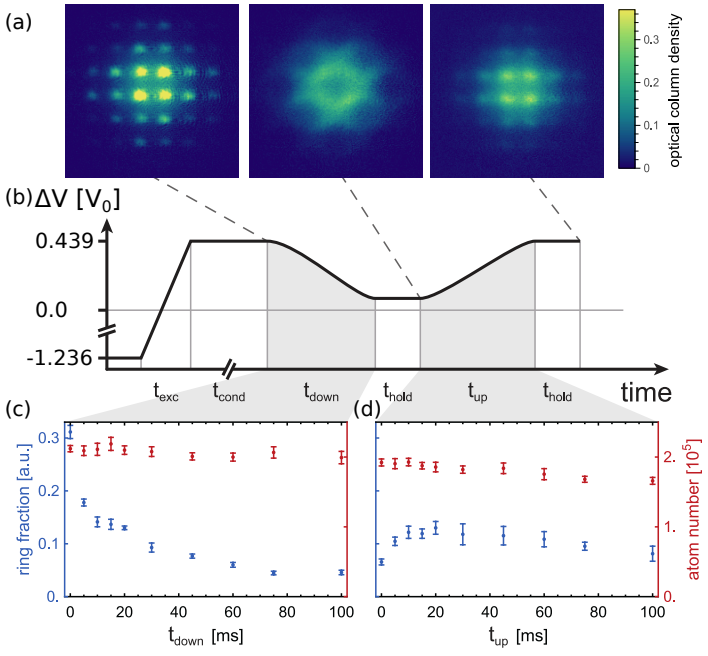


**Figure 5.3:** Collapse and revival of coherence. Three momentum spectra are shown in (a) for characteristic values of $\Delta V$ tuned according to the protocol in (b). The first image at $\Delta V = 0.439\,V_0$ shows coherent condensate fractions at the $X_\pm$ points of the second band. In the second image at $\Delta V = 0.063\,V_0$ one sees that coherence has completely vanished. The third image, recorded after ramping back to $\Delta V = 0.439\,V_0$, shows partially restored coherence.

| $t_{nm}$ | 0 | 1 | 2 |
|---|---|---|---|
| 0 | -13.97 | $1.4 \cdot 10^{-3}$ | $-6 \cdot 10^{-6}$ |
| 1 | $1.4 \cdot 10^{-3}$ | $9.7 \cdot 10^{-4}$ | $-4 \cdot 10^{-6}$ |
| 2 | $-6 \cdot 10^{-6}$ | $-4 \cdot 10^{-6}$ | $-6 \cdot 10^{-7}$ |

**Table 5.1:** Tunnelling matrix for the parameters $V_0 = 10E_{\mathrm{R}}$ and $\Delta V = 0.063V_0$. The first diagonal term gives the onsite energy, the terms $(0,1)$ and $(1,0)$ are the nearest neighbours tunnelling rates $J_1$, and $(1,1)$ the next nearest neighbours tunnelling rate $J_2$ and so on. These parameters are used in the experiment described in the next section.

to $10\,E_{\mathrm{R}}$ for $\Delta V = -1.236\,V_0$. After the system settled, a quench was applied by rapidly increasing $\Delta V$ to $0.439\,V_0$. This quench causes the atoms to be excited to the metastable second Bloch-band [40]. Allowing the system time to settle in this stage cause the atoms to condense at the two energy minima of the band. Afterwards, by decreasing $\Delta V$ to $\Delta V = 0.063\,V_0$, one enters the third stage of the experiment. Here, the energy-momentum dispersion of the second band is almost degenerated along the edge of the first Brillouin zone II. The atoms are observed to spread over the entire edge of the second Bloch band populating all available Bloch states along the edge. The fourth and final stage of the experiment is included to exclude the possibility that the observed vanishing of coherence is due to uncontrolled heating. This check is done by adiabatically increasing $\Delta V$ back to its initial value $\Delta V = 0.439\,V_0$. Here, one sees a revival of the condensate fraction. However, this recovery is not perfect. This last step in the experimental procedure is crucial to establish if the system has truly been frustrated or not.

In the frustrated regime, stage (II), no visible signatures of coherence are observed, which is also in agreement with numerical simulations of this stage II. However, the system begins and ends in a stage of coherence. Strictly speaking, this is no smoking gun or direct proof that the system is frustrated in stage (II). Still, the loss of coherence can be a potential signature of a frustrated phase. A similar method was used in [41] to distinguish the Mott insulating phase from a thermally incoherent phase.

## 5.4 The bipartite *s*-*p* lattice

We now turn to the bipartite *s*-*p* square lattice, and we shall again assume the tight-binding and single-band approximation. Here, the shallow lattice sites support *s*-orbital states, whereas the deep lattice sites

support $p$-orbital states. In the two-dimensional lattice, the $p_\alpha$-orbitals are double degenerated, and we, therefore, label them with an index $\alpha$. In this bipartite lattice, tunnelling between lattice sites changes the orbital state of the atom tunnelling. The Wannier functions for $s$-orbital states are even functions in both variables. However, the Wannier function for the $p_\alpha$-orbital state is odd in the $\alpha$-variable and even in the other variable. The bipartite lattice potential is also an even function in both variables. The combination of even and odd functions ensures that a $p_\alpha$-orbital state can only tunnel to an $s$-orbital state in the $\alpha$-direction.

Throughout this chapter, we assume that we are in the isotropic limit, meaning that the system exhibits no preference between the $p_x$- and $p_y$-orbital state. Thus, $\delta = 0$ for the last term in eq. (4.35), and it vanishes.

### 5.4.1 Bose-Hubbard Hamiltonians for the *s-p* bipartite lattice

When deriving the Bose-Hubbard Hamiltonian for optical lattice systems back in Chapter 4, we used the $s$-$p$-bipartite lattice as a model system and discussed the different terms contributing to this Hamiltonian. Thus, we refer back to Chapter 4 for a detailed discussion about this Hamiltonian. Here, we will only give the expressions for the Bose-Hubbard Hamiltonians for the $s$-$p$-bipartite lattice. We will, however, provide the expressions for both the resonant limit and the large detuned limit.

In the resonant limit, the energy levels of the $s$-orbital states and the $p$-orbital states are resonant, and hence also $\Delta = 0$ in eq. (4.35). From eq. (4.35)- (4.37) the full Bose-Hubbard Hamilton can therefore be found to have the form

$$\begin{aligned} H_{sp} = &-\sum_{\alpha}^{x,y} \sum_{\langle \mathbf{i},\mathbf{j}\rangle_\sigma} \left( t_{\alpha s}^{\sigma} \hat{a}_{\alpha_\mathbf{i}}^\dagger \hat{a}_{s_\mathbf{j}} + \text{h.c.} \right) + \sum_{\mathbf{j}} \frac{U_{ss}}{2} \hat{n}_{s_\mathbf{j}} \left( \hat{n}_{s_\mathbf{j}} - 1 \right) \\ &+ \sum_{\mathbf{i}} W \sum_{\alpha}^{x,y} \frac{U_{\alpha\alpha}}{2} \hat{n}_{\alpha_\mathbf{i}} \left( \hat{n}_{\alpha_\mathbf{i}} - 1 \right) + 2 \sum_{\mathbf{i}} \frac{U_{xy}}{2} \hat{n}_{x_\mathbf{i}} \hat{n}_{y_\mathbf{i}} \\ &+ \sum_{\mathbf{i}} \frac{U_{xy}}{4} \left( \hat{a}_{x_\mathbf{i}}^\dagger \hat{a}_{x_\mathbf{i}}^\dagger \hat{a}_{y_\mathbf{i}} \hat{a}_{y_\mathbf{i}} + \text{h.c.} \right), \end{aligned} \tag{5.9}$$

In the large detuned limit, then for an isotropic system, the Hamiltonian

becomes

$$\begin{aligned}\hat{H}_{\mathrm{sp}}^{(\Delta)} = &-\sum_{\alpha}^{x,y}\sum_{\{\mathbf{i},\mathbf{j}\}_\sigma}\tau_\alpha^\sigma \hat{a}_{\alpha_\mathbf{i}}^\dagger \hat{a}_{\alpha_\mathbf{j}} - \sum_{\substack{\alpha\beta,\\ \alpha\neq\beta}}^{x,y}\sum_{\langle\mathbf{i},\mathbf{j}\rangle}\left(\tau^{\alpha\beta}\hat{a}_{\alpha_\mathbf{i}}^\dagger \hat{a}_{\beta_\mathbf{j}} + \mathrm{h.c.}.\right)\\ &-\sum_{\alpha}^{x,y}\sum_{\mathbf{j}}\tau_\alpha \hat{n}_{\alpha_\mathbf{j}}\\ &+\sum_{\alpha}^{x,y}\sum_{\mathbf{j}}\frac{U_{\alpha\alpha}}{2}\hat{n}_{\alpha_\mathbf{j}}\left(\hat{n}_{\alpha_\mathbf{j}}-1\right) + \sum_{\substack{\alpha\beta,\\ \alpha\neq\beta}}^{x,y}\sum_{\mathbf{j}}U_{\alpha\beta}\hat{n}_{\alpha_\mathbf{j}}\hat{n}_{\beta_\mathbf{j}}\\ &+\sum_{\substack{\alpha\beta,\\ \alpha\neq\beta}}\sum_{\mathbf{j}}^{x,y}\frac{U_{\alpha\beta}}{4}\left(\hat{a}_{\alpha_\mathbf{j}}^\dagger \hat{a}_{\alpha_\mathbf{j}}^\dagger \hat{a}_{\beta_\mathbf{j}}\hat{a}_{\beta_\mathbf{j}} + \mathrm{h.c.}.\right). \end{aligned} \tag{5.10}$$

Here $\tau_\alpha = |t_\alpha|^2/\Delta$ and $\tau^{\alpha\beta} = t_x t_y/\Delta$ give the tunnelling amplitudes along nearest and next nearest neighbours respectively. If we had been interested in an anisotropic system the Hamiltonian would only change slightly as $\delta \neq 0$ causes the inclusion of the term $\frac{\delta}{2}\sum_\mathbf{j}\left(\hat{n}_{x_\mathbf{j}} - \hat{n}_{y_\mathbf{j}}\right)$.

### 5.4.2 The mean-field approach in the superfluid limit

As we are in the superfluid limit we may again follow the procedure from Chapter 4 and replace the annihilation and creation operators with their coherent function

$$\psi_{\alpha_\mathbf{i}} = e^{i\phi_{\alpha_\mathbf{i}}}\left|\psi_{\alpha_\mathbf{i}}\right|. \tag{5.11}$$

Here $\alpha \in \{s, x, y\}$. Again we wish to express a mean-field version of the Bose-Hubbard Hamiltonians such that we can minimise them with respect to the variables $\phi_{\alpha_\mathbf{i}}$ and $|\psi_{\alpha_\mathbf{i}}|$ and find the groundstate configuration.

In the isotropic limit, the density is equally distributed between the allowed states such that $|\psi| = \left|\psi_{s_\mathbf{j}}\right| = |\psi_{x_\mathbf{i}}| = |\psi_{y_\mathbf{i}}|$, and one only has to minimise the effective Hamiltonian with respect to the phases, to find the configuration of order parameters that minimises the energy.

While the overall phase does not affect the system's energy, the orbital-changing terms can do so as they link the phases of different orbital states. We again introduce the energy functional $E\left[\phi_{\alpha,\mathbf{i}}\right]$ to find the configuration of the order parameter that minimise the groundstate energy. When the energy functional is minimised with respect to these phases, it can thus result in a phase-locking throughout the lattice. For

the bipartite $s$-$p$ lattice, the energy functional will in the resonant limit become

$$E_{sp}\left[\phi_{\alpha,\mathbf{i}}\right] = -\sum_{\alpha}^{x,y}\sum_{\langle \mathbf{i},\mathbf{j}\rangle} t\cos\left(\phi_{\alpha_\mathbf{i}} - \phi_{\beta_\mathbf{j}}\right) + \sum_{\mathbf{i}\in\mathcal{D}} \tilde{U}_{xy}\cos\left(2\left(\phi_{\alpha_\mathbf{i}} - \phi_{\beta_\mathbf{i}}\right)\right). \tag{5.12}$$

Here we have introduced $\tilde{U}_{xy} = U_{xy}\left|\psi\right|^2$. In the large detuned limit, the $s$-orbital sites are frozen out such that the energy functional becomes

$$\begin{aligned} E^{\Delta}_{sp}\left[\phi_{\alpha_\mathbf{i}}\right] = &-2\tau\sum_{\alpha}\sum_{\{\mathbf{i},\mathbf{j}\}_\alpha}\cos\Big(\phi_{\alpha_\mathbf{i}} - \phi_{\alpha_\mathbf{j}}\Big) - 2\tau\sum_{\alpha\neq\beta}\sum_{\langle\mathbf{i},\mathbf{j}\rangle_\alpha}\cos\Big(\phi_{\alpha_\mathbf{i}} - \phi_{\beta_\mathbf{j}}\Big) \\ &+\sum_{\mathbf{j}}\tilde{U}_{xy}\cos\Big(2(\phi_{x_\mathbf{j}} - \phi_{y_\mathbf{j}})\Big). \end{aligned} \tag{5.13}$$

Taking the derivative of the energy functional with respect to the phases $\phi_\alpha\mathbf{i}$ gives us the configuration of the order parameter that minimises the system's energy. We are interested in finding, if possible, this configuration. Such a configuration will depend on the strength and sign of the different coupling coefficients. When it exists, it will cause a phase-locking throughout the system. However, as we are searching for frustration, we are, in reality, interested in exploring when it is not possible to identify such a configuration. The energy functional for the resonant limit only has couplings between the nearest neighbouring lattice sites, and it can not host a frustrated phase. However, this means that we should be able to find a configuration of the order parameters that minimises the system's energy. If the tunnelling parameter $t$ is positive then we see that the first term is minimised whenever $\cos\Big(\phi_{\alpha_\mathbf{i}} - \phi_{s_\mathbf{j}}\Big) = 1$, which indicates that $(\phi_{\alpha_\mathbf{i}} - \phi_{s_\mathbf{j}}) = 0$, whereas when $t$ is negative, we see that the energy functional is minimised when $\cos\Big(\phi_{\alpha_\mathbf{i}} - \phi_{s_\mathbf{j}}\Big) = -1$, which requires $(\phi_{\alpha_\mathbf{i}} - \phi_{s_\mathbf{j}}) = \pi$,

In both cases, only the relative phase between two lattice sites is relevant, not the absolute phases. We always have the (gauge) freedom to pick an overall constant phase of the condensate that will not appear in any observable.

### Large detuning limit - a systematic approach to frustration

For large detuning, $\Delta$, the Hamiltonian (5.10) has both nearest and next-nearest neighbouring tunnelling terms, with the sign of these being adjustable through the detuning itself, and thus a $J_1$-$J_2$-model arises. This model is a prime candidate for hosting a frustrated phase [4; 11].

The energy-functional consists of three terms, a nearest-neighbour coupling that links the phase of two different orbital states, a next-nearest-neighbour coupling that links the phase of two orbital states of the same kind, and an onsite interaction that links the phase of two different orbital states at the same lattice sites. Hence, we can represent this graphically as a two-layered bipartite lattice, as seen in Fig. 5.4.

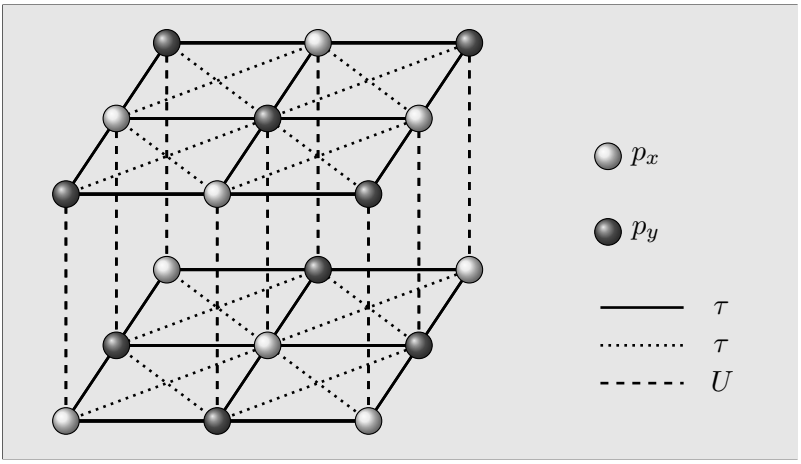


**Figure 5.4:** White (black) spheres represent $p_x$- ($p_y$-)orbitals, so the two orbitals alternate between neighbouring sites. The full black lines represent exchange interaction between orbitals of a different type, the dotted lines exchange interaction between orbitals of the same type, and the dashed lines onsite interaction. Without onsite interaction the two layers decouples.

This model is a two-flavor *rotor model* and is very similar to the classical $XY$ model I,[42] that arose for the bipartite *s*-*s*. However, a difference is that each site contains two classical rotors instead of one, which is coupled on site with $U$ (see fig. (5.4)).

### Phase-locking for the $J_1$-$J_2$ model

The problem we now have to solve is to determine if a configuration exists that allows for a phase-locking throughout the entire system. Noting, that $J_{1(2)} > 0$ then the term $J_{1(2)} \cos\left(\phi_{\alpha_\mathbf{i}} - \phi_{\beta_\mathbf{j}}\right)$ is minimised for $(\phi_{\alpha_\mathbf{i}} - \phi_{\beta_\mathbf{j}}) = \pi$, whereas when $J_{1(2)} < 0$ it is minimised for $(\phi_{\alpha_\mathbf{i}} - \phi_{\beta_\mathbf{j}}) = 0$. For the onsite coupling, when $U > 0$ the optimal phase locking is $(\phi_{\alpha_\mathbf{i}} - \phi_{\beta_\mathbf{i}}) = \pi/2$, whereas when $U < 0$ it is $(\phi_{\alpha_\mathbf{i}} - \phi_{\beta_\mathbf{i}}) = 0$.

When only one of $J_1$ and $J_2$ are zero, the two layers will order according to the sign of the non-zero coupling. If the $J_1$ coupling is fer-

romagnetic, the two layers order ferromagnetic, whereas if $J_1$ is anti-ferromagnetic, they order accordingly. When $J_1 = 0$ and $J_2 \neq 0$, each layer decouples into two sublattices, ordering according to the $J_2$ coupling. Introducing even a small onsite coupling, positive as well as negative, locks the two layers accordingly two one another.

When both $J_1$ and $J_2$ are non-zero, if both couplings are ferromagnetic, each layer of the lattice orders accordingly. With an onsite interaction, the two layers will phase-lock with respect to one another. Suppose the $J_1$ coupling is anti-ferromagnetic and the $J_2$ coupling is ferromagnetic. In that case, achieving a phase-locking throughout the entire system is still possible. If both couplings are anti-ferromagnetic or if $J_1$ is ferromagnetic and $J_2$ is anti-ferromagnetic, the competition between the couplings becomes destructive, and it is not possible to build up a phase-locking throughout either layer.

When both $J_1$ and $J_2$ are anti-ferromagnetic, then as long as one of the couplings is dominating, the lattice will align accordingly. When $J_1 = 2J_2$, we reach the fully frustrated double-layered $XY$ model.

The fully frustrated double-layered XY-model is interesting because of the spin-glass phase that exists for the single-layered XY-model despite the lack of disorder to break the translational symmetry [9; 43–49]. When moving into this phase from the ferromagnetic phase, the following symmetries are broken, a continuous one which is represented by the global transition $\phi_{\alpha,\mathbf{j}} \to \phi_{\alpha,\mathbf{j}} + \nu$, and a chiral $\mathbf{Z}_2$-symmetry is represented by $\phi_{\alpha,\mathbf{j}} \to -\phi_{\alpha_\mathbf{j}}$. There are three different possible explanations for this phase transition. It can be (*i*) a Kosterlitz-Thouless transition followed by an Ising type transition (which seems to be the consensus), (*ii*) a mixture of the two occurs for the critical temperature, or (*iii*) a transition belonging to a new universality class [43–49]. While consensus is that the phase transition is of type (*i*), this has yet to be realised experimentally.

### 5.4.3 The validity of the large detuned limit

While we know that the tight-binding approximation is valid for the *s*-*p* bipartite square lattice at resonance [50], it remains to be checked if it is also valid in the large detuned limit.

Checking this is not as straightforward as it was for the bipartite *s*-*s* lattice, as the *s*- and *p*- bands hybridise. However, one should note that even if tunnelling processes between the nearest nearest nearest lattice sites are also allowed, such process will still support an $J_1$-$J_2$ model. The question will then become if we sit at the point of frustration or

not.

## 5.5 A systematic route to frustrations in bipartite lattices

Even if it remains an open question whether the tight-binding approximation is valid or not, the treatment of the *s*-*s* and *s*-*p*- bipartite lattice in the large detuned limit shows something interesting. We see that for a bipartite square lattice, where every second lattice site freezes out, we realise a nearest-next-nearest neighbour model in which there are twice as many ways to connect nearest neighbours as next nearest neighbours.

This feature gives rise to the factor of two that the nearest neighbour couplings are stronger than the next-nearest ones. It is important to stress that it is an attribute of the bipartite square lattice. If we were to study other bipartite square lattice models, such as the *s*-*d* or the *p*-*f* bipartite square lattice, this factor of two would also show up.

# 6. A road to quantum frustration

In Chapter 5, we saw how, at least theoretically, bipartite lattice systems in the superfluid limit could be systematically used to realise models with competing nearest and next-nearest neighbour couplings. This alone makes bipartite square lattices interesting, but what can make them even more interesting is if they allow us to realise quantum frustration.

In the superfluid limit the quantum operators can be replaced by a mean-field version, and quantum correlations are suppressed. If we were to study a frustrated quantum phase, we must search in the limit where quantum fluctuations must be included. Here, we are in the the Mott phase where onsite interaction dominates over tunnelling. Thus, the atoms become almost frozen in the lattice, and we can derive an effective Hamiltonian by treating the tunnelling processes perturbatively.

In this chapter, we aim to understand how one may realise a frustrated quantum phase in the Mott phase of bipartite optical lattice systems. As we have seen before, in a square lattice a frustrated quantum phase emerges when nearest and next-nearest neighbour couplings compete in such a way that they can not simultaneously be satisfied. In this chapter, as opposed to the previous one, we study the *s*-*p* bipartite square lattice in the Mott phase. Here, the *s*-orbital states freeze out, and one is left with a $SU(2)$ spin model with both nearest and next-nearest neighbouring sites.

The spin model that emerges for the *s*-*p* lattice is not the full $J_1$-$J_2$-model. However, it does show some similarities, allowing us to compare the behaviour of the two models. Using this comparison as a starting place, we can explore more systematically what type of bipartite lattice model can lead to competing nearest and next-nearest neighbour couplings and thereby pave the route to quantum frustration.

## 6.1 The Mott phase for bipartite lattices

To understand the connection between the tunnelling processes and the spin-model they give rise to, we must understand how the tunnelling process can be expressed in the form of Schwinger Bosons which was

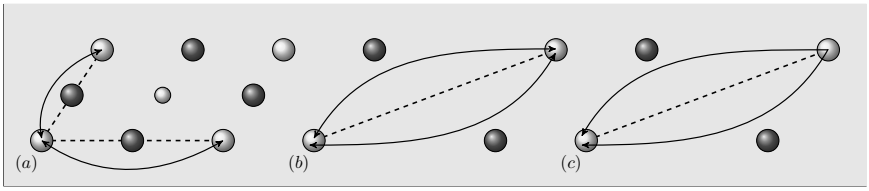


**Figure 6.1:** Transitions in a bipartite lattice leading to next-nearest neighbour ($a$) and nearest neighbour ($b$) and ($c$) couplings. For the next-nearest neighbour processes, the transitions take place along the same path out and back. For nearest neighbour processes, the transitions happen either along the same path out and back or in a loop.

discussed in Chapter 4.

As discussed in Chapter 4, the effective Hamiltonian is a summation of all allowed tunnelling processes. The $\mathcal{S}$-sites only provide an energy shift but cannot change the system's state. Hence, the effects from the $\mathcal{S}$-sites are effectively frozen out, and one can express an effective Hamiltonian for the entire system in terms of only the $\mathcal{P}$-sites.

For any bipartite square lattice, one must include fourth-order tunnelling processes to couple two of the same type of lattice sites. Thus, any lattice site will be coupled to its nearest neighbours and next-nearest neighbours of the same kind.

### 6.1.1 The fourth order transitions in the bi-bipartite lattice

For the next-nearest neighbour, there is only one way of realising a coupling between lattice sites, and that is to tunnel two steps in the $\alpha$-direction and then back along the same path (see Fig. 6.1 (a)). However, for the nearest neighbour, there are two ways of realising the coupling. In both, one starts by tunnelling one step in the $\alpha$-direction, then one tunnels one step in the $\beta$-direction. Thus, creating an atom in a $p_\beta$-orbital state at the nearest neighbour lattice site. On the way back to the original lattice site, there are two options. Either the atom tunnels back along the same path it came, by first tunnelling one step in the $\beta$-direction and then a step in the $\alpha$-direction (see Fig. 6.1 (b)). Or the atom tunnels in a loop by continuing its transition by first tunnelling a step in the $\alpha$-direction and then a step in the $\beta$-direction (see Fig. 6.1 (c)).

In the resonant limit, all lattice sites are initially occupied by the same number of atoms, and we assume that this occupation number is 1. In this limit, atoms can start and end their transitions from both

$\mathcal{P}$- and $\mathcal{S}$-sites. In the large detuned limit, only $\mathcal{P}$ lattice sites will be occupied. The $\mathcal{S}$-sites still act as mediators, but transitions can only start and end in a $\mathcal{P}$-site.

By comparing the resonant and large detuned limit, we see that the limitation of where the atoms can start and finish their transitions ensures that there are only half as many contributions to the effective Hamiltonian in the latter. While we are interested in both limits, when we discuss what kind of couplings the different transitions give rise to, we first assume that we are in the large detuned limit as this simplifies the discussion.

### Next-nearest neighbour transitions

We first consider the next-nearest neighbour transitions as they are simpler than the nearest neighbour ones. These transitions consist of an atom initially in the $i$'th lattice site, in a $p_\alpha$-orbital state. The atom tunnels twice in the $\alpha$-direction. Thus, the atom tunnels into the $j$'th lattice site into a $p_\alpha$-orbital state. This lattice site is already occupied by one atom, which can be either in an $p_\alpha$ or $p_\beta$-orbital state.

When deriving the effective Hamiltonian, one should, of course, take onsite interaction into account. As discussed in Chapter 4, the onsite interaction is either a density-density or an orbital-flipping interaction. However, the latter will flip two $p$-orbital states in the same state into the other orbital state. For next-nearest neighbour couplings, this can only mean flipping two $p_\alpha$-orbital states into two $p_\beta$-orbital states, as at least one of the atoms will be in a $p_\alpha$-orbital state after the interaction to be able to tunnel back to the initial lattice site, then the orbital-flipping interaction is forbidden for the next-nearest neighbour couplings.

Thus we see how next-nearest neighbour tunnelling processes give rise to a density-density coupling between orbital states of the same type but at different lattice sites. Using the Schwinger boson mapping leads to a Schwinger boson coupling on the form $\hat{S}^Z_{\mathbf{i}}\hat{S}^Z_{\mathbf{j}}$.

### Nearest-neighbour transitions

For nearest neighbour couplings we have two kinds of tunnelling processes, transitions that take place along the same path out and back and transitions that take place in a loop.

We consider first those transitions that take place along the same path out and back. These transitions are similar to the one we encountered for next-nearest neighbour couplings, and we find that it again leads to an $J_1^Z\hat{S}^Z_{\mathbf{i}}\hat{S}^Z_{\mathbf{j}}$ coupling. However, there are twice as many paths

that connect nearest neighbours as the path that connects next-nearest neighbours. This, combined with the couplings involving both the orbital states, thus leads to the relation between the two coupling coefficients $J_1^{ZZ} = -2J_2^{ZZ}$.

Between nearest neighbour sites, we will also have loop transitions. Here, the atom tunnels in a loop. Thus, tunnelling into an intermediate $p$-sites creates an atom in one orbital state. When it tunnels away from the site, it will annihilate an atom in the other orbital state. The onsite interaction for these processes can be either density-density interaction between different orbital states or orbital flipping interaction. Such transitions will lead to Schwinger boson couplings on the form $K\hat{S}_{\mathbf{i}}^{+}\hat{S}_{\mathbf{j}}^{-} + h.c$ and $\gamma\hat{S}_{\mathbf{i}}^{\pm}\hat{S}_{\mathbf{j}}^{\pm}$ which can be rewritten as $J_1^X\hat{S}_{\mathbf{i}}^X\hat{S}_{\mathbf{j}}^X + J_1^Y\hat{S}_{\mathbf{i}}^Y\hat{S}_{\mathbf{j}}^Y$. Here, $J_1^X = K + \gamma$ while $J_1^Y = K - \gamma$

### 6.1.2 The effective Hamiltonian for *s*-*p* lattice

To find an effective Hamiltonian for the $s$-$p$ lattice in the Mott insulating phase, we have to sum over all nearest and next-nearest neighbour transitions and determine the couplings.

Summing over all transitions means that we have to sum over not only the transitions starting and ending in $\mathcal{P}$-site but also those that start and end in an $\mathcal{S}$-site. However, the transitions that start and end in an $\mathcal{S}$-site will contribute to the same Schwinger Boson couplings, for both nearest and next-nearest neighbour lattice sites, as the transitions that started in $\mathcal{P}$-sites.

If we piece all of this together, we find that the effective Hamiltonian will be in the form

$$\begin{aligned} H_{sp} = C &+ J_{nnn}^{ZZ}\sum_{\{i,j\}} S_i^Z S_j^Z - 2J_{nnn}^{ZZ}\sum_{\langle i,j\rangle} S_i^Z S_j^Z \\ &+ J_{nn}^{XX}\sum_{\langle i,j\rangle} S_i^X S_j^X + J_{nn}^{YY}\sum_{\langle i,j\rangle} S_i^Y S_j^Y . \end{aligned} \tag{6.1}$$

While the Hamiltonian have the same terms in both the resonant and the large detuned limit, the coupling coefficients will differ. The different coupling coefficients can be found in Tab. 6.1 for both the resonant and adiabatic limit. In both limits, we see that several couplings are lacking compared to the full $J_1$-$J_2$ model. Furthermore, we also see that the sign on the nearest and next nearest neighbour couplings will differ for the $\hat{S}_{\mathbf{i}}^Z\hat{S}_{\mathbf{j}}^Z$-terms. We refer to [I] for a more detailed derivation of the coupling coefficients.

### 6.1.3 From the *s*-*p* lattice towards frustration

We are still interested in exploring if and when a Hamiltonian in the form of eq. (6.1) can support a frustrated phase in any parameter regime for the couplings.

We first note that the effective Hamiltonian in eq. (6.1) has similarities with the full $J_1$-$J_2$ model for which the Hamiltonian is

This model is one of the prime candidates for realising a Quantum Spin Liquid (QSL) phase [4; 12; 51; 52]. There is consensus that for this model, in the range of $0.41 \leq J_2/J_1 \leq 0.6$, a new quantum phase emerges. However it is still an open question if it is QSL [4; 12; 51] or if it is instead a so-called *plaquette valence-bond* phase [52].

$$\hat{H}_{J_1-J_2} = J_1 \sum_{\langle \mathbf{i},\mathbf{j} \rangle} \hat{S}_{\mathbf{i}} \cdot \hat{S}_{\mathbf{j}} + J_2 \sum_{\{\mathbf{i},\mathbf{j}\}} \hat{S}_{\mathbf{i}} \cdot \hat{S}_{\mathbf{j}} \tag{6.2}$$

Compared to the effective Hamiltonian in eq. (6.1) we see that the Hamiltonian for the full $J_1$-$J_2$ spin model has couplings of the form $\hat{S}^Z_{\mathbf{i}} \hat{S}^Z_{\mathbf{j}}$, $\hat{S}^X_{\mathbf{i}} \hat{S}^X_{\mathbf{j}}$ and $\hat{S}^Y_{\mathbf{i}} \hat{S}^Y_{\mathbf{j}}$ for both nearest and next nearest neighbouring lattice sites. The effective Hamiltonian for the *s*-*p*-lattice does not have all these couplings. However, it is still interesting to study if a "weaker" Hamiltonian could also support a truly quantum phase.

Even with state-of-the-art numerical methods, it is hard (if not impossible) to fully characterise such quantum phases. We do not aim for a complete characterisation but rather to see if it is possible that "weaker" versions of the $J_1$-$J_2$-model can also host novel quantum phases.

#### The phase diagram for the "weaker" $J_1$-$J_2$-models

Our starting point for exploring the possibility of realising frustrated quantum phases for "weaker " $J_1$-$J_2$ models is first to consider the classical $J_1$-$J_2$ models phase diagram. To do so, we replace the Schwinger Bosons with Ising spins $s = \pm 1$. This model gives has a phase diagram consisting of four phases (see Fig. 6.2(a)) [8]. The phase diagram shows two antiferromagnetic phases, the Néel and striped phases, which both survive at zero fields, and a ferromagnetic/polarised phase that first appears for sufficiently strong fields. Finally, a *disordered phase* that also only exists for non-vanishing fields.

To see how the quantum fluctuations which arise for non-zero $J_1^X$ and $J_1^Y$ affect the phase diagram, we introduce an energy functional. This energy functional can be minimised to find a first approximation for the ground state by replacing the Schwinger boson operators in the effective Hamiltonian eq. (6.1) with coherent spin states.

| | Resonant $s$-$p$ | Adiabatic limit |
|---|---|---|
| $C_{NN}$ | $-2t^4\left(\frac{3V_{zz}}{U_{ss}^2}+\frac{9V_{zz}^2}{4}\right)$ | $-2t^4\frac{3V_{zz}}{4\Delta^2}$ |
| $J_{NN}^{XX}$ | $-4t^4\left(\frac{V_{xx}}{U_{ss}^2}-\frac{V_{xx}^2}{U_{ss}}\right)$ | $-t^4\left(\frac{V_{xx}}{\Delta^2}\right)$ |
| $J_{NN}^{YY}$ | $-4t^4\left(\frac{V_{yy}}{U_{ss}^2}+\frac{V_{yy}^2}{U_{ss}}\right)$ | $-t^4\left(\frac{V_{yy}}{\Delta^2}\right)$ |
| $J_{NN}^{ZZ}$ | $-2t^4\left(\frac{4V_{zz}}{U_{ss}^2}+V_{zz}^2\right)$ | $-2t^4\frac{V_{zz}}{\Delta^2}$ |
| $C_{NNN}$ | $t^4\left(\frac{3V_{zz}}{U_{ss}^2}+\frac{9V_{zz}^2}{4}\right)$ | $t^4\frac{3V_{zz}}{4\Delta^2}$ |
| $J_{NNN}^{ZZ}$ | $t^4\left(\frac{4V_{zz}}{U_{ss}^2}+V_{zz}^2\right)$ | $t^4\frac{V_{zz}}{\Delta^2}$ |

**Table 6.1:** The coupling coefficients for $s$-$p$ bipartite square lattice. To make the expression above as compact as possible, we have used the notation $V_{xx}=-\frac{U^2-120U_{xy}^2}{U^2U_{xy}}$, $V_{yy}=\frac{U^2+120U_{xy}^2}{U^2U_{xy}}$, $V_{zz}=\frac{4\tilde{U}}{U^2}+\frac{1}{2U_{xy}}$, and $V_x=\frac{U^2+6(\tilde{U}-5U_{xy})U_{xy}}{U^2U_{xy}}$. Note the relation between $V_{xx}$ and $V_{yy}$. One could choose another notation where one could express them as $V_{xx}=K-\gamma$ and $V_{yy}=K+\gamma$.

We introduce a coherent spin state

$$\left(\hat{S}_{\mathbf{i}}^X,\hat{S}_{\mathbf{i}}^Y,\hat{S}_{\mathbf{i}}^Z\right)=\left(S\sin(\theta_{\mathbf{i}})\cos(\phi_{\mathbf{i}}),S\sin(\theta_{\mathbf{i}})\sin(\phi_{\mathbf{i}}),S\cos(\theta_{\mathbf{i}})\right), \tag{6.3}$$

where the size of the spin is $S=1/2$.

To distinguish different phases, we introduce a quantity that we call the *full correlator* $\mathcal{C}_{\text{full}}$

$$\mathcal{C}_{\text{full}}=\frac{1}{N}\left(\sum_{\mathbf{i}}\langle S_{\mathbf{i}}^Z\rangle+\frac{1}{2}\sum_{\langle\mathbf{i},\mathbf{j}\rangle}C^{zz}(\mathbf{i},\mathbf{j})+\frac{1}{2}\sum_{\{\mathbf{i},\mathbf{j}\}}C^{zz}(\mathbf{i},\mathbf{j})\right). \tag{6.4}$$

$\mathcal{C}_{\text{full}}$ is limited by $-1\leq\mathcal{C}_{\text{full}}\leq 1$, and we note that for the four phases mentioned above we find that $\mathcal{C}_{\text{full}}=1$ for the ferromagnetic phase, $\mathcal{C}_{\text{full}}=0$ for the Néel phase, $\mathcal{C}_{\text{full}}=-1$ for the striped phase, and that $\mathcal{C}_{\text{full}}=-1/2$ for the disordered phase.

When $J_x=J_y=0$, we find that the disordered phase first emerges for a field of $2J_1\leq h\leq 4J_1$ depending on the ration $J_2/J_1$. This limit has also been studied in the quantum limit, where one finds that a magnetisation plateau caused by an order-by-disorder mechanism emerges for $h=4J_1$ [53; 54]. In the quantum limit, the phase is called *uuud* (up-up-up-down), which describes how the spins for a single plaquette align.

When $J_x$ and $J_y$ become non-zero, our model is no longer integrable and quantum fluctuations set in (see Fig.6.2). Here the phase transitions between the disordered, the ferromagnetic, and the striped phases become continuous. As we increase $J_1^X$ and $J_1^Y$ we see how the classical disordered phase (pink in (a)) is reduced, and how a potentially new phase emerges even for zero field $h = 0$ (light pink in (f)), which is given the name *transverse disordered* in [53].

When $J_1^X$ ($J_1^Y$ ) is of the same order as $J_1^Z$, the new phase seems to survive down to $J_2^Z/J_1^Z \approx -1$, the survival of this phase gives us hope that, even in the parameter regime where our *s-p* model exists, something interesting could happen for $J_2^Z/J_1^Z = -1/2$.

However, with mean-field analysis, one cannot further distinguish this region, *e.g.*, determine if this is the sign of the *uuud* phase or other exotic phases emerging [55]. If we return to the full $J_1$-$J_2$ model, it has been shown that the new quantum phase that emerges for $0.42 \lesssim J_2/J_1 \lesssim 0.62$ only survives for moderate fields, while if the field becomes strong enough, a 'transverse disordered' phase is likely to emerge [53–55].

While we would like to explore how our model behaves in the quantum limit, it will, even for very small lattice systems, be computationally hard to do so, and one would have to realise such a phase to determine if it is a QSL or not. With this disclosure, we, of course, do not expect a definitive answer to whether our model can host a QSL or not.

However, when the full correlator $\mathcal{C}_{\text{full}}$ is found using exact diagonalisation for a $4 \times 4$ lattice, we see that though, as expected, the finite-size effects cause the crossover region between the two antiferromagnetic phases to extend further, a plateau still forms in the parameter regime where we from mean-field analysis predicts that a fifth phase could arise (see Fig. 6.3).

## 6.2 From transitions to quantum spin-couplings

We have seen an example of how a nearest-next-nearest neighbour spin model emerges for a bipartite lattice in the Mott phase. While the spin-model that the *s-p*-bipartite lattice gives rise to does not host a frustrated phase, we saw how the competing couplings arise naturally in a bipartite lattice system where we can freeze out one type of the lattice sites.

A first step towards designing (bipartite) lattice systems in such a way that we, through controllable parameters, can realise interesting quantum spin-models is to understand the connection between transitions and the spin-couplings they give rise to. Taking a step back, we

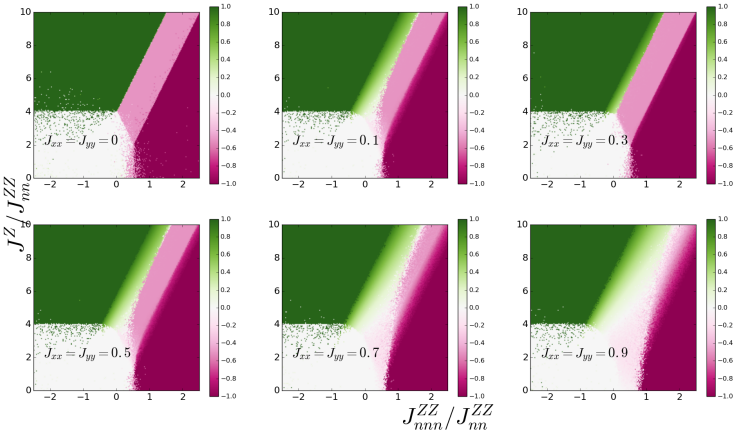


**Figure 6.2:** Fig.(a) shows the phase diagram for the "weaker" $J_1$-$J_2$ spin model for increasing $J_{XX}$ and $J_{YY}$ couplings. As this coupling increases a potential new fifth phase emerges.

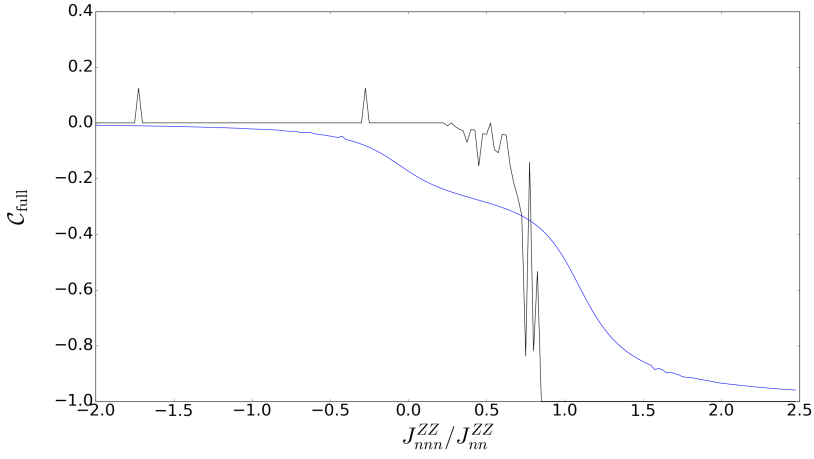


**Figure 6.3:** The full correlator $\mathcal{C}_{\text{full}}$ found using exact diagonalisation for a $4 \times 4$ lattice for the the "weaker" $J_1$-$J_2$ spin model. Here a plateau still forms in the regime where the mean-field analysis predicts that a fifth phase could emerge.

can summarise what we have learned. The contribution from the $\mathcal{P}$-sites causes the quantum spin-model. These contributions can be understood by what kind of contribution each of the lattice sites gives rise to two. Each lattice site can give rise to either a *density term* $\hat{n}_\alpha = \hat{a}^\dagger_\alpha \hat{a}_\alpha$ or a *flip term* $\hat{a}^\dagger_\alpha \hat{a}_\beta$. The density term can be expressed in terms of the $\hat{S}^Z_{\mathbf{i}}$ operator, whereas the flip term can be expressed in terms $\hat{S}^\pm$ depending on if it flips an $x$-orbital state to a $y$-orbital state or vice versa.

- When the contribution from both $\mathcal{P}$-sites are density contributions, we have density-density couplings. From eq.(4.52) we see that such couplings can be expressed as $\hat{S}^Z_{\mathbf{i}} \cdot \hat{S}^Z_{\mathbf{j}}$ couplings. There are two possibilities, depending on if densities associated with the two lattice sites are for the same orbital state or not.

  - If the two densities are for the same orbital state, *i.e.* $\hat{n}_{x_{\mathbf{i}}}$ and $\hat{n}_{x_{\mathbf{j}}}$, then the sign on the coupling will be positive.
  - If the two densities are different orbital states, *i.e.* $\hat{n}_{x_{\mathbf{i}}}$ and $\hat{n}_{y_{\mathbf{j}}}$ ,the sign on the coupling will be negative

- When the contributions from both $\mathcal{P}$-sites are flip contributions they give rise to either an $\hat{S}^+_{\mathbf{i}}$ or $\hat{S}^-_{\mathbf{i}}$ from each lattice site. Thus, when combining two flip terms, then as with the density-density terms, there will be two types.

  - For terms where the flip associated with each lattice site is different, that is $\hat{a}^\dagger_{\alpha,\mathbf{i}} \hat{a}_{\beta,\mathbf{i}}$ and $\hat{a}^\dagger_{\beta,\mathbf{j}} \hat{a}_{\alpha,\mathbf{i}}$, we have what we shall call a flip-coupling. In terms of Schwinger bosons, such a coupling will have the form $\hat{S}^+_{\mathbf{i}} \hat{S}^-_{\mathbf{j}} + \hat{S}^-_{\mathbf{i}} \hat{S}^+_{\mathbf{j}} = \hat{S}^X_{\mathbf{i}} \hat{S}^X_{\mathbf{j}} + \hat{S}^Y_{\mathbf{i}} \hat{S}^Y_{\mathbf{j}}$
  - For terms where the flip associated with each lattice site is the same, that is $\hat{a}^\dagger_{\alpha,\mathbf{i}} \hat{a}_{\beta,\mathbf{i}}$ and $\hat{a}^\dagger_{\alpha,\mathbf{j}} \hat{a}_{\beta,\mathbf{i}}$, we have what we shall call a double-flip-coupling. In terms of Schwinger bosons, such a coupling will have the form $\hat{S}^-_{\mathbf{i}} \hat{S}^-_{\mathbf{j}} + \hat{S}^-_{\mathbf{i}} \hat{S}^-_{\mathbf{j}} = \hat{S}^X_{\mathbf{i}} \hat{S}^X_{\mathbf{j}} - \hat{S}^Y_{\mathbf{i}} \hat{S}^Y_{\mathbf{j}}$

- Finally there is also **density-flip** terms. Here one lattice site give rise to a density term,*i.e.* $\hat{n}_{x_{\mathbf{i}}}$, while the other lattice site give rise to a flip term, *i.e.* $\hat{a}^\dagger_{\beta_{\mathbf{j}}} \hat{a}_{\alpha_{\mathbf{i}}}$. Thus, the **density-flip** terms give rise to couplings on the form of $S^Z_{\mathbf{i}} S^X_{\mathbf{j}}$. These couplings more general expressed as $\hat{S}_{\mathbf{i}} \times \hat{S}_{\mathbf{j}}$ and are called *Dzyaloshinskii–Moriya* terms.

## 6.3 Three different routes towards a potential frustrated phase

With the quantum spin model that emerged for the bipartite $s$-$p$ lattice there were several obstacles in terms of realising the full $J_1$-$J_2$ model. Most notable were that it lacked some of the couplings between next-nearest neighbour lattice sites.

In the following, we discuss three approaches toward regaining these lost terms. First we consider a $p$-square lattice with both nearest and next nearest neighbour tunnelings, then we look at a $s$-$d$-bipartite lattice, and finally we look at the $p$-$f$-bipartite lattice in the large detuned limit. Each of these approaches has advantages and disadvantages, and neither gives us the full $J_1$-$J_2$-model.

However, our main interest is to understand the connection between the tunnelling processes and Schwinger boson couplings. We shall in all three examples assume we are in the isotropic limit, an that we can ignore any contributions from a $\hat{S}^Z$ field.

While the inclusion of onsite interaction is of course crucial for the dynamics of the system, the exact contribution has less interest. For the two last systems we are about to study, we label the onsite interaction that preserves the orbital state by $K_1$ and one that flip the orbital state by $K_2$. While this distinction for these two systems, it is not sufficient for the $p$-square lattice. Here, we must include a third coupling and thus we shall for this system label the onsite contributions by

### 6.3.1 Frustration in the $p$-square lattice

The easiest way to realise a frustration in the Mott phase would be to explore if there is a regime where the $p$-square lattice have both nearest and next-nearest neighbour tunnelling processes.

In the regular $p$-square lattice an $p_\alpha$-orbital state can tunnel to another $p_\alpha$-orbital state in both the $\alpha$ and $\beta$-direction. In an isotropic system, the tunnelling coefficient depends on if the strength of the tunnelling process depends on if the tunnelling process takes place in the direction of the node. If it takes place in the direction of the node we label it $t_1$ and if it takes place . Here, the effective Hamiltonian can be expressed on the form

$$\hat{H}^{pp}_{\text{eff}} = \sum_{\langle i,j \rangle} (t_1^4 + t_2^4) J^{ZZ} \hat{S}^Z_{\mathbf{i}} \hat{S}^Z_{\mathbf{j}} + 2t_1^2 t_2^2 \left( J^{XX} \hat{S}^X_{\mathbf{i}} \hat{S}^X_{\mathbf{j}} + J^{YY} \hat{S}^Y_{\mathbf{i}} \hat{S}^Y_{\mathbf{j}} \right)$$

To include next-nearest neighbour couplings in an isotropic system, we introduce the tunnelling strength $t_3$. If the system is isotropic, then

next-nearest neighbour tunnelling processes will look similar to the nearest neighbour ones, and the next nearest neighbour couplings can be found by replacing $t_1$ and $t_2$ in the nearest neighbour couplings by $t_3$. Thus, including next-nearest neighbor tunnellings leads to an effective Hamiltonian on the form

$$\begin{aligned}\hat{H}_{\text{eff}}^{pp} = &\sum_{\langle i,j\rangle}(t_1^4+t_2^4)J^{ZZ}\hat{S}_{\mathbf{i}}^Z\hat{S}_{\mathbf{j}}^Z + 2t_1^2t_2^2\left(J^{XX}\hat{S}_{\mathbf{i}}^X\hat{S}_{\mathbf{j}}^X + J^{YY}\hat{S}_{\mathbf{i}}^Y\hat{S}_{\mathbf{j}}^Y\right)\\ &+2t_3^4\sum_{\{i,j\}}J^{ZZ}\hat{S}_{\mathbf{i}}^Z\hat{S}_{\mathbf{j}}^Z + \left(J^{XX}\hat{S}_{\mathbf{i}}^X\hat{S}_{\mathbf{j}}^X + J^{YY}\hat{S}_{\mathbf{i}}^Y\hat{S}_{\mathbf{j}}^Y\right)\end{aligned} \tag{6.5}$$

While this looks promising. However, as we are aiming for a $J_1$-$J_2$ model where $J_1 \approx 2J_2$ there will be a lot of conditions that needs to be fulfilled simultaneously, and as the three tunnelling coefficients are not independent it might be hard to do in a regime where this model has competing nearest and next-nearest neighbour couplings.

### 6.3.2 The *s*-*p* bipartite lattice

One of the limitations with the $s$-$p$ bipartite lattice was that it only allowed a $p_\alpha$-orbital state to tunnel in the $\alpha$-direction. The mechanism behind the restriction on allowed tunnellings can be understood by looking at the harmonic approximation. In this limit, the Wannier functions approaches the Hermite polynomials. For the $p_\alpha$-orbital state, the Hermite polynomial is odd in the $\alpha$-variable, and even in the $\beta$-variable, the Hermite polynomial for the $s$-orbital state is even in both variables, and so is the potential. Thus, due to the even and odd nature tunnelling will only be allowed in the direction of the node. However, had the Hermite polynomials for the $p_\alpha$-orbitals instead been even functions in both variables, then tunnelling would have been allowed in both directions.

Hence, a natural starting point when searching for spin models where nearest and next-nearest couplings compete is to search for a system where tunnelling is allowed in both directions for the double degenerated orbital state. While there are three $d$-orbital states in in two dimensions, only two of them will be degenerated [30]. Since the $d$-orbital states are double degenerated, we may apply the Schwinger boson mapping for this system as well. Thus, we will also for the $s$-$d$-lattice reach a Schwinger boson model.

#### An effective Hamiltonian for *s*-*d*-lattice

For the $d$-orbital states, even though the Hermite polynomial are even functions in both variables, they still have a shape with a node in one

direction (see Fig. 4.2). Intuitively this means, that in an isotropic lattice, there are two relevant tunnelling coefficients. One for tunnelling in the direction parallel to the node of the relevant orbital state, and one for tunnelling in the direction perpendicular to the node of the relevant orbital state. We shall label them $t_1$ and $t_2$ respectively. We assume that we are in the large detuned limit, and thus all process starts and end in a $\mathcal{D}$-site, but we can use the same argument as for the *s-p* lattice to see that if we were not in the large detuned limit the transitions that starts and end in a $\mathcal{S}$-site would give contributions on the same form.

With all of this in mind, and using that $2\hat{S}^X = \left(\hat{S}^+_{\mathbf{j}} + \hat{S}^-_{\mathbf{j}}\right)$, we may express the contributions to the effective Hamiltonian from the transitions that travels out and back along the same path as

$$\begin{aligned}\hat{H}^{sd}_{\text{path}} = \sum_{\mathbf{i},\mathbf{j}} &\left(\tilde{t}_1^2 + (-1)^{\sigma}\tilde{t}_2^2\hat{S}^Z_{\mathbf{i}} + 2\tilde{t}_3^2\hat{S}^X_{\mathbf{i}}\right) \\ &\left(\tilde{t}_1^2 K_1 + (-1)^{\sigma'}\tilde{t}_2^2 K_1\hat{S}^Z_{\mathbf{j}} + 2\tilde{t}_3^2 K_2\hat{S}^X_{\mathbf{j}}\right)\end{aligned} \tag{6.6}$$

here $\sigma$ and $\sigma'$ are used to label the direction of the path, taking the value 1 for the $x$ direction and $-1$ for the $y$-direction, and we have introduced the the notation $\tilde{t}_1^2 = t_1^2 + t_2^2$, $\tilde{t}_2^2 = t_1^2 - t_2^2$, and $\tilde{t}_3^2 = t_1 t_2$. The contribution from the loop term is slightly different. Here,

$$\hat{H}^{sd}_{\text{loop}} = \sum_{\langle \mathbf{i},\mathbf{j}\rangle} \left[\tilde{t}_3^2 + \tilde{t}_1^2\hat{S}^X_{\mathbf{i}}\right]\left[\tilde{t}_3^2 K_1 + 2\tilde{t}_1^2 K_2\hat{S}^X_{\mathbf{j}}\right] \tag{6.7}$$

Introducing the notation $J^X = C_X\tilde{t}_3^2\tilde{t}_1^2(K_1+K_2)$, $J^{XX} = 4K_2\tilde{t}_3^4$, $J^{ZZ} = \tilde{t}_2^4 K_1$ and $J^{ZX} = \tilde{t}_3^2\tilde{t}_2^2(K_1+K_2)$. Thus the non-loop terms contribution to the effective Hamiltonian takes the form,

$$\begin{aligned}\hat{H}^{sd}_{\text{path}} = J^X\sum_{\mathbf{i}} S^X_{\mathbf{i}} + 2\sum_{\langle \mathbf{i},\mathbf{j}\rangle} J^{XX}\hat{S}^X_{\mathbf{i}}\hat{S}^X_{\mathbf{j}} - J^{ZZ}\hat{S}^Z_{\mathbf{i}}\hat{S}^Z_{\mathbf{j}} \\ + \sum_{\{\mathbf{i},\mathbf{j}\}_\sigma} J^{XX}\hat{S}^X_{\mathbf{i}}\hat{S}^X_{\mathbf{j}} + J^{ZZ}\hat{S}^Z_{\mathbf{i}}\hat{S}^Z_{\mathbf{j}} + (-1)^{\sigma}J^{ZX}(\hat{S}^X_{\mathbf{i}}\hat{S}^Z_{\mathbf{j}} + \hat{S}^Z_{\mathbf{i}}\hat{S}^X_{\mathbf{j}}).\end{aligned} \tag{6.8}$$

and the loop terms contribution takes the form

$$\hat{H}^{sd}_{\text{loop}} = J^X\sum_{\mathbf{i}}\hat{S}^X_{\mathbf{i}} + 2\sum_{\langle \mathbf{i},\mathbf{j}\rangle}\frac{\tilde{t}_1^4}{\tilde{t}_3^4}J^{XX}\hat{S}^X_{\mathbf{i}}\hat{S}^X_{\mathbf{j}}. \tag{6.9}$$

### 6.3.3 The *p-f* bipartite lattice in the large detuned limit

We have now seen how, both for the *s-p* and the *s-d* bipartite lattice, the density-density couplings between nearest and next nearest neighbour

lattice sites will have different signs. The reason for this is that for the $s$-$p$, the $s$-orbital sites wipes the memory of the previous state of the system.

To circumvent this, we wish to realise a system where the $s$-orbital states preserve the memory of the orbital state that the atom occupied in the $\mathcal{P}$-sites. This, is not possible for $s$-orbital states as there is only one type of $s$-orbital state. However, if we instead envision a $p$-$f$ bipartite lattice, then both types of lattice sites orbital states that are double degenerated.

To see that the $f$-orbital states are also double degenerated, we recall that there are four $f$-orbital states in two dimensions. These four functions come in two pairs of two. A pair consisting of the $f_{x^3}$- and $f_{y^3}$- orbital state, and a pair consisting of the $f_{x^2y}$- and the $f_{xy^2}$-orbital state. We may thus assume that for an isotropic system, the energies are only two times and not four times degenerated.

If we consider the first of these pairs, then the relevant Hermite polynomial are odd functions in the direction of the node, and we tunnelling between an $\mathcal{F}$ site and a $\mathcal{P}$ site will therefore only be allowed for a $p_\alpha$-orbital state to an $f_\alpha$-orbital state and vice versa.

### Adiabatic elimination

In the large detuned limit one type of lattice site will be empty to begin with, and we assume that the empty lattice sites are the $\mathcal{F}$-sites. Even though the $\mathcal{F}$-sites are initially empty, they can still act as mediators that serves at coupling $p$-sites. Thus, we can realise an effective model with both nearest and next-nearest neighbour couplings. To see this, we apply the adiabatic elimination as we did in Chapter 4

$$\begin{aligned}
\partial_t \hat{f}_{\alpha_{\mathbf{i}}} &= +it_\alpha^\alpha \left(\hat{p}_{\alpha_{\mathbf{i}+\mathbf{1}_\alpha}} + \hat{p}_{\alpha_{\mathbf{i}-\mathbf{1}_\alpha}}\right) + t_\alpha^\beta \left(\hat{p}_{\alpha_{\mathbf{i}+\mathbf{1}_\beta}} + \hat{p}_{\alpha_{\mathbf{i}-\mathbf{1}_\beta}}\right) \\
&\quad -i\Delta \hat{f}_{\alpha_{\mathbf{i}}} + \text{int. terms}, \\
\partial_t \hat{p}_{\alpha_{\mathbf{j}}} &= it_\alpha^\alpha \left(\hat{f}_{\alpha_{\mathbf{j}+\mathbf{1}_\alpha}} + \hat{f}_{\alpha_{\mathbf{j}-\mathbf{1}_\alpha}}\right) + it_\alpha^\beta \left(\hat{f}_{\alpha_{\mathbf{j}+\mathbf{1}_\beta}} + \hat{f}_{\alpha_{\mathbf{j}-\mathbf{1}_\beta}}\right) \\
&\quad +\text{int. terms}.
\end{aligned} \tag{6.10}$$

We find the steady state solution for the $f$-orbitals by assuming that $\partial_t \hat{f}_\alpha = 0$. As the $\mathcal{F}$-sites initially are empty, we shall also assume the

contributions from onsite interaction at these sites are zero.

$$\hat{f}^{(\mathrm{ff})}_{\alpha_{\mathbf{i}}} = \frac{t^{\alpha}_{\alpha}}{\Delta}\left(\hat{p}_{\alpha_{\mathbf{i}+\mathbf{1}_{\alpha}}} + \hat{p}_{\alpha_{\mathbf{i}-\mathbf{1}_{\alpha}}}\right) + \frac{t^{\beta}_{\alpha}}{\Delta}\left(\hat{p}_{\alpha_{\mathbf{i}+\mathbf{1}_{\beta}}} + \hat{p}_{\alpha_{\mathbf{i}-\mathbf{1}_{\beta}}}\right). \tag{6.11}$$

Expressing the time evolution of the $p$-orbitals requires slightly more care. Here, we have divided the contributions into nearest $\hat{h}_1$ and next-nearest neighbour $\hat{h}_2$ ones.

$$\partial_t \hat{p}_{\alpha_{\mathbf{j}}} = \hat{h}_2 + \hat{h}_1 + \text{int. terms}. \tag{6.12}$$

We look at the next-nearest neighbour contribution first, which we may express as

$$\begin{aligned} \hat{h}_2 \;=\; & i\tfrac{(t^{\alpha}_{\alpha})^2}{\Delta}\left(\hat{p}_{\alpha_{\mathbf{j}+\mathbf{2}_{\alpha}}} + \hat{p}_{\alpha_{\mathbf{j}-\mathbf{2}_{\alpha}}} + 2\hat{p}_{\alpha_{\mathbf{j}}}\right) \\ & + i\tfrac{(t^{\beta}_{\alpha})^2}{\Delta}\left(\hat{p}_{\alpha_{\mathbf{j}+\mathbf{2}_{\beta}}} + \hat{p}_{\alpha_{\mathbf{j}-\mathbf{2}_{\beta}}} + 2\hat{p}_{\alpha_{\mathbf{j}}}\right), \end{aligned} \tag{6.13}$$

Similarly, there are terms which describe a coupling in the diagonal directions between two $\mathcal{P}$-lattice sites, these are nearest neighbouring (NN) couplings, and such terms take the form

$$\hat{h}_1 = i\frac{2t^{\alpha}_{\alpha}t^{\beta}_{\alpha}}{\Delta}\left(\hat{p}_{\alpha_{\mathbf{j}+\mathbf{1}_{\alpha}+\mathbf{1}_{\beta}}} + \hat{p}_{\alpha_{\mathbf{j}+\mathbf{1}_{\alpha}-\mathbf{1}_{\beta}}} + \hat{p}_{\alpha_{\mathbf{j}-\mathbf{1}_{\alpha}+\mathbf{1}_{\beta}}} + \hat{p}_{\alpha_{\mathbf{j}-\mathbf{1}_{\alpha}-\mathbf{1}_{\beta}}}\right). \tag{6.14}$$

From these equations, it is straightforward to derive an effective Hamiltonian for the $p$-orbital via

$$\partial \hat{p}_{\alpha_{\mathbf{j}}} = -i\left[\hat{p}_{\alpha_{\mathbf{j}}}, \hat{H}_{\mathrm{eff}}\right]. \tag{6.15}$$

and we find that

$$\begin{aligned} \hat{H}_{\mathrm{eff}} \;=\; & \tfrac{2t^{\alpha}_{\alpha}t^{\beta}_{\alpha}}{\Delta}\textstyle\sum_{\langle i,j\rangle}\sum_{\alpha}\hat{p}^{\dagger}_{\alpha}\hat{p}_{\alpha_{\mathbf{j}}} + \tfrac{(t^{\alpha}_{\alpha})^2}{\Delta}\sum_{\alpha}\sum_{\{i,j\}_{\alpha}}\hat{p}^{\dagger}_{\alpha_{\mathbf{i}}}\hat{p}_{\alpha_{\mathbf{j}}} \\ & + \tfrac{(t^{\beta}_{\alpha})^2}{\Delta}\textstyle\sum_{\beta}\sum_{\{i,j\}_{\alpha_{\mathbf{i}}}}\hat{p}^{\dagger}_{\alpha}\hat{p}_{\alpha_{\mathbf{j}}} + \text{int. terms}. \end{aligned} \tag{6.16}$$

**Couplings in the $p$-$f$-bipartite lattice**

The mediating $\mathcal{F}$-site will preserve the orbital state of the tunnelling atom ensures that all tunnelling processes, no matter their path, can be considered to be on one of two types.

- The atom is initially in a $p_\alpha$-orbital state, and thus it tunnels into another $p_\alpha$-orbital state. An onsite interaction takes place, before the atom tunnels back. The atom that tunnels back is also in an $p_\alpha$-orbital state .Thus, this term gives rise to a density-density-coupling, between atoms in the same orbital state.

- The atom is initially in a $p_\alpha$-orbital state, and thus it tunnels into another $p_\alpha$-orbital state. An onsite interaction takes place, before the atom tunnels back. The atom that tunnels back is also in an $p_\beta$-orbital state .Thus, this term gives rise to only a flip-coupling but no double-flip-coupling.

That the density-density coupling between atoms in different orbital states and the double flip coupling are forbidden follows as both requires that the mediating $\mathcal{F}$-site does not preserve the orbital state.

**The effective Hamiltonian**

In an isotropic system we can assume that $t_x^x = t_y^y = t_1$ and that $t_x^y = t_y^x = t_2$. Thus the contributions to the effective Hamiltonian coming from the non-loop transitions can be expressed as

$$\begin{aligned}\hat{H}_{\text{eff}}^{\text{loop}} &= 4t_1^2 t_2^2 \textstyle\sum_{\langle i,j\rangle} K_1 \left(\frac{3}{4} + \hat{S}_{\mathbf{i}}^Z \hat{S}_{\mathbf{j}}^Z\right) + K_2 \left(\hat{S}_i^X \hat{S}_{\mathbf{j}}^X + \hat{S}_{\mathbf{i}}^Y \hat{S}_{\mathbf{j}}^Y\right) \\ &\quad + \textstyle\sum_{\{i,j\}} \left(t_1^4 + t_2^4\right) K_1 \left(\frac{3}{4} + \hat{S}_{\mathbf{i}}^Z \hat{S}_{\mathbf{j}}^Z\right) + 2t_1^2 t_2^2 K_2 \left(\hat{S}_i^X \hat{S}_{\mathbf{j}}^X + \hat{S}_{\mathbf{i}}^Y \hat{S}_{\mathbf{j}}^Y\right)\end{aligned} \tag{6.17}$$

and the contributions from the loop terms is

$$\hat{H}_{\text{eff}}^{\text{loop}} = 4t_1^2 t_2^2 \sum_{\langle i,j\rangle} K_1 \left(\frac{3}{4} + \hat{S}_{\mathbf{i}}^Z \hat{S}_{\mathbf{j}}^Z\right) + K_2 \left(\hat{S}_i^X \hat{S}_{\mathbf{j}}^X + \hat{S}_{\mathbf{i}}^Y \hat{S}_{\mathbf{j}}^Y\right) \tag{6.18}$$

which are identically to the other next nearest neighbour contributions.

What we note is that without the loop contributions, the nearest neighbour couplings would be roughly a factor two stronger than the next nearest ones. However, with the inclusion of the loop terms their relative strength increases to a factor four.

## 6.4 Outlook

Frustration in a square lattice arises when nearest, and next-nearest neighbour couplings compete. A systematic way to realise such competition is to work with bipartite lattice systems.

In the superfluid phase, when saw how the bipartite lattice when it is in the large detuned limit, brings us exactly at the point of frustration. In the Mott-phase we are not guaranteed frustration in the same way, but the bipartite nature of the lattice, ensures that both for in the resonant and the large detuned limit, that there are more transition paths between nearest neighbours than between next-nearest neighbors, something that the standard square lattice fails to do.

While non of the bipartite lattices we discussed in this chapter reproduces the full $J_1$-$J_2$, they do increase our insight into how such a model can be realised and what obstacles we face in an optical lattice setting.

One of the strengths of working with in an optical lattice setting, it is theoretically possible to control both the relative depth of the lattice sites and what orbital states they support. Thus we can at least theoretically design systems in both the resonant and large detuned limit with the purpose of realising specific spin couplings.

When it comes to actually realising a full $J_1$-$J_2$ model, the system of those we have discussed that comes the closest is the $p$-$f$-bipartite square lattice. Here, the couplings between nearest and next-nearest neighbors are almost identical up to a factor of four. However, at first glance the nearest neighbor couplings are a factor of four stronger than the the next-nearest ones, which makes it likely that they will dominate rather than compete. We can however address this, by letting the contributions from the loop processes enclose a flux $\phi$. If we can realise this, then we may replace the contribution in eq. (6.18) by

$$\hat{H}_{\text{eff}}^{\text{loop}} = 4t_1^2 t_2^2 \cos(\phi) \sum_{\langle i,j \rangle} K_1 \left( \frac{3}{4} + \hat{S}_{\mathbf{i}}^Z \hat{S}_{\mathbf{j}}^Z \right) + K_2 \left( \hat{S}_i^X \hat{S}_{\mathbf{j}}^X + \hat{S}_{\mathbf{i}}^Y \hat{S}_{\mathbf{j}}^Y \right) \quad (6.19)$$

Doing so, introduces a tuneable parameter $\phi$. By controlling this $\phi$, we can control the couplings and we see how the that for $\phi = 0$ the nearest neighbor coupling is a factor for stronger than the next nearest neighbour ones, then for $\phi = \frac{\pi}{2}$ it will be a factor two stronger, and for $\phi = \pi$ the nearest neighbour coupling will almost vanish.

# Part III

# Fock state lattices

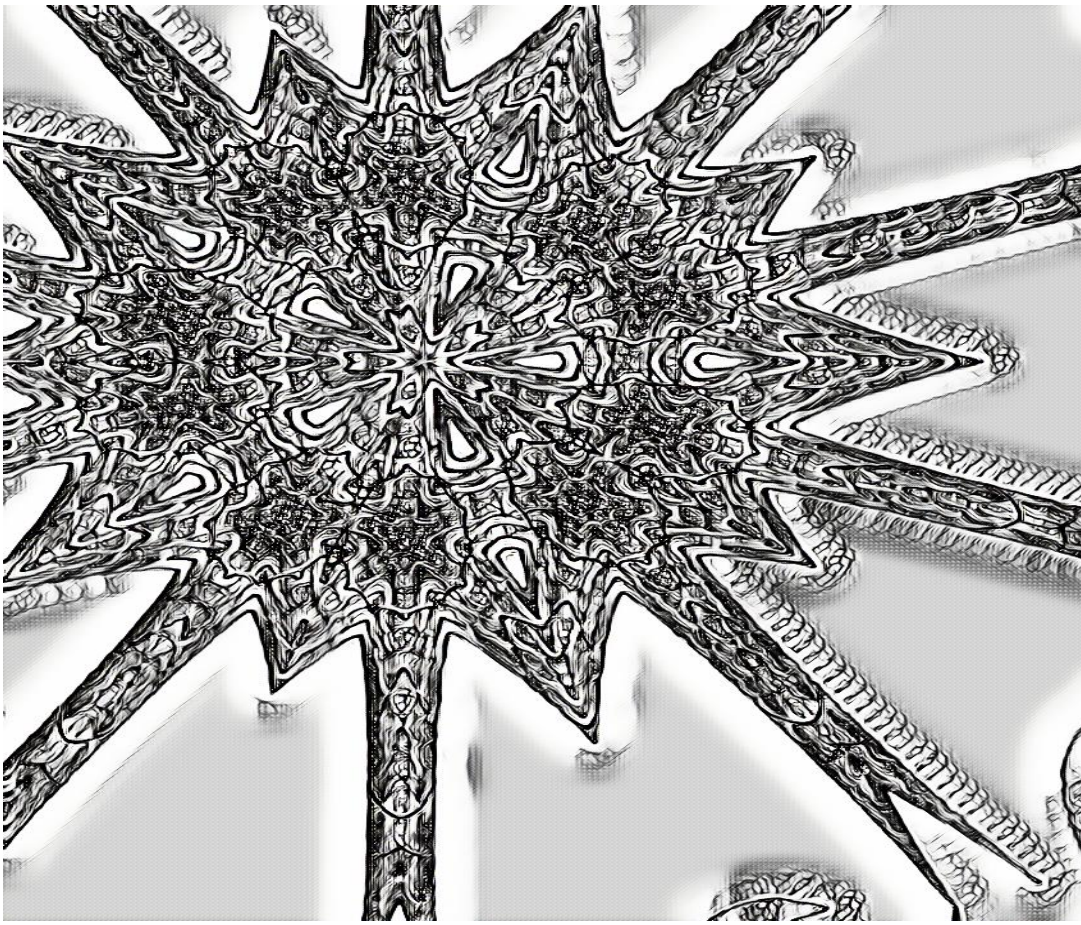

# 7. Fock state lattices

The quantum lattice structures we have thought about so fare are structures in real space. Here, the lattice geometry were linked to the spatial dimensions and we envisioned lattices in low dimensions. Mathematically speaking there is no such restriction and physically there does not need to be one either.

In physical lattices, higher dimensions may be realised by introducing one or more *synthetic dimension* by considering internal particle state [56–59]. Thus, the lattice is a structure in a mixture of real and state space. As a general strategy, one can expand a $D$-dimensional lattice structure to a $(D+1)$-dimensional one, where the extra dimension emerges due to an internal atomic degree-of-freedom [56].

Taking it one step further, one may consider entire lattice structures living in state space. Here, the system's quantum states play the role of lattice sites. Transitions between any two states play the role of tunnellings in the lattice, thus ordering the lattice into a geometric structure. Though this has already been done by some [59–61] as a general approach, it remains largely unexplored. Thus, this part (Chapter 7 - Chapter 9) of the thesis aims to explore such a state-space-lattice approach.

This chapter focuses on how state space lattices emerge and how their geometries connected to their Hamiltonian. We concentrate on paradigm models from quantum optics, such as the *Jaynes-Cummings (JC)*. Such models typically include only a few degrees of freedom and are naturally expressed as single-particle problems in the Fock state basis. Thus, the state space lattices we are interested in, are Fock state lattices (FSL) Studying these models through the lenses of a state-space lattice can yield new insight into their behaviour.

In Chapter 8 we study the *multi-mode JC* models in the large detuned limit in detail in a state space setting to explore how this setting provides us with a deeper understanding of the system. Finally, in Chapter 9, turn the question around and ask if and how we can design state space lattices that yield interesting properties.

## 7.1 From state-space lattices to Fock-state lattices

Any quantum system can be expressed using different bases. In the context of state-space lattices, this choice of basis is crucial, as the states spanning this basis are the potential lattice sites. In principle, we may use any choice of basis as our starting point. However, not all choices of basis will lead to interesting lattice-like structures. To see this, consider the eigenstate basis. For this basis, the Hamiltonian will leave any given pure state unchanged. Thus, it will not connect to other eigenstates, and thus no lattice-like structure will emerge.

For many-body quantum systems, the Fock space is a natural starting point for searching for state space lattices. A Fock space lattice (FSL) is an example of a state-space lattice. Here, we express the many-body system in its Fock state basis, and these states play the role of lattice sites.

When the state of the system is pure, we see this as localization in the lattice. Vice versa, when the system is in a mixed state, the state will be spread out in the lattice. Thus, the FSL provides a natural way of viewing how localised or spread out a given state is.

Many-body system in terms of such states turns the Hamiltonian into a single particle Hamiltonian, characterised by its corresponding matrix representation. When the Hamiltonian is quadratic, the diagonal terms serve as onsite energies, representing the state conserving terms of the many-body Hamiltonian. The off-diagonal terms give the tunnelling between the lattice sites.

This approach will typically not yield many useful insights for many many-body systems, as the lattice structures that emerge quickly grow in complexity, making it hard to study anything besides small systems in terms of numbers of particles this way.

## 7.2 The Jaynes-Cummings model

The JC model was introduced by Edwin Jaynes and Fred Cummings in 1963 [62]. It is one of the earliest fully quantum mechanical treatments of an atom interacting with an electromagnetic field, as it treats not only the atom quantum mechanically but also the electromagnetic field. The model depicts the atom as a spin half system that interacts with an electric field in the form of a single boson mode. This model captures the essence of the spin and field interaction by describing it as the exchange of excitations between them. It has since then been

extended by allowing for more complicated interactions, having several boson modes, or considering larger spins, etc. [63]. However, also for such models the principle of viewing the interaction as an exchange of excitations remains the same. This viewpoint makes the Fock state basis the convenient one to work with as it gives us a clear picture of how interaction in the system changes the state of the system. In this basis, a clear lattice-like structure emerges, where the Fock states represent the lattice points, and the interaction can be understood as tunnelling between them.

### 7.2.1 The model Hamiltonian

As we have already mentioned, the key ingredients of this model are the spin and the boson mode. The spin is a two-level system, and we shall follow the usual convention and denote the ground state by $|g\rangle$ and the excited state by $|e\rangle$. These two states typically represent two different electronic states of an atom [63]. We call the energy difference between these two internal spin states for $\Omega$ (with $\hbar = 1$). The two-level structure makes it practical to introduce *Pauli matrices*, the raising $\hat{\sigma}^+$ and the lowering $\hat{\sigma}^-$ operators being

$$\hat{\sigma}^{\pm} = \hat{\sigma}^x \pm i\hat{\sigma}^y, \tag{7.1}$$

where $\hat{\sigma}^x$ and $\hat{\sigma}^y$ are the standard Pauli matrices. In quantum optics, they are often called the *dipole operators*, whereas $\sigma^z$ is referred to as the *inversion operator*. The expectation value of $\sigma^z$ gives the difference between the population in the excited state and the ground state $\langle\sigma^z\rangle = P_e - P_g$, and thereby the reason for its name. The boson mode can hold any number of photons, and we shall use the Fock state basis and denote the state of $n$ photons in a given mode for $|n\rangle$. The exchange of excitations between the spin and the boson mode means that whenever the spin is excited from its ground state to its excited state, the boson mode loses a photon and vice versa. This can be expressed schematically as

$$|n, e\rangle \longleftrightarrow |n+1, g\rangle\,, \tag{7.2}$$

and depicted graphically as in fig. 7.1 (a). Here, we see the first indication of what is meant by an FSL.

#### The JC Hamiltonian

To continue we need to specify the Hamiltonian [62; 64; 65]. We break the Hamiltonian into a *bare* part $\hat{H}_0$ and an interacting part $\hat{H}_I$. Thus,

it can be expressed as

$$\hat{H} = \hat{H}_0 + \hat{H}_I. \tag{7.3}$$

The bare part of the Hamiltonian, $\hat{H}_0$, can further be split into two contributions, one from the spin and one from the boson mode. Defining the zero energy to be halfway between the ground and the excited spin state, the contribution from the spin may be written as

$$\hat{H}_A = \frac{\Omega}{2}\hat{\sigma}^z, \tag{7.4}$$

while the boson mode can be expressed as

$$\hat{H}_B = \omega\hat{n} = \omega\hat{a}^\dagger\hat{a}. \tag{7.5}$$

We return to the interaction, here both the spin and the boson mode will emit and absorb excitations. We may thus write a general interaction Hamiltonian on the form [64]

$$\hat{H}_I = g\left(\hat{\sigma}^+ + \hat{\sigma}^-\right)\left(\hat{a} + \hat{a}^\dagger\right). \tag{7.6}$$

Here the coupling constant $g$ is assumed to be real, which for the original model can always be reached by a unitary transformation [64]. This Hamiltonian has four different contributions, two of which we have described before. These are the terms where the spin absorbs a boson excitation or vice versa. However, the other terms correspond to the situation where both a spin and a boson mode are simultaneously excited or de-excited. Neither of these terms conserves energy, and these terms are therefore dropped in the JC model. This approximation is called *the Rotating Wave Approximation (RWA)*, and it leads to the interaction Hamiltonian being on the form

$$\hat{H}_I = g\left(\hat{\sigma}^+\hat{a} + \hat{\sigma}^-\hat{a}^\dagger\right). \tag{7.7}$$

The full Hamiltonian, therefore, takes the form

$$\hat{H} = \frac{\Omega}{2}\hat{\sigma}^z + \omega\hat{n} + g\left(\hat{\sigma}^+\hat{a} + \hat{\sigma}^-\hat{a}^\dagger\right). \tag{7.8}$$

In terms of state space lattices, the bare part of the Hamiltonian will only contribute with an energy shift. It is therefore often convenient to move into the interaction picture with respect to $\omega\hat{N}$, where $\hat{N} = \hat{n} + \frac{1}{2}\hat{\sigma}_z$ is the *number operator*. Here, the number of free parameters is reduced

with one, such that we are left with the coupling $g$ and the spin field detuning $\Delta = \Omega - \omega$, which reads

$$\hat{H}_{JC} = \frac{\Delta}{2}\hat{\sigma}^z + g\left(\hat{\sigma}^+\hat{a} + \hat{\sigma}^-\hat{a}^\dagger\right). \tag{7.9}$$

It follows that in the Fock state basis, the Hamiltonian takes a Block form

$$\hat{H}_{JC} = \begin{pmatrix} \hat{h}_0 & & & \\ & \hat{h}_1 & & 0 \\ & & \ddots & \\ & 0 & & \ddots \\ & & & & \hat{h}_n \end{pmatrix}, \tag{7.10}$$

with $\hat{h}_n$ being the $2 \times 2$ matrix

$$\hat{h}_n = \begin{pmatrix} \frac{\Delta}{2} & g\sqrt{n+1} \\ g\sqrt{n+1} & -\frac{\Delta}{2} \end{pmatrix}, \tag{7.11}$$

acting on the states $|n, e\rangle$ and $|n+1, g\rangle$. These Fock states are called the *bare states* [64], and while they provide an intuitive basis for understanding the interaction, it should be remembered that they are not the eigenstates of the system. Hence, when the Hamiltonian acts on them, they will change and be connected to other Fock states, such that a lattice-like structure emerges. By diagonalizing the Hamiltonian, one can find the eigenstates of the JC model [64]

$$|\psi_{\pm,n}\rangle = \sin\left(\frac{\theta}{2}\right)|n, e\rangle \pm \cos\left(\frac{\theta}{2}\right)|n+1, g\rangle, \tag{7.12}$$

with

$$\tan(\theta) = \frac{2g\sqrt{n+1}}{2}, \tag{7.13}$$

and with the corresponding interaction picture eigenvalues being

$$E_{\pm,n} = \pm\Omega_n = \pm\sqrt{\frac{\Delta^2}{4} + g^2(n+1)}. \tag{7.14}$$

Such that the full eigenvalues become

$$\mathcal{E}_{\pm,n} = \omega\left(n \pm \frac{1}{2}\right) \pm \Omega_n. \tag{7.15}$$

The eigenstates are also called the *dressed states*, and from eq. (7.14) we see that there depending on $\Delta$ are two limits of interest; the resonant

limit where $\Delta \to 0$, and the large detuned limit where $|\Delta| \gg g\sqrt{n}$. When $\Delta = 0$, it entails that $\Omega - \omega = 0$, and hence there is perfect resonance. Here the angle $\theta$ from (7.13) does not depend on $n$, and the solutions of the eigenstates simplify significantly and become

$$|\psi^0_{\pm,n}\rangle = \frac{1}{\sqrt{2}}\left(|n,e\rangle \pm |n+1,g\rangle\right), \tag{7.16}$$

with the eigenvalues

$$E^0_{n,\pm} = \pm g\sqrt{n+1}, \tag{7.17}$$

One of the many ways to expand the original JC model is to allow for more than one boson mode. Labelling each boson mode by an index $i$ and assuming that the spin couples to each boson mode with a corresponding coupling strength $g_i$, the multi-mode JC model takes the form

$$\hat{H} = \frac{\Omega}{2}\hat{\sigma}^z + \sum_i \omega_i \hat{n}_i + g_i\left(\hat{\sigma}^+\hat{a}_i + \hat{\sigma}^-\hat{a}_i^\dagger\right). \tag{7.18}$$

The Fock state of this $m$-mode model takes the form $|n_1, \cdots, n_m, g(e)\rangle$.

### 7.2.2 The large detuned limit

In the large detuned limit $|\Delta| \gg g\sqrt{n}$, where $n$ is the average photon number. Here an effective Hamiltonian can be obtained by treating the spin and the boson mode as approximately decoupled. Here one assumes that the spin degrees-of-freedom follows the boson one adiabatically. To see how this comes about, we consider the Heisenberg equations of motion again

$$\begin{aligned}
\partial_t \hat{a} &= -i\left[\hat{a}, \hat{H}\right] = -ig\hat{\sigma}^-, \\
\partial_t \hat{\sigma}^- &= -i\left[\hat{\sigma}^-, \hat{H}\right] = -i\Delta\hat{\sigma}^- + ig\hat{a}\hat{\sigma}^z, \\
\partial_t \hat{\sigma}^z &= -i\left[\hat{\sigma}^z, \hat{H}\right] = 2ig\hat{a}^\dagger\hat{\sigma}^-.
\end{aligned} \tag{7.19}$$

Assuming $\Delta \gg g$ implies that the spin operators evolve on a very fast time scale compared to the boson operators. With this assumption, we replace the Pauli spin matrices with their steady-state solutions, *e.g.*,

$$\partial_t \hat{\sigma}^- = 0, \tag{7.20}$$

such that for the steady state, one finds

$$\hat{\sigma}^- = \frac{g\hat{a}\hat{\sigma}^z}{\Delta}. \tag{7.21}$$

Inserting this into the equations-of-motion for the boson degrees-of-freedoms leads to an effective dynamical equation for the boson operator $\hat{a}$

$$\partial_t \hat{a} = -\tfrac{g^2}{\Delta} = \hat{a}\hat{\sigma}^z, \qquad \partial_t \hat{a} = -i\left[\hat{a}, \hat{H}_{\text{eff}}\right]. \tag{7.22}$$

In the second step above, we introduced an effective Hamiltonian $\hat{H}_{\text{eff}}$, which takes the form

$$H_{\text{eff}} = \frac{\Delta}{2}\hat{\sigma}^z + \frac{2g^2}{\Delta}\hat{n}\hat{\sigma}^z. \tag{7.23}$$

In the case of multi-mode JC models, the *adiabatic elimination scheme* is straightforward to generalise. The effective Hamiltonian will include a summation over indices $i, j$ on the boson modes, but otherwise, it stays the same, such that the Heisenberg equations become

$$\begin{aligned} \partial_t \hat{a}_i &= -ig_i\hat{\sigma}^-, \\ \partial_t \hat{\sigma}^- &= -i\Delta\hat{\sigma}^- + i\sum_i g_i\hat{a}_i\hat{\sigma}_z, \\ \partial_t \hat{\sigma}_z &= 2i\sum_i g_i\hat{a}_i^\dagger\hat{\sigma}^-, \end{aligned} \tag{7.24}$$

and with $\partial_t\hat{\sigma}^- = 0$ one obtains $\hat{\sigma}^- = \sum_i \frac{g_i\hat{a}_i\hat{\sigma}_z}{\Delta}$, and reach an expression for the effective multi-mode Hamiltonian on the form

$$\hat{H}_{\text{eff}} = \sum_{i,j}\frac{2g_ig_j}{\Delta}\hat{a}_i^\dagger\hat{a}_j\hat{\sigma}^z. \tag{7.25}$$

## 7.3 Fock state lattices for JC models

The bare part of the JC Hamiltonian is diagonal in the Fock basis, and it leaves the Fock states unchanged up to a multiplication factor. Hence, the lattice-like structures emerges from the interaction Hamiltonian.

To understand how these lattices appear, we let the (interaction) Hamiltonian work on a Fock state. For an $m$-mode system, this means that a boson will be annihilated from, say, the boson mode $k$, and thereby exciting the spin-state. Afterwards, the spin-state gets de-excited, relaxing into its ground state by creating a boson in, say, the boson mode $l$. Or expressed schematically

$$\begin{array}{c} |n_1,\cdots,n_k,\cdots,n_l,\cdots,n_m,g\rangle \\ \updownarrow \\ |n_1,\cdots,n_k-1,\cdots,n_l,\cdots,n_m,e\rangle \\ \updownarrow \\ |n_1,\cdots,n_k-1,\cdots,n_l+1,\cdots,n_m,g\rangle \end{array} \tag{7.26}$$

This expression is for a general multi-mode Fock-state, but we in this chapter we only look at the multi-mode JC model for up to three boson modes. In fig. 7.1 the lattice-like structures for these models are shown in both the resonant limit (dashed lines) and the large detuned limit (solid lines). We have fixed the number of excitations, the total number of bosons and spin excitations, to $N = 2$. Had $N$ been different, the shape of these lattices would have remained the same. While the single-mode lattice would always consist of two lattice sites, the size of the FSLs for the two- and three-mode JC models scale with the total number of excitations ($N$).

The basic lattice structure for the single-mode JC model is a zero-dimensional/quasi-one-dimensional lattice. This structure consists of exactly two lattice points, namely the pair $|n+1, g\rangle$ and $|n, e\rangle$, as shown in fig.7.1(a). The coupling between these two lattice points scales with $\sqrt{n}$, which means that no two copies are identical. For the two-mode JC model, fig 7.1(b), the basic structure is a chain of length $2N+1$ where $N$ is the number of bosons occupying the two modes, and for the three-mode JC model, the basic lattice will be triangular-shaped (see fig. 7.1(c)). For the two- and three-mode JC models, the tunnelling scales with the number of bosons created or annihilated, $\sqrt{n_i}$, in a given mode. The basic lattice structures thus grow in size as the number of bosons grows. In the large detuned limit, we may also consider multi-mode models. Here, the spin-degree-of freedom is effectively frozen out, and the FSL that emerges, the lattice sites will have no spin component. Thus it will only consist of the white lattice sites and the thick lines in fig. 7.1. In the resonant limit, the lattice structure size scales with the number of bosons of the system. Also in this limit the tunnellings will scale as $\sqrt{n_k(n_l+1)}$.

## 7.4 A systematic approach for generating FSLs

The JC models are not the only models that give rise to FSLs. To explore what lattices may emerge, we study light-matter models similar to the JC models to see what lattice structure emerges. However, we shall choose another route and flip the question. As the strength of the tunnelling is proportional to the number of bosons, it creates and annihilates. The terms we are interested in are those that only raise or lower the number of bosons in a Fock state by one. The strength of these kinds of terms scales with $\sqrt{n}$.

From a Fock state $|n, g\rangle$ point of view, we may define the nearest neighbours as exactly those Fock states which can be reached by raising

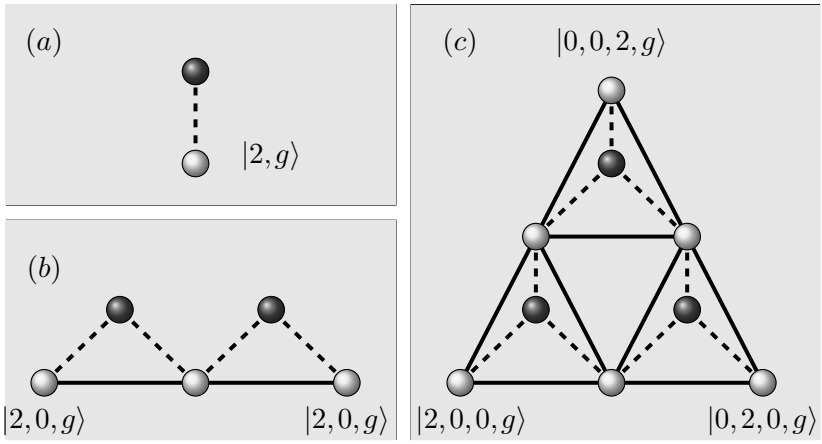


**Figure 7.1:** The FSL with $\hat{N} = 2$ for the single-mode JC (a), two-mode JC (b), and three-mode JC models, with white (black) spheres marking the atomic $|g(e)\rangle$ states. The dashed lines indicate the non-zero tunnellings of the lattice in the resonant limit, these scales with $\sqrt{n_i}$. Similarly, the dolifr lines (in the two- and three-mode model) are the tunnellings in the large detuned limit, these scales with $\sqrt{n_a n_b}$. Hence, these lattices are not translationally invariant.

or lowering the number of bosons in the state by one. These connections are schematically shown in Fig. 7.2. Here, the possible nearest neighbour connections are labelled by Roman numerals $(\mathrm{I}) - (\mathrm{III})$. The term (I) is the JC exchange which we have already discussed. The term labelled (II) the term we together with its hermitian conjugated dropped from eq. (7.6) in the RWA, *i.e.* terms are the counter-rotating terms. Finally, the two terms labelled by (III) are called *drive* or *pump* terms. Here the number of bosons is raised or lowered by one without affecting the spin part of the Fock state. The contribution in the Hamiltonian due to these terms involves one boson annihilation or creation operator. The terms of type (I) preserves the number of excitations, *i.e.*, $\hat{N}$ is a constant of motion. As a result, it generates a continuous $U(1)$ symmetry, which, however, reduces to a $\mathbb{Z}_2$ parity symmetry upon including terms of type (II), which then again disappears when terms of type (III) are included.

A final connection is shown in Fig 7.2, namely $|n,g\rangle \longleftrightarrow |n,e\rangle$. This connection only changes the spin part of the Fock state. While such a term, of course, changes the Fock state, it does not include any boson annihilation or creation operators, and thus tunnelling terms that arise from this term do not scale like those discussed before. At the same time, the spin is finite, meaning that it will only give rise to a quasi-

dimension in the lattice. For these reasons, we shall focus on the other terms in the remaining part of this chapter.

### 7.4.1 The quantum Rabi model

In fig. 7.3 four different lattice structures are shown. These structures all involve different combinations of JC terms, the counter-rotating terms and drive terms. We start by including the terms we dropped from eq. (7.6) in the Hamiltonian *i.e.* the counter-rotating terms marked by (II) in fig. 7.2. This model is called the *quantum Rabi model* [64; 66] with the interaction Hamiltonian expressed as

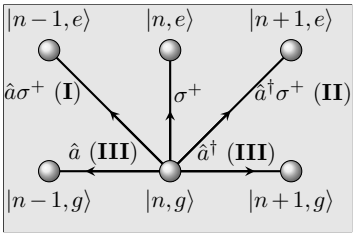


**Figure 7.2:** Schematic representation of the zeroth and first-order couplings of Fock states. The order of the coupling refers to the number of participating boson creation or annihilation operators in each tunnelling process.

$$\hat{H}_{int} = g(\hat{a}^\dagger + \hat{a})\hat{\sigma}_x. \tag{7.27}$$

As opposed to the JC Hamiltonian Eq. (7.9), this Hamiltonian does not preserve the number of excitations, and hence in the FSL, the terms in the Hamiltonian that change the number of excitations by one will ensure that each Fock state now couples to two neighbouring Fock states;

$$\ldots|e,-2\rangle \longleftrightarrow |g,n-1\rangle \longleftrightarrow |e,n\rangle \longleftrightarrow |g,n+1\rangle \ldots, \tag{7.28}$$

With two neighbours the FSL becomes a 1D chain (see Fig. 7.3). The $\mathbb{Z}_2$-symmetry highlights that the FSL will decouple into two parity sectors, such that the full lattice consists of two copies of the chain, one for each sector. The FSL lattice is shown in fig. 7.3(c).

If we allow the couplings of eq. (7.27) to be *anisotropic*, meaning that the counter-rotating terms have a different coupling amplitude than the JC terms, the interaction Hamiltonian takes the form [67]

$$\hat{H}_{\text{int}} = g_{\text{jc}}\left(\hat{\sigma}_+\hat{a} + \hat{a}^\dagger\hat{\sigma}_-\right) + g_{\text{ajc}}\left(\hat{\sigma}_-\hat{a} + \hat{a}^\dagger\hat{\sigma}_+\right). \tag{7.29}$$

Allowing for different couplings does not change the FSL but gives rise to an alternation between two different tunnellings. The translational invariant version of this is the *Su-Schrieffer–Heeger* (SSH) Hamiltonian [68; 69]. This model hosts exponentially localised topologically protected zero-energy edge states and while the FSL for the Quantum-Rabi model is not translational invariant, a kind of edge state is found for anisotropic couplings [(III)].

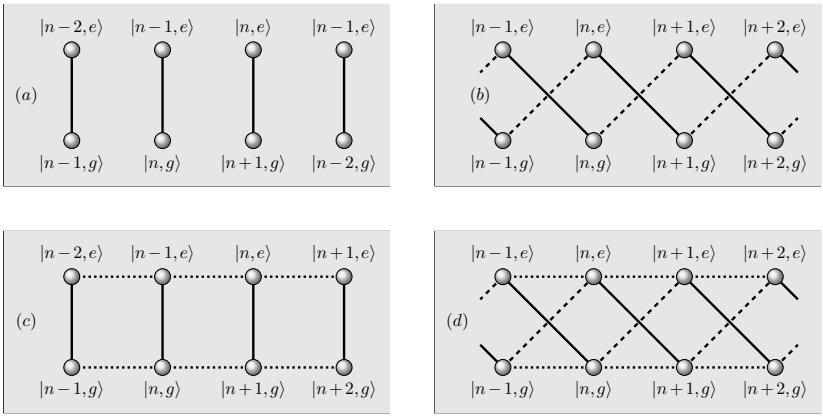


**Figure 7.3:** Four FSLs for models consisting of only a single boson and a two-level atomic degree-of-freedom. In (a), the lattice of the single-mode JC model (7.9) is shown again. In (b) the FSL for the quantum Rabi model (7.29) is shown. Here the dashed lines mark the tunnelling due to the counter-rotating terms, and the solid lines the JC interaction terms. The second row of FSLs shows the driven JC model in (c) and the driven quantum Rabi model in (d). The dotted lines mark the tunnelling stemming from the drives, *i.e.*, by removing them, we return to lattices in the first row.

### 7.4.2 Driven Jaynes-Cummings like systems

Including the counter-rotating terms is not the only way to break the continuous $U(1)$ number conservation symmetry in the JC model. Another way is to include a boson drive term

$$\hat{H}_{\mathrm{dr}} = \eta\left(\hat{a} + \hat{a}^{\dagger}\right). \tag{7.30}$$

With such a term, the excitation number is no longer preserved. In fig. 7.3 we see how such a term will cause horizontal tunnellings in the FSL (compare Fig. 7.3 (a) with (c), and Fig. 7.3 (b) with (d)). If included in the quantum Rabi model, the drive will realise a *Creutz ladder* [70] (without translational invariance) as seen Fig. 7.3 (d). The translational invariant Creutz ladder attracts attention as it may host dispersionless, *i.e.*, flat bands. We return to this model in Chapter 9.

## 7.5 A note on symmetries, geometry and lattice dimensions

We have seen several examples of FSLs and how the lattice changes when the Hamiltonian changes. There is *per se* nothing surprising about the lattice-like structures changing as the Hamiltonian is modified.

However, to fully explore the potential of FSLs, one must also explore the symmetries of the Hamiltonian. Given some Hamiltonian, its FSL will typically support some discrete point symmetries. For the three-mode JC model, its FSL, as shown in fig. 7.1(c), has both a $2\pi/3$ rotational symmetry around its centre and three mirror reflections. Such lattice symmetries originate from the symmetries of the Hamiltonian, *e.g.*. the rotational symmetry translates to the unitary transformation $\hat{a} \to \hat{b}$, $\hat{b} \to \hat{c}$, and $\hat{c} \to \hat{a}$ .

The Hamiltonian may also possess symmetries tied to the number of excitations of the relevant Fock states. For Hamiltonians, such as the multi-mode JC models, the number of excitations is preserved by the Hamiltonian. The preservation of excitation leads to a continuous $U(1)$ symmetry, which reduces the lattice dimension of the FSL by one. For the quantum Rabi model, the Hamiltonian preserves the number of excitations modulo 2. This preservation leads to a discrete $\mathbb{Z}_2$ symmetry of the Hamiltonian that decouples the lattice into two sublattices.

#### The lack of translational invariance

Recalling our discussion in Chapter 2 on symmetries, the FSLs that emerge for the JC models (see fig. 7.1) possess some symmetries usually associated with lattices but not the translational one. That the tunnelling depends on the boson number, *i.e.*, lattice site index, implies that the strength of the tunnelling varies throughout the lattice and that the lattice is not translationally invariant.

## 7.6 The potential of Fock state lattices

Throughout this chapter we have seen how different coupling terms manifest themselves as tunnelling rates in the FSL and gained an understanding how these various couplings shape the lattice-like structure.

The lattice geometry, *e.g.*, the number of neighbours, is determined by the specific form of the interaction Hamiltonian when expressed in terms of raising/lowering operators (*e.g.* $\hat{a}$ and $\hat{\sigma}^-$), and the number of terms in $\hat{H}_{\text{int}}$ gives the maximum number of possible neighbours.

Fig. 7.2 can be used as a starting point for a recipe on how to construct and design more elaborated FSLs. Though we in the figure consider a system of a single boson mode and a two-level spin, it can be expanded to several boson modes, a spin with more than two levels, or a combination of these. Each boson mode adds an extra dimension to the system, and thus higher-dimensional lattices can emerge. Adding these ingredients proves a root for systematically building lattice-like systems in high dimensions. In Chapter 9, we shall use our understanding of how the couplings to design specific lattice like. However, before we do so we shall explore what we gain from the FSL approach when looking at the multi-mode JC model in the large detuned limit.

# 8. Multi-mode detuned Jaynes-Cummings models

Having seen in Chapter 7 how FSLs emerge we also wish to show how such FSLs can lead to new knowledge about the models they represent. Previously, FSLs have been used to study used to study multi-photon systems in ref. [59] and the multi-mode JC models in the resonant limit in ref. [61] were they have let to new insight.

We will also study the multi-mode JC models, but in the large detuned limit instead of the resonant limit. In this limit, the spin degrees-of-freedom freezes out, and we are left with a model consisting only of the boson modes. Here, we shall allow the coupling between different Fock states to carry a phase and thus they become complex. According to *Peierls substitution* a complex amplitude can be envisioned as a magnetic flux $\phi$ through a plaquette [69]. Similarly, a complex coupling term of the boson model will be manifested in a flux through each plaquette of the corresponding FSL.

We first compare the effective Hamiltonian of the two- and three-mode JC models in the large detuned limit. Seeing how the three-mode model allows one to study FSLs under the presence of a flux through the plaquettes, we shall explore the behaviour of the energy spectrum for the three- and higher-mode models as a function of this flux. We find that the three-mode model gives rise to a quasi-equidistant energy spectrum, only to vanish again for four or higher mode models. We explore how one may construct higher-dimensional FSLs with similar properties of a quasi-equidistant energy spectrum and introduce the *Ring-like models*, thus seeing an example of how we can use our knowledge to design models of interest. We return to the three-mode model and study what consequences the quasi-equidistant spectrum has on the evolution of initial Fock states, beffore we summarise our findings.

## 8.1 The Jaynes-Cummings models in the detuned limit

The full multi-mode JC model couples a spin-half degree-of-freedom to multiple boson modes, and the interaction Hamiltonian takes the form

$$\hat{H}_{\text{int}} = \sum_i g_i(\hat{a}_i^\dagger \hat{\sigma}^- + \hat{a}_i \hat{\sigma}^\dagger). \tag{8.1}$$

Here, the index $i$ labels the boson modes, and the coupling between the spin and the $i$'th boson mode is labelled $g_i$. In the large detuned limit, the spin degrees-of-freedom adiabatically follow the bosons, and thus, in this limit, the spin mode decouples from the boson ones provided that we consider an initial spin state $|g\rangle$ or $|e\rangle$. Hence, in the large detuned limit one is left with an effective Hamiltonian for only the boson modes

$$\hat{H}_{\text{eff}} = \sum_{i,j}(\tau_{ij}\hat{a}_i^\dagger \hat{a}_j + h.c.). \tag{8.2}$$

Here, the sum runs over boson modes $i, j$, and we label the coupling by $\tau_{ij}$ and it is determined by (7.25). The terms where $i = j$ are included in $\hat{H}_0$ in (7.3). Thus, we shall only consider the terms $i \neq j$, but we will allow the couplings to carry a phase such that the effective Hamiltonian will take the form.

$$\hat{H}_{\text{eff}} = \sum_{i,j}(\tau_{ij}e^{i\phi_{ij}}\hat{a}_i^\dagger \hat{a}_j + h.c.). \tag{8.3}$$

### 8.1.1 The two-mode Jaynes-Cummings model

We first consider the case for two boson modes. Here the Hamiltonian in (8.3) reduces to

$$\hat{H}_2 = \tau\left(\hat{a}^\dagger \hat{b} e^{i\phi} + \hat{b}^\dagger \hat{a} e^{-i\phi}\right). \tag{8.4}$$

For this Hamiltonian, we can remove the phase with a gauge transformation, and hence we are left with the Hamiltonian

$$\hat{H}_2 = \tau\left(\hat{a}^\dagger \hat{b} + \hat{b}^\dagger \hat{a}\right). \tag{8.5}$$

As the Hamiltonian is quadratic, it is straightforward to find its eigenvalues and thereby its entire spectrum by diagonalising it. Noticing that

$$\dot{\hat{a}} = -i\left[\hat{a}, \hat{H}_2\right], \qquad \ddot{\hat{a}} = -i\left[\dot{\hat{a}}, \hat{H}_2\right], \tag{8.6}$$

we find that $\ddot{\hat{a}} = -\tau^2 \hat{a}$. Similarly, one will also find $\ddot{\hat{b}} = -\tau^2 \hat{b}$. Thus, the time-dependent expressions for $\hat{a}(t)$ and $\hat{b}(t)$ becomes

$$\begin{aligned} \hat{a}(t) &= \hat{a}(0) \cdot \cos\left(\tau^2 t\right) + \hat{b}(0) \cdot \sin\left(\tau^2 t\right), \\ \hat{b}(t) &= \hat{b}(0) \cdot \cos\left(\tau^2 t\right) - \hat{a}(0) \cdot \sin\left(\tau^2 t\right). \end{aligned} \tag{8.7}$$

Both $\hat{a}(t)$ and $\hat{b}(t)$ are periodic with period $T_{\mathrm{R}} = \frac{2\pi}{g^2}$, and thus for any choice of the initial state, the system exhibits perfect revivals and return to this state after multiple of the revival time. For the two-mode JC model in the large detuned limit, the FSL is simply a 1D chain with tunnelling amplitudes that vary throughout the lattice. The length of the chain is determined by the number of bosons $N$, and the end states will be $|N,0\rangle$ and $|0,N\rangle$ respectively. Suppose we assume that the initial state was $|N,0\rangle$ as time progresses. In that case, the population will move from one edge of the lattice to the other edge, such at $t = T_{\mathrm{R}}/2$ only $|0,N\rangle$ will be populated, and at $t = T_{\mathrm{R}}$ the entire population will have returned to $|N,0\rangle$. The FSL is similar to the spin model considered in [71], which was introduced as a lattice model that could realise the perfect transfer of quantum states between two sites.

### 8.1.2 Three- and higher modes

We now turn to the three mode model. While the phase in the couplings can be gauged away for two modes, this is not the case for three or more modes [72]. Instead, a phase results in complex couplings in the FSLs. The effective Hamiltonian for the three-mode JC model in the large detuned limit takes the form

$$\begin{aligned} \hat{H}_3 = \tau_{ab} \hat{a}^\dagger \hat{b} e^{i\phi_{ab}} + \tau_{ca} \hat{c}^\dagger \hat{a} e^{i\phi_{ca}} \\ + \tau_{cb} \hat{b}^\dagger \hat{c} e^{i\phi_{bc}} + h.c. \end{aligned} \tag{8.8}$$

While the tunnelling strengths *a priori* depend on the details of the system, we shall assume, for three as well as higher mode models, that for all pairs $i, j$ that $\tau_{ij} = \tau$. With this assumption, the effective Hamiltonian becomes

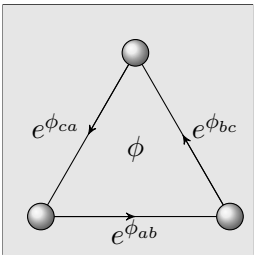


**Figure 8.1:** The flux through the smallest loop for the three-mode model. Here the tunnelling phases sum up to the plaquette flux; $\phi = \phi_{ab} + \phi_{bc} + \phi_{ca}$.

$$\hat{H}_3 = \tau \left( \hat{a}^\dagger \hat{b} e^{i\phi_{ab}} + \hat{c}^\dagger \hat{a} e^{i\phi_{ca}} + \hat{c}^\dagger \hat{b} e^{i\phi_{bc}} \right). \tag{8.9}$$

Not only does the phase result in complex tunnelling rates, but from Peierls substitution, we know that such phases will also mimic a synthetic magnetic flux. For a lattice with a flux penetrating a loop perpendicularly, the flux $\phi$ equals the sum of the phases of the corresponding couplings [69]. To characterise the system, we are interested in the flux through the smallest of such loops (see fig. 8.1). For the three boson modes we have the three phases $\phi_{ab}$, $\phi_{bc}$, and $\phi_{ca}$. While each of these can be changed via a gauge transformation, the sum $\phi = \phi_{ab} + \phi_{bc} + \phi_{ca}$ will be gauge invariant. Hence, any choice of $\phi_{ab}, \phi_{ac}$, and $\phi_{bc}$ will lead to a flux that will alternate between $\pm\phi = \pm(\phi_{ab} + \phi_{bc} - \phi_{ac})$.

As the Hamiltonian preserves the number of particles in eq. (8.2). The Hamiltonian has a corresponding $U(1)$-symmetry. This symmetry lowers the lattice dimension from three dimensions (the number of boson modes) to two dimensions. Hence, the corresponding FSL is a triangular lattice with a staggered magnetic flux, *i.e.*. alternating $\pm\phi$ fluxes through each triangular plaquette, see fig. 8.2. Furthermore, for a given particle number $N$, the lattice is finite, such that for $N$ bosons, the number of sites in this FSL will be

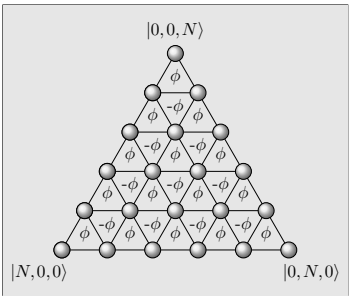


**Figure 8.2:** The three-mode triangular FSL. A synthetic magnetic flux $\pm\phi$ penetrates each plaquette in a staggered pattern.

$$\mathcal{S} = (N+1)(N+2)/2. \tag{8.10}$$

For higher mode models including phases in the couplings leads to a more complicated situation. However, for any number of modes, the unit cell is a *d-simplex*, where $d$ is one less than the number of boson modes, *e.g.*, for three boson modes, it is a (2D) triangle, for four boson modes it is a (3D) tetrahedron and so on.

Here, one finds that any given plane of three modes labelled $i, j$ and $k$ will exhibit the same pattern of staggered flux $\phi_{ijk}$ through the smallest plaquettes in the plane. For the particular choice of the phase, where for all pairs $i < j$ where $\phi_{ij} = \phi$, then for choosing a plane spanned by any three modes of the full FSL, this plane will display the same triangular lattice structure with a staggered $\pm\phi$ flux as found for the three-mode model.

## 8.2 The energy spectrum

The Hamiltonian for the detuned JC model is quadratic. Hence, assuming that $\tau = 1$, and including the phases that lead to a staggered flux pattern, it will take the matrix form

$$\hat{H}_{\text{eff}} = \hat{\psi}_n^\dagger \begin{pmatrix} 0 & & & & \\ & 0 & & e^{i\phi} & \\ & & \ddots & & \\ & e^{-i\phi} & & \ddots & \\ & & & & 0 \end{pmatrix} \hat{\psi}_n, \tag{8.11}$$

where $\hat{\psi}_n^\dagger = \left(\hat{a}_1^\dagger, \cdots, \hat{a}_n^\dagger\right)$. By labeling the eigenvalues, for an $m$-mode system $\{\gamma_0, \gamma_1, \cdots, \gamma_{m-1}\}$, one may express the energy eigenvalues of the full system, as

$$E_m = \sum_{i=0}^{n-1} m_i \gamma_i. \tag{8.12}$$

Here, the constraint $\sum_{i=0}^{m-1} m_i = N$ ensures that we have exactly $N$ particles distributed in the $m$ different modes. In general, one will need to find eigenvalues numerically, but for three and four modes, it can always be done analytically as characteristic polynomial for the matrix in eq. (8.11) becomes a polynomial of degree three and four, respectively. Thus, one can analytically express how the full energy spectrum depends on the flux for three and four modes.

### 8.2.1 A quasi equidistant spectrum

We start our analysis of the full energy spectrum by considering the three-mode model. Here, the expression in eq. (8.11) simplifies to

$$\hat{H}_3 = \left(\hat{a}^\dagger, \hat{b}^\dagger, \hat{c}^\dagger\right) \begin{pmatrix} 0 & e^{i\phi} & e^{i\phi} \\ e^{-i\phi} & 0 & e^{i\phi} \\ e^{-i\phi} & e^{-i\phi} & 0 \end{pmatrix} \begin{pmatrix} \hat{a} \\ \hat{b} \\ \hat{c} \end{pmatrix}. \tag{8.13}$$

Here, the characteristic polynomial $P_3$, takes the form

$$P_3 : \gamma^3 - 3\gamma - 2\cos(\phi) = 0. \tag{8.14}$$

This expression leads to the three single-particle eigenvalues,

$$\gamma_k = 2\cos\left(\frac{\phi - 2 \cdot \pi \cdot k}{3}\right) \quad , \quad k \in \{0, 1, 2\}. \tag{8.15}$$

We are here interested in understanding the full energy spectrums' dependence on the flux $\phi$. To do so, the first question we seek to answer is what interval of $\phi$ we must explore.

When looked upon individually, the three eigenvalues each have a period of $\phi = 6\pi$. However, if one considers the spectra of all three eigenvalues collectively, its period reduces to $\phi = 2\pi$ instead. This is so, because at $\phi = 2\pi$, $\gamma_0(2\pi) = \gamma_1(0)$, $\gamma_1(2\pi) = \gamma_2(0)$, and $\gamma_2(2\pi) = \gamma_0(0)$. Hence, we can at least restrict ourselves to the interval $\phi \in [0; 2\pi[$. Furthermore, one can show that $\gamma_0(\phi) = \gamma_1(2\pi - \phi)$ and $\gamma_2(\phi) = \gamma_2(2\pi - \phi)$. Hence, taking this into account, we may restrict $\phi$ even further, such that $\phi \in [0; \pi]$. In fig. 8.3 $\gamma_0$, $\gamma_1$, and $\gamma_2$ are plotted for this interval.

### 8.2.2 Decomposition of the energy eigenvalues

We return to the question of exploring the energy eigenvalues dependence on the flux.

To do so, we start by decomposing the energies of the full spectra in terms of the eigenvalues given in (8.15). As described in (8.12) one can, for any number of particles $N$, decompose any eigenvalue for the full three-mode system, as follows

$$E_m = m_0\gamma_0 + m_1\gamma_1 + m_2\gamma_2, \tag{8.16}$$

where $m_0 + m_1 + m_2 = N$. This can be rewritten as

$$E_m = N\gamma_0 + (\gamma_1 - \gamma_0)m_1 + (\gamma_2 - \gamma_0)m_2, \tag{8.17}$$

From this expression, we see that the energy difference between two energy levels can be expressed as

$$E_m - E_{\tilde{m}} = (\gamma_1 - \gamma_0)(m_1 - \tilde{m}_1) + (\gamma_2 - \gamma_0)(m_2 - \tilde{m}_2). \tag{8.18}$$

Noting that since $m_0, m_1, m_2 \in \mathbb{N}$, then whenever

$$\frac{\gamma_0(\phi_j) - \gamma_1(\phi_j)}{\gamma_0(\phi_j) - \gamma_2(\phi_j)} = q \quad , \quad q \in \mathbb{Q}, \tag{8.19}$$

the distance between any two energy levels in the spectrum can be expressed as $E_m - E_{\tilde{m}} = n\Delta_j$, where $n \in \mathbb{N}$ and $\Delta_j = |\min(\gamma_l - \gamma_k)|$ with $l < k$. When $\phi \in [0; \pi]$, then $\Delta_j = \gamma_0 - \gamma_1$.

If we disregard the singularity at $(\gamma_0(\phi_j) - \gamma_2(\phi_j))$, then as $N \to \infty$, we see that there will be infinitely many $\phi_j$'s which will fulfil the condition in eq. (8.19), see fig. 8.4 (a) and (b). At these $\phi_j$'s the spectrum exhibits a highly degenerate structure, and the energy differences

between the neighbouring energies can be ordered in terms of a basic energy difference $\Delta_j$, such that the energy difference will arrange like $\Delta_j$, $2\Delta_j$, $3\Delta_j$,...$j\Delta_j$. Note that while the basic energy difference $\Delta_j$ is different for different $j$'s, for any $j$ it will be such that the maximal energy difference will be $j\Delta_j$. Thus, the relevant time-scale of the system will be

$$\mathrm{T}_j = \frac{2\pi}{\Delta_j}. \tag{8.20}$$

When the energy difference between any two neighbouring energies has this form, the spectrum will be "quasi equidistant". If we plot the distances $\delta E(\phi)$ between any energy level $E_m$ and its neighbouring energy (that is, its nearest different energy level) $E_{m'}$, then $\delta E(\phi)$ will exhibit the fractal-like structure of a quasi-equidistant energy spectrum, as seen in fig. 8.4. We note that at $\phi = 0$, $\phi = \pi/2$, and $\phi = \pi$, the energy spectrum is not only quasi-equidistant but equidistant since here there exists only a single energy difference between neighbouring energy levels.

### Quasi energy distant $\phi$'s

Returning to the expression (8.19) we can use it to solve for $\phi$ such that we can find these quasi-equidistant fractal points. First, we take care of the singularity at $\gamma_0 - \gamma_2 = 0$. Noting that this requires $\gamma_0 = \gamma_2$, which corresponds to $\phi = 2\pi$, the singularity happens outside the interval of $\phi$, and we can therefore disregard it.

We note that for $\phi \in [0, \pi]$, the $q$ given in (8.19) fulfills

$$\begin{cases} q = 1 & \text{if} \quad \phi = 0, \\ 0 < q < 1 & \text{if} \quad 0 < \phi < \pi, \\ q = 0 & \text{if} \quad \phi = \pi. \end{cases} \tag{8.21}$$

The first condition requires that $\gamma_1 = \gamma_2$, which happens at $\phi = 0$. As for $\phi = 2\pi$, this leads to a situation where the spectrum is equidistant, and the net flux is zero. When $q = 0$, it instead requires that $\gamma_0 = \gamma_1$, which happens at $\phi = 2\pi$. The energy spectrum will be equidistant, even though the net flux is $\pi$.

When $0 < q < 1$ we rewrite (8.19) in terms of the analytical expressions for $\gamma_0, \gamma_1$, and $\gamma_2$,

$$\frac{\gamma_0 - \gamma_1}{\gamma_0 - \gamma_2} = \frac{\cos\left(\frac{\phi}{3}\right) - \cos\left(\frac{\phi}{3} - \frac{2\pi}{3}\right)}{\cos\left(\frac{\phi}{3}\right) - \cos\left(\frac{\phi}{3} - \frac{4\pi}{3}\right)}. \tag{8.22}$$

Using that $\cos A - \cos B = 2\sin\left(\frac{A+B}{2}\right)\sin\left(\frac{A-B}{2}\right)$, we can reach

$$\frac{\gamma_0-\gamma_1}{\gamma_0-\gamma_2} = \frac{\sin\left(\frac{\phi-\pi}{3}\right)}{\sin\left(\frac{\phi-2\pi}{3}\right)}, \tag{8.23}$$

which can be rewritten using $\sin(A-B) = \sin A\cos B - \cos A\sin B$

$$\frac{\gamma_0-\gamma_1}{\gamma_1-\gamma_2} = -\frac{\sin\left(\frac{\phi}{3}\right)-\sqrt{3}\cos\left(\frac{\phi}{3}\right)}{\sin\left(\frac{\phi}{3}\right)+\sqrt{3}\cos\left(\frac{\phi}{3}\right)} \quad . \tag{8.24}$$

Since $\frac{\gamma_0-\gamma_1}{\gamma_0-\gamma_2} = q = \frac{j}{j'}$ where both $j, j' \in \mathbb{N}$ and $j < j'$, we reach

$$j'\left(\sqrt{3}\cos\left(\frac{\phi}{3}\right)-\sin\left(\frac{\phi}{3}\right)\right) = j\left(\sqrt{3}\cos\left(\frac{\phi}{3}\right)+\sin\left(\frac{\phi}{3}\right)\right), \tag{8.25}$$

which leads to the requirement on $\phi$ that

$$\tan\left(\frac{\phi}{3}\right) = \frac{\sqrt{3}(j'-j)}{j'+j} \quad , \quad j, j' \in \mathbb{N}. \tag{8.26}$$

For any pair $j, j' \in \mathbb{N}$ we can find a new pair $k, k' \in \mathbb{N}$ such that

$$j + j' = k', \qquad j' - j = k. \tag{8.27}$$

Thus, for $k = 1$ then $k' = 2j+1$ and we find that $\phi$ must fulfill

$$\tan\left(\frac{\phi}{3}\right) = \frac{\sqrt{3}}{2j+1}, \qquad j \in \mathbb{N}. \tag{8.28}$$

At first glance, it may look like this expression will only give us the conditions for $\phi$ when $q = 1/n$. However, using that $2\tan A = \tan(2A)(1-\tan^2 A)$, one can find $\phi$ for all other combinations of $j, j'$.

In tab. 8.1 we list the first few $\phi_j$'s for the three-mode JC model in the large detuned limit. We will return to what thi fractal structure implies for the system's behaviour, but before doing so, we will first study how to realise a similar result for higher dimensional lattice-like structures.

### 8.2.3 Higher mode Jaynes-Cummings models

Adding extra an extra boson modes increase the lattice dimension by one, so our first attempt to reproduce the fractal-like structure of the

| Model | **j** | 0 | 1 | 2 | 3 | 4 |
|---|---|---|---|---|---|---|
| 3 mode JC | $\phi_j$ | $\pi$ | $\pi/2$ | $0.3188\pi$ | $0.2316\pi$ | $0.1816\pi$ |
| 4 mode ring | $\phi_j$ | $\pi$ | $\pi/2$ | $0.2952\pi$ | $0.2048\pi$ | $0.156\pi$ |
| 6 mode ring | $\phi_j$ | $0.3156\pi$ | $0.1584\pi$ | $0.1056\pi$ | $0.0798\pi$ | $0.0636\pi$ |

**Table 8.1:** Some values of $\phi_j$ for which the three-mode detuned JC model, the four-mode ring model, and the six-mode ring model exhibit degenerated points.

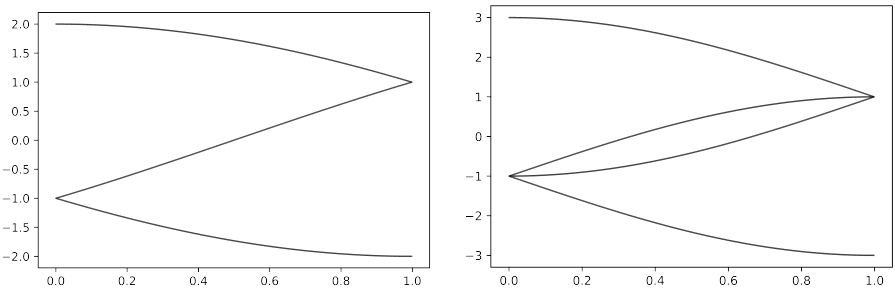


**(a)** **(b)**

**Figure 8.3:** The eigenvalues for the matrix given in (8.11) for three (a) and four modes (b). The plot shows how there are two versus three relevant energy differences for three versus four modes.

energy spectrum in higher dimensions, is to consider the four-mode JC model. For four modes however, the characteristic polynomial becomes

$$P_4 := \gamma^4 - 6\gamma^2 - 8\cos\phi - 2\cos\phi, \tag{8.29}$$

which leads to the following four solutions for the eigenvalues

$$\gamma_k = (-1)^k + 2\cos\left(\frac{\phi + 2\pi\cdot k}{2}\right). \tag{8.30}$$

The interesting question is, of course, what happens if the spectrum for the four-mode JC model in the detuned limit shows the same fractal structure as we saw the three-mode JC model did. If one looks at 8.4(c), it is clear that it does not do so. Though there seem to be a few $\phi$'s that exhibit the fractal behaviour, as N grows, there will not be infinitely many quasi-equidistant points. To understand why this is so, we rewrite the energy difference for the four-mode JC model, as we did for the three-mode JC model. For the four-mode JC model, this leads to the following expression

$$E_m = m_0\gamma_0 + m_1\gamma_1 + m_2\gamma_2 + m_3\gamma_3, \tag{8.31}$$

where $m_0 + m_1 + m_2 + m_3 = N$, such that

$$E_m = N\gamma_0 + (\gamma_1 - \gamma_0)m_1 + (\gamma_2 - \gamma_0)m_2 + (\gamma_3 - \gamma_0)m_3, \tag{8.32}$$

and the energy difference between any two energy levels may be expressed as

$$\begin{aligned} E_m - E_{\tilde{m}} = (\gamma_1 - \gamma_0)(m_1 - \tilde{m}_1) + (\gamma_2 - \gamma_0)(m_2 - \tilde{m}_2) \\ + (\gamma_3 - \gamma_0)(m_3 - \tilde{m}_3). \end{aligned} \tag{8.33}$$

Hence, for the energy spectrum to exhibit fractal structure, this requires that

$$\frac{\gamma_3 - \gamma_0}{\gamma_1 - \gamma_0} = q, \qquad \frac{\gamma_2 - \gamma_0}{\gamma_1 - \gamma_0} = q', \qquad q, q' \in \mathbb{Q}. \tag{8.34}$$

These two conditions must be fulfilled simultaneously for the energy spectrum to exhibit a fractal structure. While two conditions, as opposed to one, do not sound like a huge difference, it is. We are always guaranteed that there exist (an infinite number of) solutions to each of these two equations, but not that these solutions occur simultaneously.

The more modes we add to the full model, the more conditions as the ones on the form (8.34) will have to be fulfilled at the same time, and the more unlikely it becomes that the energy spectrum shows a large degeneration as characteristic for a fractal structure.

However, a question remains if it, by some other means, is possible somehow to design higher-dimensional models exhibiting a similar fractal-like structure to that of the three-mode JC model.

### 8.2.4 A Ring-like model

We start by looking at a set of related models, where each boson mode is only connected to two other boson modes instead of being connected to all other boson modes. Therefore we name it the Ring-like model. This gives a nearest neighbour kind of model, for which we can write the Hamiltonian as

$$\hat{H}_{\text{ring}} = \sum_i \hat{a}_i^\dagger \hat{a}_{i+1} e^{i\phi/n} + h.c., \tag{8.35}$$

where we assume periodic boundary conditions. For four modes, the characteristic polynomial becomes

$$\gamma^4 - 4\gamma^2 + 4\sin^2\left(\frac{\phi}{2}\right) = 0, \tag{8.36}$$

By substituting $\gamma^2 = \lambda$, one can reach an expression for a cubic polynomial which can be solved analytically, and one finds that the four roots can be expressed as

$$\gamma_k = \pm\cos\left(\frac{\phi + \pi \cdot k}{2}\right), \tag{8.37}$$

with $k \in \{0,1\}$ which leads to the following condition

$$\phi = 2\tan^{-1} q, \qquad q \in \mathbb{Q}. \tag{8.38}$$

Similarly, for the Ring-like model with six modes, the characteristic polynomial becomes

$$\gamma^6 - 6\gamma^4 + 9\gamma^2 - 4\cos^2\left(\frac{\phi}{2}\right) = 0. \tag{8.39}$$

By again substituting $\gamma^2 = \lambda$, one can reach an expression for a cubic polynomial which can be solved analytically. Here, one finds that the six roots can be expressed as

$$\gamma_k = \pm 2\cos\left(\frac{\phi + 2\pi \cdot k}{6}\right), \tag{8.40}$$

with $k \in \{0,1,2\}$. These eigenvalues allow us to express the spectrum in terms of three different energy differences $\Delta, \delta$, and $\eta$. There are several different ways to choose $\Delta, \delta$, and $\eta$, but one choice is

$$\Delta = \gamma_0 - \gamma_1, \quad \delta = \gamma_1 - \gamma_2, \quad \eta = \gamma_2 - \gamma_3.$$

However, we may rewrite $\eta$ as follows

$$\eta = 2(\Delta - \delta), \tag{8.41}$$

thus the number of relevant energy differences reduces to two, and one can find the following condition on $\phi$

$$\tan\left(\frac{\phi_m}{6}\right) = \left(\frac{1}{2\sqrt{3} \cdot (m+1)}\right). \tag{8.42}$$

## 8.3 Evolution of Fock states

Going back to the three-mode model, where we wish to explore the manifestation of the fractal spectrum. To do so, we study the system's evolution over time. Recalling that for the two-mode model, the system showed perfect revival after a time $T_{\mathrm{R}} = 2\pi/g^2$, and so it will for the three-mode model when $\phi = \pi/2$, and we are of course interested in seeing if it does so for other fluxes as well.

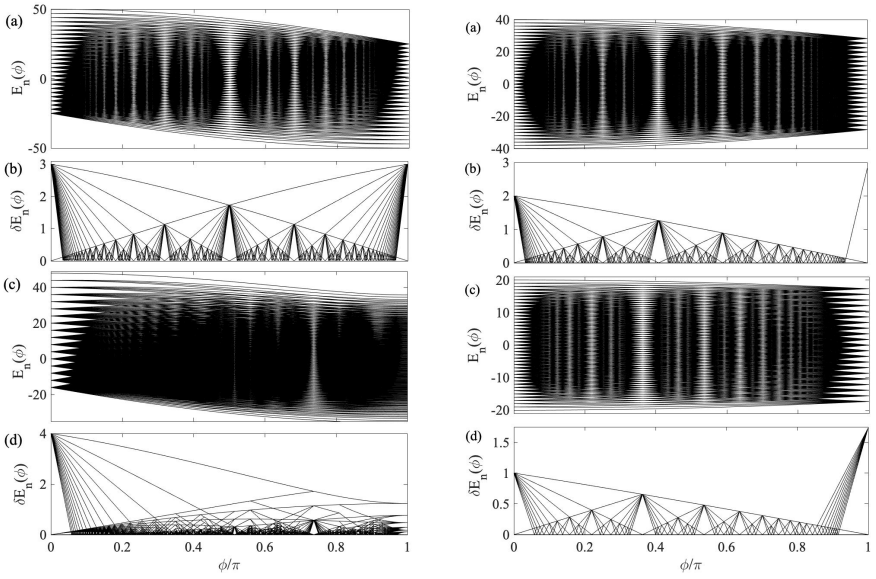


**Figure 8.4:** The upper two plots, (a) and (b), in the left panel show the energy spectrum and the distances between neighbouring energies as a function of the flux $\phi$, for the three-mode model with $N = 25$ bosons III. In the lower two plots, (c) and (d), the same is shown for the four-mode case with $N = 16$. In the right panel, the same is shown but for the four upper two plots (e) and (f), and six modes, lower two plots (g) and (h), for the ring models. Here, the number of bosons are $N = 20$ and $N = 10$ for the two cases, respectively. For the three-mode case, the fractal structure is evident, while the four-mode spectrum does not display the same fractal properties. By disregarding some of the terms in the Hamiltonian (8.3) to obtain the ring Hamiltonian (8.35), the number of conditions for having a quasi-equidistant spectrum is reduced, and thereby the fractal structure will reappear in both the four- and six-mode Ring-like model.

### 8.3.1 Initial states and physical observable

We consider a system of $N = 15$ bosons. Here, the Fock are expressed as $|n_a, n_b, n_c\rangle$, where $n_i \in \mathbb{N}$ and $n_a + n_b + n_c = 15$. For such a system, we know from eq. (8.10) that the number of states is 136.

To study the time evolution of the system, we look at the evolution of three initial states: $|15, 0, 0\rangle$, $|11, 4, 0\rangle$, and $|5, 5, 5\rangle$. These states are chosen as they are at respectively the corner, on an edge, and exactly in the centre in the FSL. Studying the time evolution of different initial states allows us to distinguish what properties of the time evolution depend on the initial state versus the flux. We will explore the time-

evolution of several different $\phi$'s. Here, we primarily focus on the time evolution for the flux $\phi_1 = \pi/2$, but we shall also present results for $\phi_2, \phi_3$, and $\phi_4$ (see tab. 8.1). In addition, we choose a flux that does not coincide with one of the quasi-equidistant points, namely $\tilde{\phi} = \pi/100$.

In order to explore the systems behaviour we introduce three quantities. The first is the inverse partition ratio (IPR)

$$IPR(t) = \sum_{\mathbf{n}} |\langle \mathbf{n}|\psi(t)\rangle|^4, \tag{8.43}$$

which gives the degree of localisation in the FSL, and where the sum is over all possible Fock states (*i.e.* sites) $|\mathbf{n}\rangle$. For a fully localised state, we will have $IPR = 1$. For a maximally delocalised, or spread out, state, we instead have an $IPR = 1/\mathcal{S}$, where we recall that $\mathcal{S}$ is the number of states in the FSL.

The second quantity we introduce is the fidelity

$$F(t) = |\langle \phi(0)|\phi(t)\rangle|^2, \tag{8.44}$$

which is a measure of the overlap between the initial state and the time evolved state.

The third quantity we introduce is the mean position of the Fock state distribution

$$P(\mathbf{n}, t) = |\langle \mathbf{n}|\psi(t)\rangle|^2. \tag{8.45}$$

This expression is a three-component vector, where the entries are the mean number densities of the three boson modes. When this quantity is plotted as a trajectory, it shows how the time-evolved state moves around in the lattice.

### 8.3.2 Points of perfect revival

We begin by looking at how the IPR evolves for all three initial states and the fluxes $\phi_1$ and $\phi_2$. In fig. 8.5 we plot the $IPR$ for the three initial states, for both $\phi_1$ and $\phi_2$. Here, one sees how, after time $t = T_1$ and $t = T_2$, the $IPR$ indicates that all the time-evolved states return to become fully localised ($IPR = 1$). However, we also see how for $\phi_1$ that time-evolved state becomes fully localised at $t = T_1/3$ and multiple thereof. Had we used other initial states or equidistant flux, the resulting plot would have show the same behaviour. To get a better feeling of how the states spread out between revival times, we study the evolution of the initial state $|0, 0, 15\rangle$ in fig. 8.6, for the time interval $t \in [0; T_1/3]$. Here, we plot the $IPR$ along with the fidelity in the second panel. At

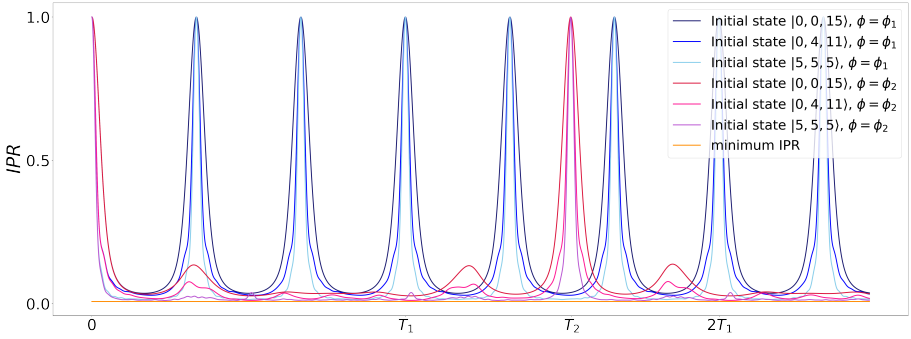


**Figure 8.5:** This plot shows the $IPR$ (8.43) for the three initial states (see inset), with $\phi = \phi_1$ (blue lines) and $\phi = \phi_2$ (red lines) respectively. Both flux choices correspond to equidistant points, and both display perfect revivals. The revival times differ between the two fluxes but not between the states. As a comparison, we also give the minimum possible $IPR$ (yellow line). Though the distribution spreads out, the $IPR$ does not come close to the minimum $IPR$ and thus remains fairly localised at all times. This localisation can be hard to see in the figure since we compare small numbers, *e.g.*, the minimum $IPR = 1/136$ in this example.

the time $t = T_1/3$, though the state is fully localised ($IPR = 1$), we see that it has not yet returned to its initial state as $F(t) = 0$. What has happened can be seen in the lower panel of the figure. Here the number densities of each mode are plotted as a function of time. Here, we see how the states are moved from mode $a$ to mode $b$ and only slightly populate the $c$-mode. Finally, in the upper panel, the light blue triangles show snapshots of how the time-evolved states are distributed in the Fock state lattice. Here, one sees how the state remains fairly localised at any time and how it moves along the edge of the lattice.

In fig. 8.7, we show the same plots but for the initial state $|5,5,5\rangle$. The initial state is completely symmetric in the three boson modes, and thus after a time $t = T_1/3$, the initial state is revived. However, in between revival times, the state becomes highly delocalised and spreads out through the entire lattice. As the number density remains unchanged at all times, we do not plot it.

## 8.4 Spirograph like trajectories

To explore the depth of the system's structure, we look closer at the mean distribution in (8.45) of the time-evolved states for the fluxes $\phi_1, \phi_2, \phi_3$, and $\phi_4$. From the previous figures, we know that for such

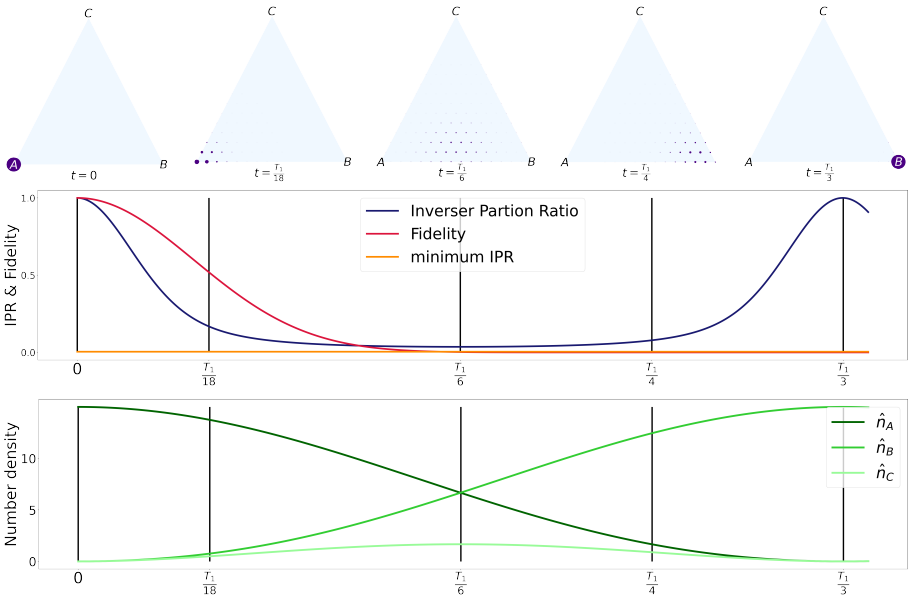


**Figure 8.6:** The upper light blue triangles display snapshots of the Fock state distributions for the initial state $A = |0,0,15\rangle$ and for the flux $\phi_1 = \pi/2$. Initially, the distribution occupies a single corner site, and after $T_R/3$, it has been transferred to another corner site. In between, it stays well localised and traverses along the lower edge of the lattice. The middle plot gives the corresponding $IPR$ (8.43) along with the fidelity (8.44), with the vertical lines indicating the time instances used for the distribution snapshots. Note that for the centre distribution at $T_1/6$, we have $IPR \ll 1$, but still, the distribution is well localised according to the upper figure. The lower plot shows the density distribution between the three modes.

fluxes, the state is fully revived at a later time $T_j$. As the number of particles is kept fixed, we have that at any time $t$

$$n = \langle \hat{n}_a(t) \rangle + \langle \hat{n}_b(t) \rangle + \langle \hat{n}_c(t) \rangle. \tag{8.46}$$

This ensures that, if we plot all three number operators simultaneously as $\vec{n}(t) = (\langle \hat{n}_a(t) \rangle, \langle \hat{n}_b(t) \rangle, \langle \hat{n}_c(t) \rangle)$, it will be a trajectory in a two dimensional plane. Recall that the constraint stemming from particle conservation will remove one degree-of-freedom. This is what ensures that $\vec{n}(\phi, t)$ lives in a 2D plane, *i.e.*. the FSL. Thus, the trajectory can give us insight into how the full distribution moves around in the FSL, even though it only captures the mean occupation. In fig. 8.8(a), we show examples of such trajectories for two of the initial Fock states, $|0,0,15\rangle$ and versus $|0,4,11\rangle$, we used in fig. 8.5. First, one should notice how the

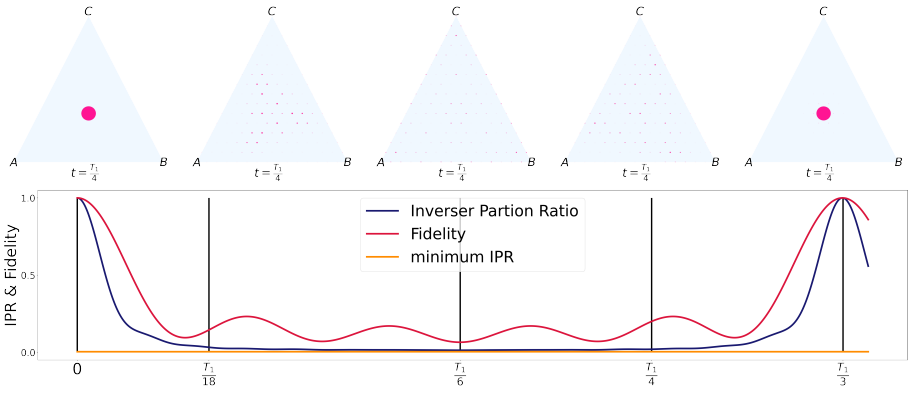


**Figure 8.7:** The same plots as the upper two for fig. 8.6 but for an initial state $|5,5,5\rangle$. Initially, the distribution occupies the centre site, and after $T_R/3$, we see how it has returned fully to this state. In between, the state spreads out throughout the lattice.

trajectory $\vec{n}(\phi_1,t)$ sets an outer boundary for all the other trajectories for the same initial state but different fluxes. Secondly, when comparing the trajectories, we find that the shape and structure remain intact. However, it has been rotated and contracted.

As pointed out, when $\phi_j$ agrees with one of the equidistant points, we encounter perfect revivals at times $T_j$. The revivals manifest as closed trajectories of $\vec{n}(t)$ in the FSL. These trajectories form a highly symmetric pattern in the FSL, *i.e.* the number of full 360° turns the trajectories make before closing upon themselves are found to be $2j-1$. Thus, for $j=1$ (i.e. $\phi_1=\pi/2$) the distribution makes a single loop around the lattice. For $\phi_2$, the distribution makes three loops and so on instead. In that sense, the trajectory shows a Spirograph-like structure for quasi-equidistant fluxes, whereas for a flux that does not correspond to a quasi-equidistant point, the trajectories will never close.

For the closed loops, there are 'clustering points' in which many trajectories cross, the lattice centre being the most noticeable. In fig. 8.8(b) the trajectories for $\phi_1,...,\phi_4$ are shown for initial state $|0,0,15\rangle$. Here, one sees how both the $j=2$ and $j=3$ trajectories pass through the point $n_a(t)=n_b(t)=n_c(t)=N/3$, for all $\phi_j$ with $j=2,3,5,6,8,9,....$

## 8.5 Conclusion and outlook

Throughout this chapter, we have seen an example of how studying the large detuned three-mode JC model through its FSL strengthens our

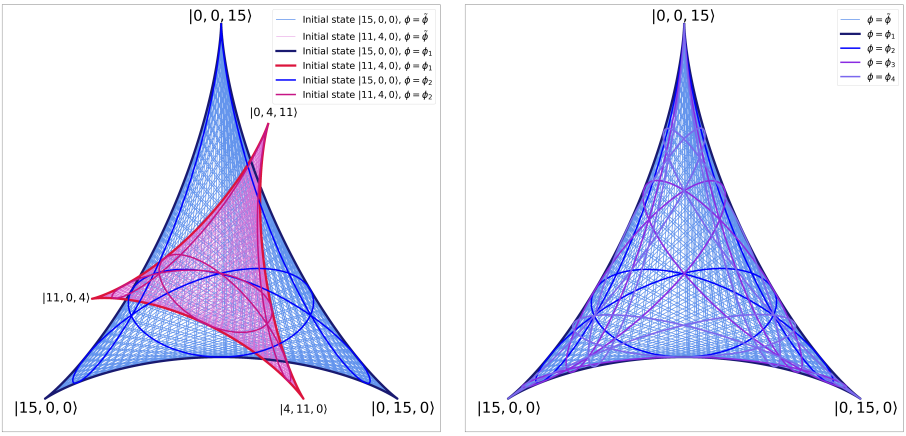


**Figure 8.8:** Examples of the evolution of the occupation vector $\vec{n}(t) = (n_a(t), n_b(t), n_c(t))$, with $n_i(t) = \langle \hat{n}_i \rangle$ in the FSL for the three-mode model. The initial states are $|0,0,15\rangle$ (blue curves) and $|0,4,11\rangle$ (red curves), and the fluxes for the different curves are given in the inset.

understanding of this model. We have seen how allowing the couplings to carry a phase gives rise to a flux through the plaquettes of the FSL. When the flux of the FSL is staggered the energy spectrum becomes quasi-equidistant.

We explored how the evolution of Focks states depends on the initial state and the flux through the plaquettes. At the quasi-equidistant points $\phi_j$, the initial state is perfectly revived after time $T_j$. For these fluxes the distribution $P(\mathbf{n}, t)$ remains well localised and follows closed loops. The index $j$ was seen to determine how many twists the distribution makes before it returns to the initial site. We found that these loops have mirror symmetry with respect to the axis through the centre of the lattice and the lattice site of the initial state. The direction of the initial state's propagation can be clockwise or counterclockwise depending on the sign of $\phi_j$, which reflects the breaking of time-inversion as soon as the flux is non-zero (a zero flux does not produce a favoured direction for the propagating distribution). The propagation is reminiscent of a Hall current; a perpendicular magnetic field applied to a 2D electronic gas implies a current living on the edge of the system. Finally, we also saw an inherent scale invariance of these trajectories; for a given $\phi_j$, the trajectories are identical in structure irrespective of the specific initial Fock state, *i.e.*, they only differ in orientation and size.

We have seen that at the fractal points $\phi_j$, there exists a revival time $T_{\mathrm{R}} = T_j$, given by eq. (8.20). Though perfect revivals are found for any

$j$, the evolution of the system between two consecutive revivals depends much on the index $j$.

Hopefully, this shows how FSLs can prove a useful tool for exploring the behaviour of other light-matter interaction models. As mentioned, FSLs provide a route to realising high dimensional lattice structures and having seen how we could realise a quasi-equidistant spectrum for the detuned three-mode JC model made us question if we could realise a similar spectrum for a higher dimensional FSL.

In the next chapter, we will elaborate on the potential of FSLs, and in particular, how one may flip the question around and try to design FSLs that could be interesting, but already in this chapter, we have seen an example of this.

# 9. The scope of Fock state lattices

In the introduction, quantum simulators were presented as the overarching theme of this thesis. But, so far, the state space lattices we have studied in the last two chapters can hardly be called quantum simulators.

The FSLs still present a relatively unexplored approach to studying many light-matter (spin-boson) models known from quantum optics. They highlight other features of these systems than what usually is in focus. What is particularly interesting is that they show how several of such models give rise to similar topological features to those seen for the translational invariant counterpart of these systems, FSL, which we show some examples of here. It seems possible that there is a connection between the behaviour of the state space lattice and its translational invariant partner, which gives us hope that more interesting properties are uncovered through the FSLs. Flipping the approach around, and rather than starting with a light-matter model and then from it finding its FSL, it thus makes sense to ask the question. Given some lattice models, how can we construct a light-matter model with an FSL that corresponds to this lattice model? Using such knowledge, we can then return to the question of quantum simulators and ask, can we design a quantum simulator from an FSL. The answer to this question is that we can at least try.

## 9.1 A zoo of Fock state lattices

In quantum optics, one encounters a range of models comprising a few degree-of-freedoms that describe the interaction between quantized light and matter. Many of these are extensions and generalisations of the JC model toward multi-mode and multi-level atoms [64]. Suppose we replace the two-level atom with an $S$-level atom. In that case, it will provide a pseudo dimension of $2S+1$ sites deep, while including another boson mode adds an extra full dimension (infinitely deep). Generally, the boson modes, constituting one continuous degree-of-freedom, each give rise to one lattice dimension, such that with each additional bo-

son mode, the dimension of the FSL grows with one. The atom, which provides a discrete degree-of-freedom, causes an extra lattice pseudo dimension, *i.e.*, the lattice is finite in the new dimension. These models generate interesting FSLs with known, translationally invariant counterparts in condensed matter physics. In tab. 9.1 several models are listed, with their respective interaction Hamiltonians and information about the type of FSL that represents them. Hence, given your favourite lattice with some interesting properties, *e.g.*, non-trivial topology, you can work backwards and ask for some interaction Hamiltonian that generates the corresponding FSL.

## 9.2 Topological features in Fock state lattices

In the last chapter, we saw how, in the large detuned limit, the three-mode JC model gave rise to a trajectory pattern, where when $\phi = \pi/2$, it looks like the current is moving along the edge. Thus, it is tempting to speculate if some underlying topological features cause such an edge current. Here, one finds the $E = 0$ energies are respectively $Z = N/2+1$ or $N/2+1/2$ degenerated for even and odd particle numbers $N$ III. Noting that this degeneracy does not only appear for the FSL but also appears as the degeneracy of flat bands for the translationally invariant lattice with a similar staggered field. Thus, we can understand the $E = 0$ energies as the FSL counterpart of flat bands. Similarly, if we look at the two-mode JC model, we see this model also gives rise to localisation on the edges III. However, looking closer at these edge states for both models, we see that they do not localise exponentially when the lattice grows in size.

However, the idea that we in FSL can have edge states and something corresponding to flat bands is intriguing. So, we turn to another model similar to the two-mode JC model, which has a finite 1D FSL, emerging from a (large) finite spin-$S$ instead of a boson mode. Such a model can be introduced by replacing the boson mode with spin modes.

$$\left(\hat{a}^\dagger + \hat{a}\right) \to \hat{S}_x, \quad i\left(\hat{a}^\dagger - \hat{a}\right) \to \hat{S}_y, \quad \hat{a}^\dagger \hat{a} \to \hat{S}_z, \tag{9.1}$$

where the $\hat{S}_\alpha$'s are the SU(2) spin operators for a spin-S particle. This model naturally introduces an upper and a lower bound for the lattice. When we apply this mapping to the one mode JC model, one obtains a so-called *central spin model* [73; 74]. This is a model where one single central spin-1/2 particle interacts with $N$ non-interacting spin-1/2 particles, which form the large spin-$S$ (i.e. $S = N/2$). With such a model,

one has a toy model for looking at the non-Markovian decay of a qubit and for studying quantum criticality [73; 74]. We, therefore, consider a central spin model on the form

$$\begin{aligned}\hat{H}_{int}^{cs} &= g_x\hat{\sigma}^x\hat{S}^x + g_x\hat{\sigma}^y\hat{S}^y \\ &= g_+\left(\hat{\sigma}^+\hat{S}^- + \hat{\sigma}^-\hat{S}^+\right) + g_-\left(\hat{\sigma}^+\hat{S}^+ + \hat{\sigma}^-\hat{S}^-\right),\end{aligned} \tag{9.2}$$

where $g_\pm = g_x \pm g_y$. This model is the spin analogue to the anisotropic quantum Rabi model (7.29), shown in chapter 8. When $g_+ \neq g_-$ and $g_+, g_- \neq 0$, the tunnelling rates alternate throughout the lattice and thus become similar to that of the SSH model [68]. The SSH model is known to have two $E = 0$ eigenstates that are exponentially localised at each of the edges, and we find that also the central spin model reproduces this. Also, each localised state belongs to one of the two parity sectors.

The "central spin SSH model" is not the only FSL that gives rise to degenerated $E = 0$ energies and the FSL version of flat bands. In chapter 8, we showed the FSL for both the regular and the driven quantum Rabi model in fig. 7.3. Without the drive term, a $\mathbb{Z}_2$-parity symmetry splits the lattice into two 1D chains, but when a drive term is included, the two 1D chains become connected, and a *Creutz-like ladder* emerged [70]. For the translational invariant Creutz ladder, it is known that dispersionless flat bands can emerge when the tunnellings are properly tuned [70]. These flat bands are manifested by the $E = 0$ eigenstates being infinitely degenerated. For the driven quantum Rabi model, its FSL is, of course, not translational invariant. However, one still sees something similar. When rotating the spins, $\hat{\sigma}_x \to \hat{\sigma}_z$ the Hamiltonian takes the form $\hat{H}_{\text{int}} = (\eta \pm g)\left(\hat{a}^\dagger + \hat{a}\right)$. Here the tunnelling amplitude one can tune is $g$, and when it fulfils that $g = \eta$, such that the amplitude is the same for all the tunnelling rates, the $E = 0$ eigenstates also here become infinitely degenerated.

Another translational invariant lattice model known for hosting flat bands is the *Lieb lattice*. Here, the lattice geometry provides a mechanism that can block movement in the lattice when $E = 0$, and again flat bands arise [75]. Also, here, one may find something similar for the corresponding FSL.

## 9.3 State space lattices as quantum simulators

At first, glance, since FSLs and state-space lattices generally can be understood as single-particle systems, they should be unsuitable can-

didates for realising quantum simulators. Therefore it is important to stress that state-space lattices are many-body systems in real space. If we return once more to what is required for a quantum system to be a potential quantum simulator, it must be computationally hard for a classical computer to solve. One way to fulfil this is to require that the state space grows exponentially, which translates to the state space lattice growing exponentially. So what we are searching for is an FSL that fulfils this. In general, for an $N$-dimensional lattice, each time we add a step in all directions, the lattice grows in size with $N$. Thus, to ensure that our lattice grows exponentially, we would need the lattice dimension to be infinite, or we would need the lattice to have a fractal structure. A fractal structure is a geometric structure that exhibits self similarities at all scales. There are, of course, many different fractals, and for many of them, it can seem like an impossible task to construct them in state space. However, we only need one example, to begin with, and for this purpose, we turn our eyes to the *Bethe lattice*.

### 9.3.1 The Bethe lattice

The Bethe lattice is a lattice where all vertices have the same number of neighbours. It was introduced by Hans Bethe in 1935 [76]. In a Bethe lattice, each node is connected to $z$ neighbours; the number $z$ is called the coordination number. The Bethe lattice is a loop-free lattice, meaning that if one wants to return to any node in the lattice, one must return through the same path as one left it.

If each lattice point is to have the same number of neighbours, and the lattice is to grow exponentially, then each lattice point must have at least three neighbours. We know an FSL lattice that fulfils this, namely the large detuned JC model for three boson modes. Its FSL is not a Bethe lattice, but by looking at it from the perspective of how to construct a Bethe lattice, it shows one clear obstacle to doing so. The lattice allows for loops. Had we instead considered spins-modes, the size of the spin would reduce the number of steps the lattice can grow, and we would end up with a finite lattice. So the combination of the lattice being loop-free and growing exponential does, at first glance, present an obstacle when trying to realise it through a state space lattice. Also, in a true Bethe lattice, any lattice point is the same. This we can not realise in an FSL, where the lattice points naturally are labelled by particle number. Hence, the FSL version of the Bethe lattice will have an origin, which naturally turns out to be the vacuum state.

The trick lies in combining boson and spin modes if we begin by

considering the following Hamiltonian.

$$\hat{H} = \sum_{\alpha,\beta} \hat{a}_\alpha^\dagger \hat{a}_\beta \hat{S}_{i+1}^+ + h.c, \tag{9.3}$$

where the index $i$ is used to label the lattice site. Here, the familiar terms from the large detuned JC model are now coupled directly to a spin mode, and we see an example of how boson and spin modes can be coupled in a way we have not discussed yet. Having a boson model ensures that the lattice can continue to grow. Having spin modes keeps track of the route we took, thereby ensuring that all states in a given layer of the lattice are unique. However, the spin mode imposes a limitation on the size of the lattice. To circumvent this, we shall also allow the system to have a spatial lattice dimension. For a single boson mode, this Hamiltonian then takes the form

$$\hat{H} = \sum_i \hat{a}_{i+1}^\dagger \hat{a}_i \hat{\sigma}_{i+1}^+ + h.c, \tag{9.4}$$

where instead of keeping track of the route through a large spin, we keep track of it by having spin-half modes assigned to every lattice site instead. If we generalise this Hamiltonian to include more than a single type of boson mode, we reach

$$\hat{H} = \sum_i \sum_{\alpha \neq \beta} \hat{a}_{\alpha_{i+1}}^\dagger \hat{a}_{\beta_i} \hat{\sigma}_{\alpha_{i+1}}^+ + h.c, \tag{9.5}$$

The lattice that emerges from the vacuum state is a Bethe lattice. Physically it is a one-dimensional lattice on a string in real space, but looking at the state space lattice, it is a Bethe lattice. It means that its state space lattice grows exponentially for each step we take away from the origin.

### 9.3.2 Final remarks

We have worked our way from developing the theoretical framework for FSLs to construct and study such structures. In Chapter 8 we explored the multi-mode JC model in the large detuned limit, and here have used the FSL approach to construct a model of interest.

That something can be done on paper is not the same as it can be done in the lab. However, understanding the mechanisms of constructing FSLs allows us to determine what models could be interesting.

| Model | Interaction Hamiltonian | Lattice type |
|---|---|---|
| Jaynes-Cummings | $\hat{H}_{\text{int}} = g\left(\hat{a}^\dagger\hat{\sigma}_- + \hat{a}\hat{\sigma}_+\right)$ | Double-well, fig. 7.3 (a) |
| Quantum Rabi | $\hat{H}_{\text{int}} = g\left(\hat{a}^\dagger + \hat{a}\right)\hat{\sigma}_x$ | 1D chain, fig.7.3 (b) |
| Anisotropic quantum Rabi | $\hat{H}_{\text{int}} = g_{\text{jc}}\left(\hat{\sigma}_+\hat{a} + \hat{a}^\dagger\hat{\sigma}_-\right)$ $+ g_{\text{ajc}}\left(\hat{\sigma}_-\hat{a} + \hat{a}^\dagger\hat{\sigma}_+\right)$ | Infinite SSH chain |
| $N$ atom Dicke | $\hat{H}_{\text{int}} = g\left(\hat{a}^\dagger + \hat{a}\right)\hat{S}_x$ | Square lattice |
| $N$ atom Tavis-Cummings | $\hat{H}_{\text{int}} = g\left(\hat{a}^\dagger\hat{S}^- + \hat{a}\hat{S}^+\right)$ | $N$ potential-well |
| Central spin model | $\hat{H}_{\text{int}} = g_x\hat{\sigma}_x\hat{S}_x$ $+ g_y\hat{\sigma}_y\hat{S}_y$ | Finite SSH chain, fig. |
| Driven quantum Rabi | $\hat{H}_{\text{int}} = g\left(\hat{a}^\dagger + \hat{a}\right)\hat{\sigma}_x$ $+\eta\left(\hat{a}^\dagger + \hat{a}\right)$ | Creutz ladder, fig. 7.3 (d) |
| Single mode $\Lambda$ | $\hat{H}_{\text{int}} = g\left(\hat{a}^\dagger + \hat{a}\right)\left(\hat{\lambda}^{(1)} + \hat{\lambda}^{(6)}\right)$ | Lieb ladder |
| Two-mode JC | $\hat{H}_{\text{int}} = g_a\left(\hat{a}^\dagger\hat{\sigma}_- + \hat{a}\hat{\sigma}_+\right) + g_b\left(\hat{b}^\dagger\hat{\sigma}_- + \hat{b}\hat{\sigma}_+\right)$ | SSH chain |
| Two-mode detuned JC | $\hat{H}_{\text{int}} = t\left(\hat{a}^\dagger\hat{b} + \hat{b}^\dagger\hat{a}\right)$ | CDEL chain |
| Two-mode quantum Rabi | $\hat{H}_{\text{int}} = g\left[\left(\hat{a}^\dagger + \hat{a}\right) + \left(\hat{b}^\dagger + \hat{b}\right)\right]\hat{\sigma}_x$ | (Layered) square lattice |
| Two-mode $\Lambda$ | $\hat{H}_{\text{int}} = g_a\left(\hat{a}^\dagger + \hat{a}\right)\hat{\sigma}_{12} + g_b\left(\hat{b}^\dagger + \hat{b}\right)\hat{\sigma}_{23}$ | 2D Lieb lattice |
| Three-mode JC | $\hat{H}_{\text{int}} = g_a\left(\hat{a}^\dagger\hat{\sigma}_- + \hat{a}\hat{\sigma}_+\right) + g_b\left(\hat{b}^\dagger\hat{\sigma}_- + \hat{b}\hat{\sigma}_+\right)$ $+ g_c\left(\hat{c}^\dagger\hat{\sigma}_- + \hat{c}\hat{\sigma}_+\right)$ | Hexagonal lattice |
| Three-mode detuned JC | $\hat{H}_{\text{int}} = t\left(\hat{a}^\dagger\hat{b}e^{i\varphi} + \hat{b}^\dagger\hat{c} + \hat{a}^\dagger\hat{c} + \text{h.c.}\right)$ | Triangular lattice, fig. 8.1 |
| Three-mode tripod | $\hat{H}_{\text{int}} = g_a\left(\hat{a}^\dagger + \hat{a}\right)\hat{\sigma}_{12} + g_b\left(\hat{b}^\dagger + \hat{b}\right)\hat{\sigma}_{13}$ $+ g_c\left(\hat{c}^\dagger + \hat{c}\right)\hat{\sigma}_{14}$ | Perovskite lattice |
| Three-mode quantum Rabi | $\hat{H}_{\text{int}} = g\left[\left(\hat{a}^\dagger + \hat{a}\right) + \left(\hat{b}^\dagger + \hat{b}\right) + \left(\hat{c}^\dagger + \hat{c}\right)\right]\hat{\sigma}_x$ | Cubic lattice |
| Four-mode detuned JC | $\hat{H}_{\text{int}} = t\sum_{j,i=1}^{4} e^{i\phi_{ij}}\hat{a}_i^\dagger\hat{a}_j$ | Tetrahedral lattice |
| Four-mode detuned JC2 | $\hat{H}_{\text{int}} = t\sum_{i=1}^{4} e^{i\phi_i}\hat{a}_i^\dagger\hat{a}_{i+1} + \text{h.c.}$ | Cubic lattice |

**Table 9.1:** A collection of atom-light interaction Hamiltonians and their corresponding FSLs. Many of these frequently appear in the quantum optics community. Some are discussed in some detail in this chapter. We use the notation $\hat{\sigma}_{ij} = |i\rangle\langle j| + |j\rangle\langle i|$.

# Part IV

# Conclusion and outlook

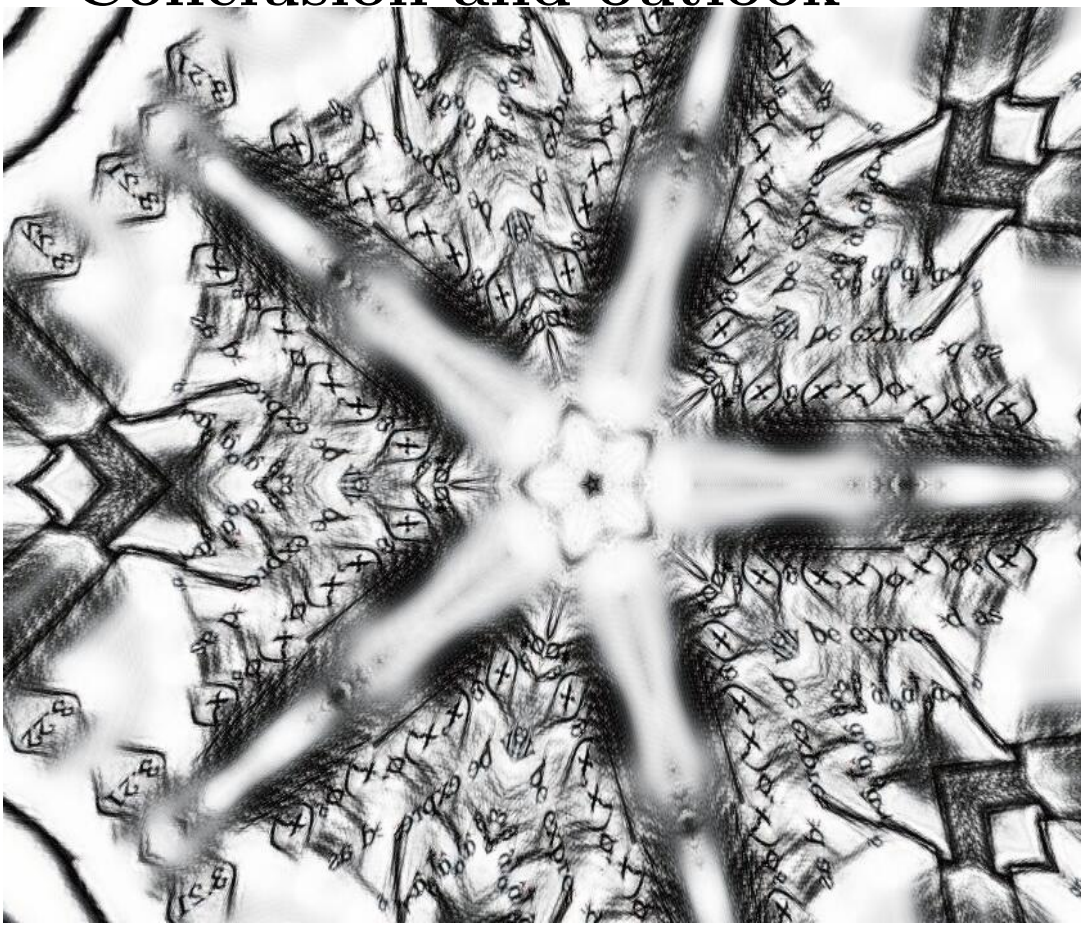

# 10. Towards a quantum for a quantum

This thesis examines exotic lattice systems and how they pave the wave to quantum simulators. It is about how to explore and exploit the lattice (or lattice-like) behaviour to design models with interesting properties.

The systems you encountered here are lattice systems, meaning they had at least two ingredients. They had lattice sites and they had connections between these lattice sites. For both types of systems, we approached them in a similar manner, trying first to understand the behaviour of the lattice sites and the connections between them, and then we tried to use this knowledge to design lattice systems with specific behaviour.

I hope you feel you learned something, even if it is just a tiny bit, but I also hope I have left you with questions that remain to be answered. I hope you wonder about the things I did and maybe even more so about things I didn't do. I have questions of my own, both about why I did certain things and why I didn't do others, and these questions lead to ideas that I would have like to pursue had there been more time. The questions I have, about why I did certain things, are not so much connected to what is presented in this thesis. They have more to do with what is not presented here. Like other PhD candidates, I had projects that failed and didn't lead to anything. I spent hours pursuing ideas that I today easily can see were doomed to fail.

The questions I have about why I didn't do something often have a simple answer, when it came around to do it, I didn't have the time to do it. Throughout the summer, when I worked on finalising this thesis, I came across several questions to which I would have wished I knew the answer. Some of these questions others have likely already answered, but for some of them, the answers are unknown. These questions presents ideas and suggestions for what direction this research can go next, and I would like to share a few of these with you.

## 10.1 From state space lattice to quantum simulators

State space lattices are still a relatively unexplored. Both in general and as a method for realising quantum simulators. In state space lattices, the lattice sites are the states of the system, and the connections between the lattice sites change the states. Some may argue that these systems are not truly lattice systems as they lack translational invariance. I guess this is a matter of preferences, and some call them graphs rather than lattices [59]. I prefer to call them lattices, as they possess a regularity that graphs do not necessarily do.

We explored this regularity in Chapter 7 and again in Chapter 9. Breaking the connections in the lattice up into connections between neighbouring lattices sites was what allowed us to construct the Ring-like models from Chapter 8 and the Bethe lattice in Chapter 9.

If I have one wish for state space lattices in general and FSLs in particular, it is that we of course explore more systematically how they emerge for more boson modes and larger spins, but in particular that explore more generally, how non-quadratic terms can be included and what state space lattice structures they can give rise to. If the aim is to design quantum simulators, it is crucial to include such terms as it is the growth of the systems state space that determines if it is a candidate for quantum simulators or not. Thus, non quadratic terms must be included if we are to have state space lattices that grows exponentially.

When it comes to searching for space lattices that could be quantum simulators, we can also search for specific models as we did with the Bethe lattice. Here, an idea could be to try to generate fractal lattice lattices, where in particular the *Koch curve* or *Koch snowflakes* [77] are interesting options as they have a simple lattice structure, that grows exponentially.

Finally we can also give up on the notion that the state space lattice has to be simple. There is nothing that stops us from visualising the many-body systems. The lattice-like structures will generally be high dimensional; each lattice site will have many connections, and the connections will be complicated. While it is unrealistic to assume that we can draw the lattice-like structures that emerge as neatly as for the Bethe lattice or for fractal lattices, it might allow us to understand how the state space of these systems looks and use this knowledge to design other systems with a similar state space structure.

## 10.2 And back again to optical lattices

It is the Mott phase that for the optical lattice from Part 2 is interesting in the context of quantum simulators. Here, we explored the connection between the effective Hamiltonians for several bipartite lattice systems and the Schwinger-boson model, which emerged from them. The $p$-$f$-bipartite lattice system has been studied in the superfluid limit [78; 79], however, for both the $s$-$d$ and $p$-$f$-bipartite models, a more in-depth study remains to be carried out. In this context, there are two directions that I find particularly interesting.

On the last page of Chapter 6 we introduced a flux to control the contributions from loop processes. Our motivations for doing so were to show that one could bring the model we had a hand closer to the perfect $J_1$-$J_2$ model. The role of the flux is one that needs to be explored, and it also opens up possibilities than the one discussed in Chapter 4. Introducing a flux also opens up for realising systems that exhibits at Hofstadter Butterfly spectrum [80]. Optical lattices have already been used to realise systems that exhibit the Hofstadter butterfly spectrum [81–83]. At resonance, one would expect that both regular and bipartite square lattice systems exhibit a similar spectrum, but an intriguing question is what happens when we move away from resonance.

In the Mott phase, all the lattice systems we explored gave rise to $SU(2)$-spin models. However, one can realise a variety of different spin models. In three dimension regular $p$-square lattice supports three orbital states $p_x$, $p_y$ and $p_z$, and thus the spin model in the Mott phase is an $SU(3)$-model [23; 30]. Thus, the other optical lattice models we discussed would also give rise to an $SU(3)$-model in three dimensions. As these models were bipartite and in three dimensions, they would give rise to spin-models with nearest and next-nearest neighbour couplings. This direction can be expanded and $SU(2) \times SU(3)$ models can also emerge.

## 10.3 Quantum simulators and beyond

The above hopefully shows many possible extensions to the work presented in this thesis. If I were to sum up, what this thesis was about in one sentence, I would answer that it is a thesis about using lattices in different ways to design potential quantum simulators. However, if I were given a chance to elaborate on this, I would say that it is also about systematising our understanding of these lattices in a way that allows us to generate new lattices that hopefully lead to new knowledge.

# Part V

# Summaries

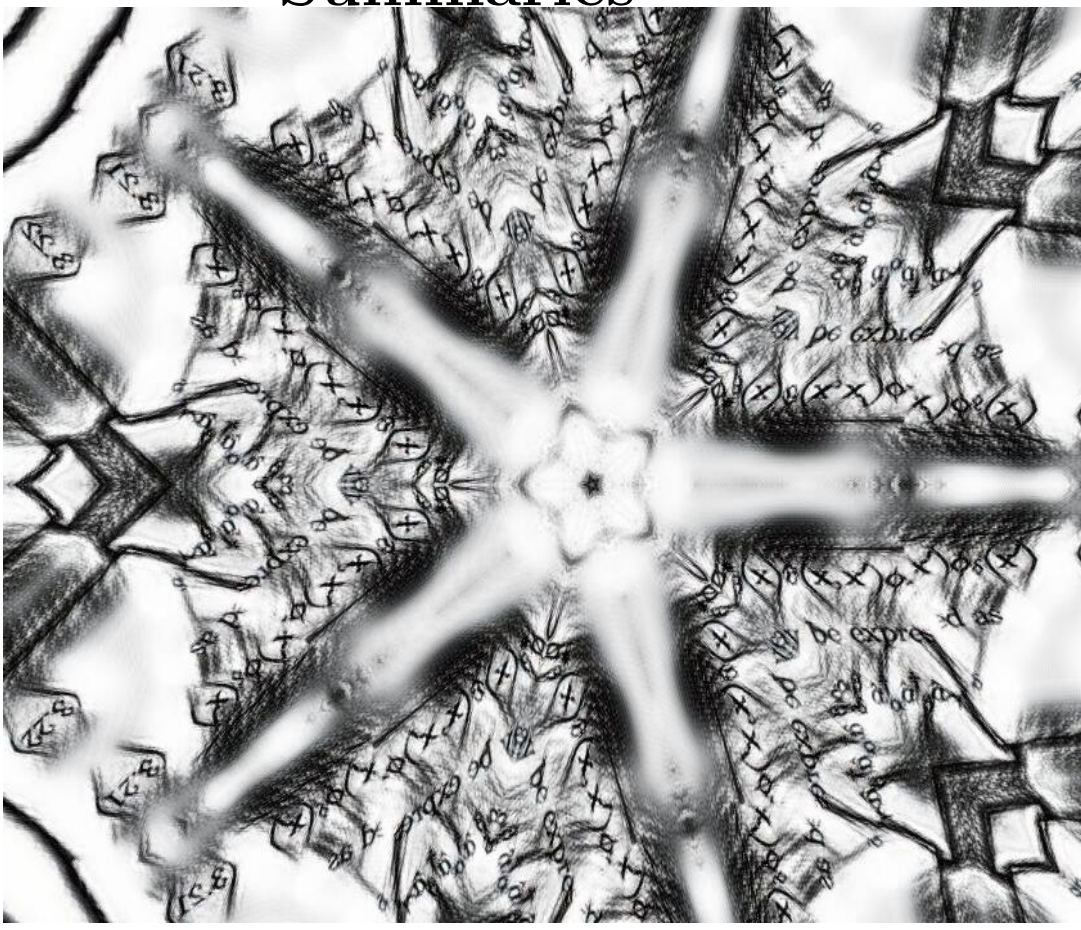

# 11. Ett kvantum för ett kvantum

I kunskapssamhället är kunskap det som formar samhället, vilket väcker frågan om vad kunskap är. En sorts kunskap den akademiska världen är specialiserad på är nämligen forskningsbaserad kunskap. Den forskning som bedrivs idag kommer förhoppningsvis att leda till ny kunskap och därmed bidra till att forma framtiden. Forskning spelar alltså en integrerad roll i kunskapssamhället, och med detta följer, menar jag, ett ansvar att se till att forskningen inte bara delas med experter, utan även med en bredare allmänhet. Det gäller alla typer av forskning, och givetvis även min egen. Titeln på min avhandling är *En kvant för en kvant* och min förhoppning är att denna sammanfattning lyckas förklara titeln och ger dig ett hum om vad du kan förvänta dig inför du ska läsa hela avhandlingen.

Jag forskar inom *kvantfysik*. Kvantfysikens rykte kommer sannolikt att nå dig innan du blir helt bekant med själva fältet. Det ryktas vara så otillgängligt att vi inte helt kan förstå den. Det finns många anledningar till detta rykte, men en av dem är att den kvantmekaniska världen är annorlunda än den vi lever våra dagliga liv i.

Den klassiska världen är deterministisk, men det är inte så i den kvantmekaniska världen. Medan Schrödingers ekvation deterministiskt bestämmer den kvantmekaniska vågfunktionen, så finns det ingen direkt relation mellan denna vågfunktion och det vi kan mäta och väga. Den indikerar inte partikelns position, utan en sannolikhetsfördelning för var partikeln mest troligtvis går att finna.

Men vi får problem om vi har mer än en partikel. Klassiska partiklar är oskiljbara, vilket innebär att vi kan numrera dem och beskriva hela systemet som en summa av varje enskild partikels bidrag. Däremot är kvantpartiklar omöjliga att särskilja, även om vi vet hur vi ska beskriva den individuella kvantpartikelns rörelse eller interaktionen mellan två kvantpartiklar, kan vi inte beskriva hela systemet som en summa av dessa bidrag. Kvantpartiklarna är vad vi kallar snärjda (entangled) och därmed kommer vi att behöva lösa systemet för alla kvantpartiklar samtidigt.

Och däri ligger ett problem: om vi är intresserade av ett system

bestående av många partiklar blir det snabbt en svår uppgift att försöka hitta systemets tillstånd. Antalet ekvationer vi måste lösa för att hitta systemets tillstånd kommer att växa exponentiellt med antalet partiklar. Det är alltså ett beräkningsmässigt svårt problem, vilket gör att den klassiska datorn inte kan lösa det när det finns många partiklar.

Att kvantpartiklarna är snärjda och att deras tillståndsrum växer exponentiellt blir ett hinder när vi försöker beskriva hur många partikelsystem beter sig. Men det behöver inte bara vara ett hinder, det kan också vara en del av lösningen. Richard Feynman föreslog att egenskapen att kvantsystem med många partiklar är snärjda också skulle kunna bana väg för hur vi kan studera dem [1; 2]. Istället för att använda en klassisk dator för att simulera mångapartikel kvantsystem bör vi istället använda en kvantdator.

Att vi studerar ett system genom att titta på ett annat är varken konstigt eller nytt. Detta är vad vi gör när vi använder en dator för att simulera hur en rymdraket färdas till månen. Det som kan tyckas vara nytt är att vi vill studera kvantsystem genom andra kvantsystem, så den typ av simulator vi letar efter är vad vi kallar en *kvantsimulator*, och är anledningen till att denna avhandling har titeln *Ett kvantum för ett kvantum*,

En kvantsimulator är ett kvantsystem som kan lära oss något om ett annat kvantsystem utan att studera detta system direkt. Det är avgörande att inget av de två systemen kan studeras på ett tillfredsställande sätt med en klassisk dator, då de båda måste vara kvantmekaniska.

## 11.1 Ultrakalla atomer i ett optiskt gitter

I denna avhandling intresserar vi oss för två typer av kvantsystem som kan användas för att realisera kvantsimulatorer. I del 2 (kapitel 4-kapitel 6) tittar vi på system av ultrakalla atomer i ett optiskt gitter. Sådana system är system där lasrar används för att bilda en gitterformad energipotential där atomer kan fångas vid gitterpunkterna.

Vi kan beskriva atomernas dynamik med en Bose-Hubbard-modell, vilket innebär att vi kan studera fasdiagrammet för dessa många partiklars kvantsystem. Ett kvantmekaniskt system kan liksom ett klassiskt system befinna sig i olika faser och det är systemets grundtillstånd som bestämmer systemets fas. I samband med kvantsimulatorer är det vi letar efter ett system med en fas, det vill säga ett grundtillstånd som vi inte kan beskriva utan att studera det med en kvantsimulator.

För att skilja olika faser från varandra kan du introducera en *ordningsparameter*, vilket är en storhet som har olika värden beroende på

fas. När ordensparameterern är noll, signalerar den att systemet är oordnat.

Både oordnade klassiska och kvantmekaniska system kan vara i en frustrerad fas. I en frustrerad fas är systemets grundtillstånd mycket degenererat på grund av konkurrerande krafter som inte kan tillfredsställas samtidigt [4; 5]. Genom att studera spinn i gitterstrukturen kan vi hitta ett systematiskt sätt att realisera sådana frustrerade faser.

Vi betraktar två gittersystem som är frustrerade. I båda exemplen antar vi att ett Ising-spinn, det vill säga ett spinn som bara kan ta värdena $\pm 1$, placeras på alla gitterpunkterna. Först tittar vi på en triangulär gitterstruktur med antiferromagnetiska kopplingar. Här måste alla kopplingar uppfylla kravet att för samtliga grannpar av Ising-spinn måste ett spinn ha värdet 1 och det andra $-1$. Det är omöjligt att uppfylla för alla spinn samtidigt, och systemets grundtillstånd kommer därför att bli frustrerat [6]. Om vi istället betraktar ett kvadratiskt gitter med båda närmaste och näst närmaste grannar antiferromagnetiska kopplingar, finner vi också att vi inte kan tillfredsställa alla kopplingar samtidigt, och systemets grundtillstånd kommer återigen att vara frustrerat. [8].

Ising-spinn är ett bra ställe att börja, men vi är främst intresserade av kvantmekaniska system med frustrerade grundtillstånd. Så istället för gitterstrukturen med Ising-spinn, vill vi studera gitterstrukturen med kvantspinn. Här kommer spinn vid olika gitterpunkter att vara snärjda och systemets tillståndsrum kommer därför att växa exponentiellt.

För en typ av frustrerade kvantsystem är grundtillståndet ett tätt packat och ett mycket snärjt tillstånd, utan statisk ordning. Ett sådant tillstånd har fått namnet kvantspinnvätska (QSL) [4] på grund av dess likhet med vanliga vätskor.

För kvantspinn är en kvadratisk gitterstruktur där det finns kopplingar mellan både närmaste ($J_1$) och näst närmaste ($J_2$) grannar intressant, eftersom det är en kandidat för att realisera en kvantspinnvätska. En av frågorna jag är intresserad av i denna avhandling är alltså hur bipartita optiska gittersystem kan användas för att realisera modeller som liknar just denna modell.

## 11.2 Focktillståndsgitterstruktur

I del 2 (Kapitel 7- Kapitel 8.5) byter vi fokus och studerar Focktillståndsgitterstrukturen. Focktillståndsgitterstrukturen är vad vi kallar tillståndsrymdsgitterstruktur och skiljer sig mycket från de optiska gittersystemen som just beskrivits.

När vi tänker på kvantgitterstrukturer tänker vi ofta på strukturer i den verkliga rymden. Här är gittergeometrin kopplad till de tre rumsliga dimensionerna. I fysiska gitter kan vi realisera högre dimensioner genom att introducera en eller flera *syntetiska dimensioner*, vilket kan göras genom att inkludera dimensioner i tillståndsrymden. Om man tar det ett steg längre kan man studera hela gitterstrukturer i tillståndsrymden. Här spelar systemets kvanttillstånd rollen som gitterpunkter, och kopplingen mellan två tillstånd spelar rollen som tunnling i gittret och arrangerar därmed gittret i en geometrisk struktur.

I samband med kvantsimulatorer och de system de simulerar, växer deras tillståndsrymd exponentiellt. Denna exponentiella tillväxt av tillståndsrummet är så att säga det som kännetecknar de system som vi refererar till som verkligt kvantmekaniska. Det betyder också att ett annat tillvägagångssätt för att söka efter kvantsimulatorer är att söka efter tillståndsrymdsgitterstrukturer som växer exponentiellt.

## 11.3 Exotiska gitterstrukturer som kvantsimulatorer

Ultrakalla atomer i optiska gittersystem och Focktillståndsgitterstrukturen är två typer av gitterstrukturer som vi kallar exotiska. De är exotiska i den mening att de är exotiska jämfört med de fysiska gitterstrukturer vi vanligtvis möter i fasta tillståndets fysik. De är exotiska genom att de inte förekommer naturligt i naturen, och de är så att säga artificiella gitterstrukturer av ljus och materia, och de är exotiska i den meningen att de kan användas för att realisera kvantsimulatorer eller *Ett kvantum för ett kvantum*.

# 12. Et kvantum for et kvantum

I vidensamfundet er viden det, der former samfundet. Det rejser spørgsmålet om, hvad viden er. En slags viden er den akademiske verden har specialiseret sig i, nemlig den forskningsbaseret viden. Den forskning, der bedrives i dag, vil forhåbentlig føre til ny viden og dermed være med til at forme fremtiden. Forskningen spiller således en integreret rolle i vidensamfundet, og hermed følger, synes jeg, et ansvar, for at forskning ikke kun deles med eksperter, men også med et bredere publikum. Det gælder for alle former for forskning, og selvfølgelig også for min egen. Titlen på mit afhandling er *Et kvantum for et kvantum kvantum* og mit håb er, at dette resume formår at forklarer titlen og skitserer, hvad du skal forvente, hvis du skal læse det hele.

Jeg forsker inden for *kvantefysik*. Kvantefysik er et felt, hvor dets omdømme sandsynligvis vil nå dig, før du bliver helt bekendt med selve feltet. Det rygtes at være så utilgængeligt, at vi ikke helt kan forstå det. Der er mange grunde til dette rygte, men en af dem er, at den kvantemekaniske verden er anderledes end den vi lever vores daglige liv i.

Hvor den klassiske verden er deterministisk, så er tingene ikke helt så enkle i den kvantemekaniske. Mens at Schrödingers ligning deterministisk bestemmer den kvantemekaniske bølgefunktionen, så vil resultatet af en måling af denne bølgefunktion være ikke-deterministisk. Det betyder, at kvantepartiklens position og impuls må beskrives ved sandsynlighedsfordelinger.

Men problemer begynder, hvis vi har mere end én partikel ved hånden. Klassiske partikler er skelnelige, hvilket betyder, at vi kan nummerere dem og beskrive det fulde system som en sum over bidraget fra hver enkelt partikel. Derimod er kvantepartikler ikke-skelnelige, så selvom vi ved, hvordan man beskriver bevægelsen af den enkelte kvantepartikel eller interaktionen mellem to kvantepartikler, så kan vi ikke beskrive det fulde system, som en sum over disse bidrag. Kvantepartiklerne er det vi kalder sammenfiltret (entaglement) og således bliver vi nødt til at løse systemet for alle kvantepartikler samtidigt.

Og heri ligger et problem: Hvis vi er interesseret i mangepartikel-

systemer, så blive det hurtigt et besvärligt arbejde at prøve at finde systemets tilstande. Det antal af ligninger, vi skal løse for at finde systemets tilstand, vil vokse eksponentielt med antallet af partikler. Det er således et beregningsmæssigt svært problem, hvilket betyder, at den klassiske computer ikke kan løæse det, når der er mange partikler.

At kvantepartiklerne er sammenfiltrede, og at deres tilstandsrum vokser eksponentielt bliver altså en hindring når vi forsøge at beskrive hvordan mangepartikelsystemer opföre sig. Men det behöver ikke kun at være en hindring, det kan også være en del af lösningen. Richard Feynman foreslog at denne egenskab, at mangepartikel kvantesystemer er sammenfiltrede, også kunne bane vejen for hvordan vi kan studerer dem [1; 2]. I stedet for at bruge en klassisk computer til at simulere mangepartikel kvantesystemer, bør vi bruge en kvantecomputer i stedet.

At vi studerer et system ved at kigge på et andet er hverken mærkeligt eller nyt. Det er, hvad vi gør, når vi bruger en computer til at simulere, hvordan en rumrakets rejse til månen. Det der måske virke nyt, er at vi ønsker at studere kvantesystemer gennem andre kvantesystemer, så den type af simulatorer vi leder efter er vi kalder for *kvantesimulator*. og hvorfor denne afhandling har titlen *Et kvantum for et kvantum*,

En kvantesimulator er et kvantesystem som vi kan lære noget et andet kvantesystem om uden at vi studerer dette system direkte. Det er det afgørende, at ingen af de to systemer kan studeres fyldsgörende på en klassisk computer.

## 12.1 Ultrakolde atomer i et optiske gitter

I denne afhandling er vi interesseret i to slags kvantesystemer, der kan bruges til at realisere kvantesimulatorer. I del 2 (kapitel 4-kapitel 6) ser vi på systemer af ultrakolde atomer i et optiske gitter. Sådanne systemer er systemer, hvor lasere bruges til at danne et gitterformet energipotentialer hvori atomer kan fanges på gitterpunkterne.

Vi kan beskrive atomernes dynamik med en Bose-Hubbard-model, hvilket betyder, at vi kan studere fasediagrammet for disse mangepartikel kvantesystemer. Kvantemekaniske systemer kan ligesom klassiske systemer være i forskellige faser, og det er systemets grundtilstand, der bestemmer systemets fase. I forbindelse med kvantesimulatorer er det, vi søger efter, et system med en fase, dvs en grundtilstand, vi ikke kan beskrive uden at studere det med en kvantesimulator.

For at skelne forskellige faser fra hinanden kan man indføre en *ordreparameter*, som er en størrelse, der har forskellige værdier afhængigt

af fasen. Når ordensparameteren er nul signalerer det at systemet er uordnet.

Både uordnede klassiske og kvantemekaniske systemer kan være i en frustreret fase. I en frustreret fase er systemets grundtilstand stærkt degenereret på grund af konkurrerende kræfter, der ikke samtidigt kan opfyldes [4; 5]. Ved at studerer spin i gitterstrukturer kan vi finde en systematisk vej til at realisere sådanne frustrerede faser.

Vi betragter to gittersystemer, der kan værer frustrerede. I begge eksempler antager vi, at et Ising-spin, det vil sige et spin, der kun kan tage værdierne $\pm 1$, placeres på alle gitterpunkterne. Først ser vi på en trekantetet gitterstruktur med antiferromagnetiske koblinger. Her vil opfyldelse af alle koblinger, betyde at for alle nabopar af Ising-spin, så skal det ene spin have værdien 1 og det andet $-1$. Det er umuligt at opfylde for alle spins samtidigt, og systemets grundtilstand vil derfor være frustreret [6]. Betragter vi istedet et kvadratisk gitter med antiferromagnetiske nærmeste og næst-nærmeste nabokoblinger, så finder vi også at vi ikke kan opfylde alle koblinger samtidigt, og systemets grundtilstand vil igen være frustreret. [8].

Isings-spins er et godt sted at starte, men vi er primært interesserede i kvantemekaniske systemer med frustrerede grundtilstande. Så i stedet for gitterstrukturer med Ising-spins studerer vi gitterstrukturer med kvantespins. Her vil spins på forskellige gitterpunkter være sammenfiltrede og systemet tilstandsrum vil derfor vokse eksponentielt,.

For en type af frustrerede kvantesystemer er grundtilstanden er tætpakket og meget sammenfiltret tilstand, uden statisk orden. Sådan en tilstand er på grund af dens lighed med almindelige vväsker blevet givet navnet kvantespinvæske (QSL) [4].

For kvantespin er en kvadratisk gitterstrukture, hvor der er både nærmeste ($J_1$) og næst nærmeste nabo ($J_2$)-koblinger interessant, idet det er en kandidat til at realisere en kvantespinvæske. Således er et af de spørgsmål, jeg er interesserede i denne afhandling, hvordan bipartite optiske gittersystemer kan bruges til at realisere modeller, der ligner netop denne model.

## 12.2 Focktilstands gitterstrukturer

I del 2 (Kapitel 7- Kapitel 9) ændre vi fokus og studerer Focktilstands gitterstrukturer. Focktilstands gitterstruktur er det, vi kalder tilstandsrums gitterstruktur, og er konceptuelt meget forskelligt fra de optiske gittersystemer, der lige er blevet beskrevet.

Når vi tænker på kvantegitterstrukturer, tænker vi ofte på strukturer i det reelle rum. Her er gittergeometrien knyttet til de tre rumlige dimensioner. I fysiske gitter kan vi realiserer højere dimensioner ved at introducere en eller flere *syntetiske dimensioner*, hvilket kan göres ved at inkludere dimensioner i tilstandsrummet. Tager man det et skridt videre, kunne man studerer hele gitterstrukturer, der er strukturer i et tilstandsrum. Her spiller systemets kvantetilstande rollen som gitterpunkter, og koblingen mellem to tilstande spiller rollen som tunnelleringer i gitteret og ordner dermed gitteret i en geometrisk struktur.

I sammenhæng med kvantesimulatorer og de systemer, de simulerer, vokser deres tilstandsrum eksponentielt. Denne eksponentielle vækst af tilstandsrummet er så at sige det, der karakteriserer de systemer, som vi omtaler som at være virkelig kvantemekaniske. Det betyder også at en anden tilgang til at søge efter kvantesimulatorer er at søge efter tilstandsrum gitterstrukturer, der vokser eksponentielt.

## 12.3 Eksotiske gitterstrukturer som kvantesimulatorer

Ultrakolde atomer i optiske gittersystemer og Focktilstands gitterstrukturer er to slags gittersystemer, som vi kalder eksotiske gittersystemer. De er eksotiske i den forstand, at de er eksotiske sammenlignet med de fysiske gitterstrukturer, vi typisk møder i faststoffysik. De er eksotiske, da de ikke forekommer naturligt i naturen, og de er så at sige kunstige gitterstrukturer af lys og materie, og de er eksotiske i den forstand, at de kan bruges til at realisere kvantesimulatorer eller *Et kvantum for et kvantum.*

# References


[1] Richard P Feynman. **Simulating Physics with Computers**. *International Journal of Theoretical Physics*, **21**(6/7), 1982. 20, 142, 146

[2] Richard P Feynman. **There's Plenty of Room at the Bottom**. *Caltech Engineering and Science*, **23:5**, 1960. 142, 146

[3] J Ignacio Cirac and Peter Zoller. **Goals and opportunities in quantum simulation**. *Nature physics*, **8**(4):264–266, 2012. 20

[4] Leon Balents. **Spin liquids in frustrated magnets**. *Nature*, **464**(7286):199–208, 2010. 21, 22, 73, 81, 143, 147

[5] Gérard Toulouse. **The frustration model**. In *Modern trends in the theory of condensed matter*, pages 195–203. Springer, 1980. 21, 143, 147

[6] GH0038 Wannier. **Antiferromagnetism. the triangular ising net**. *Physical Review*, **79**(2):357, 1950. 22, 143, 147

[7] Roderich Moessner and Arthur P Ramirez. **Geometrical frustration**. *Phys. Today*, **59**(2):24, 2006. 22

[8] Per Arne Slotte. **Phase diagram of the square-lattice ising model with first- and second-neighbour interactions**. *Journal of Physics C: Solid State Physics*, **16**(15):2935, 1983. 22, 81, 143, 147

[9] J Villain. **Two-level systems in a spin-glass model. I. General formalism and two-dimensional model**. *Journal of Physics C: Solid State Physics*, **10**(23):4793, 1977. 22, 68, 75

[10] Philip W Anderson. **The resonating valence bond state in La2CuO4 and superconductivity**. *science*, **235**(4793):1196–1198, 1987. 22

[11] Yi Zhou, Kazushi Kanoda, and Tai-Kai Ng. **Quantum spin liquid states**. *Reviews of Modern Physics*, **89**(2):025003, 2017. 73

[12] Hong-Chen Jiang, Hong Yao, and Leon Balents. **Spin liquid ground state of the spin-1 2 square J 1-J 2 Heisenberg model**. *Physical Review B*, **86**(2):024424, 2012. 22, 81

[13] Alexander Altland and Ben D Simons. *Condensed matter field theory*. Cambridge university press, 2010. 25, 52

[14] N. W. Ashcroft and N. D. Mermin. *Solid State Physics*. Holt-Saunders, 1976. 26, 28, 29, 45, 48, 49

[15] Charles Kittel. *Introduction to solid state physics Eighth edition*. John Wiley and Sons, 2021. 26, 29, 49

[16] Felix Bloch. **Über die Quantenmechanik der Elektronen in Kristallgittern**. *Zeitschrift fur Physik*, **52**(7-8):555–600, July 1929. 28, 45

[17] Alan L Mackay. **Crystallography and the Penrose pattern**. *Physica A: Statistical Mechanics and its Applications*, **114**(1-3):609–613, 1982. 29

[18] Dov Levine and Paul Joseph Steinhardt. **Quasicrystals: a new class of ordered structures**. *Physical review letters*, **53**(26):2477, 1984. 29

[19] Immanuel Bloch, Jean Dalibard, and Wilhelm Zwerger. **Many-body physics with ultracold gases**. *Reviews of modern physics*, **80**(3):885, 2008. 30, 41

[20] Immanuel Bloch, Jean Dalibard, and Sylvain Nascimbene. **Quantum simulations with ultracold quantum gases**. *Nature Physics*, **8**(4):267–276, 2012. 30, 51

[21] Henrik Bruus and Karsten Flensberg. *Many-body quantum theory in condensed matter physics: an introduction*. OUP Oxford, 2004. 33, 37, 52

[22] Dieter Jaksch and Peter Zoller. **The cold atom Hubbard toolbox**. *Annals of physics*, **315**(1):52–79, 2005. 41

[23] Fernanda Pinheiro. *Multi-species systems in optical lattices: from orbital physics in excited bands to effects of disorder*. Springer, 2016. 41, 52, 59, 60, 61, 137

[24] Maciej Lewenstein, Anna Sanpera, Veronica Ahufinger, Bogdan Damski, Aditi Sen, and Ujjwal Sen. **Ultracold atomic gases in optical lattices: mimicking condensed matter physics and beyond**. *Advances in Physics*, **56**(2):243–379, 2007. 43, 59

[25] L. Guidoni, C. Triché, P. Verkerk, and G. Grynberg. **Quasiperiodic Optical Lattices**. *Phys. Rev. Lett.*, **79**:3363–3366, Nov 1997. 43

[26] Immanuel Bloch. **Ultracold quantum gases in optical lattices**. *Nature physics*, **1**(1):23–30, 2005. 52

[27] Christopher J Pethick and Henrik Smith. *Bose–Einstein condensation in dilute gases*. Cambridge university press, 2008. 52, 59

[28] Fernanda Pinheiro, Jani-Petri Martikainen, and Jonas Larson. **Confined p-band Bose-Einstein condensates**. *Physical Review A*, **85**(3), Mar 2012. 52

[29] Fernanda Pinheiro, Georg M. Bruun, Jani-Petri Martikainen, and Jonas Larson. **XYZ Quantum Heisenberg Models with p-Orbital Bosons**. *Physical Review Letters*, **111**(20), Nov 2013.

[30] Fernanda Pinheiro, Jani-Petri Matrikainen, and Jonas Larson. **Phases of d-orbital bosons in optical lattices**. *New Journal of Physics*, **17**(5):053004, May 2015. 58, 87, 137

[31] Fernanda Pinheiro and Jonas Larson. **Disordered cold atoms in different symmetry classes**. *Physical Review A*, **92**(2), Aug 2015. 52

[32] J. Hubbard. **Electron Correlations in Narrow Energy Bands**. *Proceedings of the Royal Society of London Series A*, **276**(1365):238–257, November 1963. 55

[33] H. A. Gersch and G. C. Knollman. **Quantum Cell Model for Bosons**. *Physical Review*, **129**(2):959–967, January 1963. 55

[34] Crispin Gardiner and Peter Zoller. *The Quantum World of Ultra-Cold Atoms and Light Book I: Foundations of Quantum Optics*, **2**. World Scientific Publishing Company, 2014. 56, 58, 67

[35] K Sheshadri, HR Krishnamurthy, Rahul Pandit, and TV Ramakrishnan. **Superfluid and insulating phases in an interacting-boson model: Mean-field theory and the RPA**. *EPL (Europhysics Letters)*, **22**(4):257, 1993. 58

[36] JK Freericks and H Monien. **Phase diagram of the Bose-Hubbard model**. *EPL (Europhysics Letters)*, **26**(7):545, 1994. 58

[37] Torben Müller, Simon Fölling, Artur Widera, and Immanuel Bloch. **State preparation and dynamics of ultracold atoms in higher lattice orbitals**. *Physical Review Letters*, **99**(20):200405, 2007. 59

[38] W. Vincent Liu and Congjun Wu. **Atomic matter of nonzero-momentum Bose-Einstein condensation and orbital current order**. *Phys. Rev. A*, **74**:013607, Jul 2006. 59

[39] Assa Auerbach. *Interacting electrons and quantum magnetism*. Springer Science & Business Media, 1994. 59, 61

[40] J Vargas, M Nuske, R Eichberger, C Hippler, L Mathey, and A Hemmerich. **Orbital many-body dynamics of Bosons in the second Bloch band of an optical lattice**. *Physical Review Letters*, **126**(20):200402, 2021. 70

[41] Markus Greiner, Olaf Mandel, Theodor W Hänsch, and Immanuel Bloch. **Collapse and revival of the matter wave field of a Bose–Einstein condensate**. *Nature*, **419**(6902):51–54, 2002. 70

[42] Subir Sachdev. *Quantum phase transitions*. Cambridge university press, 2011. 74

[43] B Berge, HT Diep, A Ghazali, and P Lallemand. **Phase transitions in two-dimensional uniformly frustrated XY spin systems**. *Physical Review B*, **34**(5):3177, 1986. 75

[44] Jooyoung Lee, JM Kosterlitz, and Enzo Granato. **Monte Carlo study of frustrated XY models on a triangular and square lattice**. *Physical Review B*, **43**(13):11531, 1991.

[45] G Ramirez-Santiago and Jorge V José. **Critical exponents of the fully frustrated two-dimensional XY model**. *Physical Review B*, **49**(14):9567, 1994.

[46] Sooyeul Lee and Koo-Chul Lee. **Phase transitions in the fully frustrated XY model studied with use of the microcanonical Monte Carlo technique**. *Physical Review B*, **49**(21):15184, 1994.

[47] Peter Olsson. **Two phase transitions in the fully frustrated XY model**. *Physical review letters*, **75**(14):2758, 1995.

[48] HJ Luo, Lothar Schülke, and BO Zheng. **Dynamic approach to the fully frustrated XY model**. *Physical review letters*, **81**(1):180, 1998.

[49] Martin Hasenbusch, Andrea Pelissetto, and Ettore Vicari. **Multicritical behaviour in the fully frustrated XY model and related systems**. *Journal of Statistical Mechanics: Theory and Experiment*, **2005**(12):P12002, 2005. 75

[50] T Kock, C Hippler, A Ewerbeck, and A Hemmerich. **Orbital optical lattices with bosons**. *Journal of Physics B: Atomic, Molecular and Optical Physics*, **49**(4):042001, 2016. 75

[51] Wen-Jun Hu, Federico Becca, Alberto Parola, and Sandro Sorella. **Direct evidence for a gapless Z 2 spin liquid by frustrating Néel antiferromagnetism**. *Physical Review B*, **88**(6):060402, 2013. 81

[52] Ling Wang and Anders W. Sandvik. **Critical Level Crossings and Gapless Spin Liquid in the Square-Lattice Spin-**$1/2$ $J_1 - J_2$ **Heisenberg Antiferromagnet**. *Phys. Rev. Lett.*, **121**:107202, Sep 2018. 81

[53] OA Petrenko, A Honecker, and ME Zhitomirsky. **Field induced ordering in the frustrated square-lattice antiferromagnet**. *Phys. Rev. Lett*, **85**:3269, 2000. 82, 83

[54] Tommaso Coletta, ME Zhitomirsky, and Frédéric Mila. **Quantum stabilization of classically unstable plateau structures**. *Physical Review B*, **87**(6):060407, 2013. 82

[55] Katsuhiro Morita and Naokazu Shibata. **Field-Induced Quantum Phase Transitions in S= 1/2 J 1–J 2 Heisenberg Model on Square Lattice**. *journal of the physical society of japan*, **85**(9):094708, 2016. 83

[56] O Boada, A Celi, JI Latorre, and M Lewenstein. **Quantum simulation of an extra dimension**. *Physical review letters*, **108**(13):133001, 2012. 95

[57] Armando Perez-Leija, Hector Moya-Cessa, Alexander Szameit, and Demetrios N Christodoulides. **Glauber–Fock photonic lattices**. *Optics letters*, **35**(14):2409–2411, 2010.

[58] Hannah M Price, Tomoki Ozawa, and Nathan Goldman. **Synthetic dimensions for cold atoms from shaking a harmonic trap**. *Physical Review A*, **95**(2):023607, 2017.

[59] Konrad Tschernig, Roberto de J León-Montiel, Armando Pérez-Leija, and Kurt Busch. **Multiphoton synthetic lattices in multiport waveguide arrays: synthetic atoms and Fock graphs**. *Photonics Research*, **8**(7):1161–1170, 2020. 95, 109, 136

[60] Da-Wei Wang, Han Cai, Ren-Bao Liu, and Marlan O Scully. **Mesoscopic superposition states generated by synthetic spin-orbit interaction in Fock-state lattices**. *Physical review letters*, **116**(22):220502, 2016.

[61] Han Cai and Da-Wei Wang. **Topological phases of quantized light**. *National Science Review*, **8**(1), Aug 2020. 95, 109

[62] E.T. Jaynes and F.W. Cummings. **Comparison of quantum and semiclassical radiation theories with application to the beam maser**. *Proceedings of the IEEE*, **51**(1):89–109, 1963. 96, 97

[63] Bruce W. Shore and Peter L. Knight. **The Jaynes-Cummings Model**. *Journal of Modern Optics*, **40**(7):1195–1238, 1993. 97

[64] Jonas Larson and Themistoklis Mavrogordatos. *The Jaynes–Cummings Model and Its Descendants*. 2053-2563. IOP Publishing, 2021. 97, 98, 99, 104, 127

[65] Marlan O Scully and M Suhail Zubairy. **Quantum optics**, 1999. 97

[66] Jorge Casanova, Guillermo Romero, Ion Lizuain, Juan José García-Ripoll, and Enrique Solano. **Deep strong coupling regime of the Jaynes-Cummings model**. *Physical review letters*, **105**(26):263603, 2010. 104

[67] Qiong-Tao Xie, Shuai Cui, Jun-Peng Cao, Luigi Amico, and Heng Fan. **Anisotropic rabi model**. *Physical Review X*, **4**(2):021046, 2014. 104

[68] W_P Su, JR Schrieffer, and Ao J Heeger. **Solitons in polyacetylene**. *Physical review letters*, **42**(25):1698, 1979. 104, 129

[69] Jonas Larson, Erik Sjöqvist, and Patrik Öhberg. *Conical Intersections in Physics*. Springer, 2020. 104, 109, 112

[70] Michael Creutz. **End states, ladder compounds, and domain-wall fermions**. *Physical review letters*, **83**(13):2636, 1999. 105, 129

[71] Matthias Christandl, Nilanjana Datta, Artur Ekert, and Andrew J Landahl. **Perfect state transfer in quantum spin networks**. *Physical review letters*, **92**(18):187902, 2004. 111

[72] A Nunnenkamp, Jens Koch, and SM Girvin. **Synthetic gauge fields and homodyne transmission in Jaynes–Cummings lattices**. *New Journal of Physics*, **13**(9):095008, 2011. 111

[73] N David Mermin. **Can a phase transition make quantum mechanics less embarrassing?** *Physica A: Statistical Mechanics and its Applications*, **177**(1-3):561–566, 1991. 128, 129

[74] Heinz-Peter Breuer, Daniel Burgarth, and Francesco Petruccione. **Non-Markovian dynamics in a spin star system: Exact solution and approximation techniques**. *Physical Review B*, **70**(4):045323, 2004. 128, 129

[75] Elliott H Lieb. **Erratum: Two theorems on the Hubbard model [Phys. Rev. Lett. 62, 1201 (1989)]**. *Physical Review Letters*, **62**(16):1927, 1989. 129

[76] Hans A Bethe. **Statistical theory of superlattices**. *Proceedings of the Royal Society of London. Series A-Mathematical and Physical Sciences*, **150**(871):552–575, 1935. 130

[77] Helge von Koch. **On a continuous curve tangent constructible from elementary geometry**. *Arkiv f or Matematik, Astronomi och Fysik*, pages 681–702, 1904. 136

[78] M Ölschläger, T Kock, G Wirth, A Ewerbeck, C Morais Smith, and A Hemmerich. **Interaction-induced chiral px±ipy superfluid order of bosons in an optical lattice**. *New Journal of Physics*, **15**(8):083041, 2013. 137

[79] Georg Wirth, Matthias Ölschläger, and Andreas Hemmerich. **Evidence for orbital superfluidity in the P-band of a bipartite optical square lattice**. *Nature Physics*, **7**(2):147–153, 2011. 137

[80] Douglas R Hofstadter. **Energy levels and wave functions of Bloch electrons in rational and irrational magnetic fields**. *Physical review B*, **14**(6):2239, 1976. 137

[81] Hirokazu Miyake, Georgios A Siviloglou, Colin J Kennedy, William Cody Burton, and Wolfgang Ketterle. **Realizing the Harper Hamiltonian with laser-assisted tunneling in optical lattices**. *Physical review letters*, **111**(18):185302, 2013. 137

[82] Monika Aidelsburger, Marcos Atala, Michael Lohse, Julio T Barreiro, B Paredes, and Immanuel Bloch. **Realization of the Hofstadter Hamiltonian with ultracold atoms in optical lattices**. *Physical review letters*, **111**(18):185301, 2013.

[83] Dieter Jaksch and Peter Zoller. **Creation of effective magnetic fields in optical lattices: the Hofstadter butterfly for cold neutral atoms**. *New Journal of Physics*, **5**(1):56, 2003. 137